SISSA

International School for Advanced Studies

PhD Course in Theory and Numerical Simulation of Condensed Matter

Nonequilibrium dynamics in isolated quantum systems: absence of thermalization and dynamical phase transitions

Thesis submitted for the degree of
Doctor Philosophiae

Candidate:
Anna Maraga

Supervisors:
Prof. Alessandro Silva
Prof. Michele Fabrizio

Academic Year 2014-2015

Contents

Chapter 1

Introduction: nonequilibrium dynamics of isolated quantum systems

Equilibrium systems can often be studied using simple effective models that accurately describe low temperature experiments on complex real systems, such as interacting electrons in solids. The nonequilibrium case, however, is till now much less known, and one may wonder whether the theoretical study of the dynamics of simplified models would still allow to faithfully describe real experiments as in equilibrium [1]. In this regard, over the last years ultracold atomic gases [2] emerged as a versatile tool for benchmarking nonequilibrium theories based on simple models against the results of well-controlled experiments with tunable parameters [3].

In principle, there are many different ways in which a system can be brought out of equilibrium and, in general, the outcome is expected to be affected by the particular choice. In the following, we shall focus on isolated quantum systems taken far from equilibrium by changing in time one or more of the system parameters, i.e., by performing a quench [4]. This change can be either sudden or slow, and leads to a unitary dynamical evolution of the system. In this context, a series of intriguing natural questions arises, concerning the behavior long after the quench. Does the system display relaxation? If so, what is the nature of such a steady state? Can it be thermal?

1.1 Studying nonequilibrium dynamics with cold atoms

Ultracold atomic gases are ideal systems for the experimental study of the nonequilibrium quantum dynamics. Because of their almost-perfect isolation from the external environment, which strongly suppresses dissipative and decoherence effects, they can be regarded as closed quantum systems. Furthermore, the wide tunability of many parameters, such as interaction strength, density, temperature, and dimensionality, allows the realization of various physical scenarios.

The weak coupling with the environment and the very low densities and temperatures of these gases lead to very long coherence times (that can reach many seconds) compared to the timescales of the dynamics, typically of the order of milliseconds. Accordingly, the real-time observation of the quantum coherent dynamics is fully accessible. In a remarkable experiment, Greiner et al. [5] succeeded in observing the long-lived coherent collapse and revival dynamics of the matter wave field of a Bose-Einstein condensate. During the time evolution, induced by a sudden change of the lattice depth, the matter wave field periodically dephased and rephased, as revealed in the interference patterns obtained after turning off all trapping potentials. More recently, Lamporesi et al. [6] studied the condensate formation in an elongated Bose gas of sodium atoms cooled below the BEC transition temperature. The phase transition was crossed with different velocities, revealing the spontaneous formation of solitons (Figure 1.1(a)), whose number followed the expectations of the Kibble-Zurek mechanism [7–9]. These measurements provided also a promising way for evaluating critical exponents of the BEC transition in trapped gases. The coherence times in such experiments are so long that they can be regarded as examples of dynamic quantum simulators [10] and can be used to obtain results beyond those of numerical studies. For example, Trotzky at al. [11] observed the dynamics of a charge-density wave in a strongly correlated one-dimensional Bose gas. Local densities, currents and correlations showed a fast relaxation towards their equilibrium values and, most notably, the time-range of the experiment went well beyond that of numerical predictions obtained with time-dependent density-matrix renormalization group (t-DMRG), as shown in Figure 1.1(b).

In order to probe the dynamics of ultracold gases, absorption or fluorescence imaging is typically used. This detection process was recently employed to study a two-dimensional strongly interacting bosonic Mott insulator on a microscopic level, reaching single-atom and single-site resolution [12, 13]. The high-resolution optical imaging technique gave the opportunity to directly observe the atomic tunneling dynamics [14], measure a string order parameter [15], detect the light-cone spreading

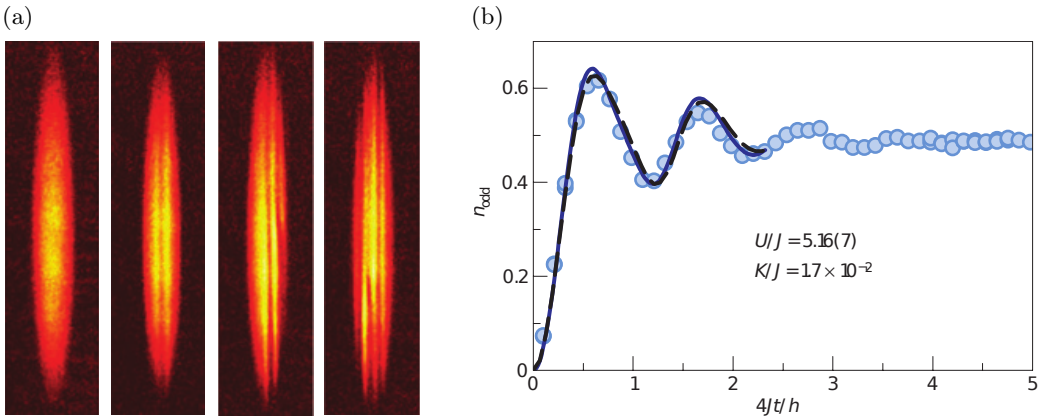

Figure 1.1: (a) Time-of-flight pictures of atomic clouds after a quench across the BEC transition. The clouds contain 0, 1, 2 and 3 solitons, from left to right. Figure adapted from [6]. (b) Relaxation of the odd-site density after a quench. The experimental dynamics (symbols) runs for longer times than t-DMRG simulations (solid and dashed lines). Figure adapted from [11].

of correlations [16], study the dynamics of a mobile spin impurity [17] and of two-magnon bound states [18]. While imaging techniques are suitable for measuring, e.g., the density and momentum distribution, they can not be used for probing the phase of the fields, which requires matter waves interference experiments. For example, interference was used to study the relaxation dynamics of a coherently split one-dimensional Bose gas and show that the system retained memory of its initial state [19–22]. Measuring the full probability distribution of the integrated interference contrast revealed that the system did not relax to thermal equilibrium, but to a different thermal-like steady state characterized by an effective temperature and identified as a long-lived prethermalized state (see Sec. 1.4).

One of the crucial feature of ultracold atomic gases for the study of nonequilibrium dynamics is the possibility of varying the interaction strength in time via Feshbach resonances [25, 26]. Recently, Hung et al. [23] performed a quench experiment in a two-dimensional atomic superfluid: sound waves were synchronously generated by suddenly changing the atomic interactions using a Feshbach resonance. In the subsequent evolution, reported in Figure 1.2(a), the density fluctuations changed drastically within the first few milliseconds, while the density profile exhibited weak collective oscillations on long time scales, evolving toward a new equilibrium corresponding to the final interaction strength. This suggests a fast local equilibration and a much slower global thermalization. Another experiment

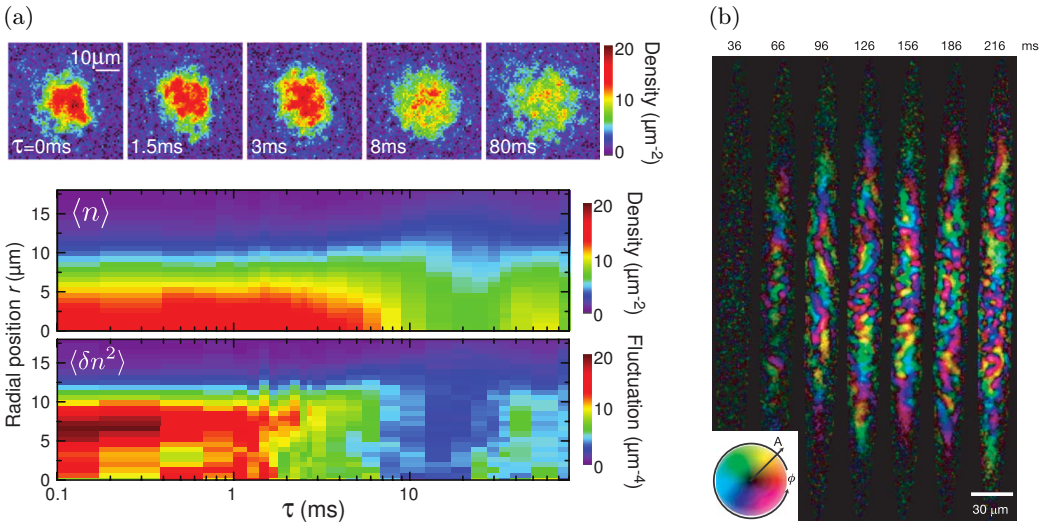

Figure 1.2: (a) Evolution after an interaction quench in atomic superfluids. Upper panel: single-shot images of the sample for the indicated hold times. Central panel: averaged radial density profile $\langle n(r)\rangle$ based on ~ 25 samples. Lower panel: averaged density fluctuations $\langle \delta n^2(r)\rangle$ based on ~ 25 samples. Figure adapted from [23]. (b) Defect generation after a quench in a spinor condensate. The images show the transverse magnetization density for variable evolution times, revealing a spatially inhomogeneous formation of ferromagnetic domains. The orientation ϕ and amplitude A are depicted by the color and brightness according to the color wheel shown. Figure adapted from [24].

by Meinert et al. [27] studied a one-dimensional atomic Bose-Hubbard chain in a tilted potential, which effectively maps onto a one-dimensional Ising model [28, 29]. Varying the tilt of the lattice, it is possible to simulate the quantum phase transition from the paramagnetic to the antiferromagnetic spin chain. The authors performed a sudden quench to the vicinity of the transition point which resulted in coherent oscillations for the orientation of effective Ising spins, detected via oscillations in the number of doubly occupied lattice sites.

Atoms contain also well-controllable internal degrees of freedom. An intriguing example are spinor gases. These gases, with a spin degree of freedom arising from a nonzero hyperfine spin F, can simultaneously exhibit superfluidity and magnetism. Sadler et al. [24] performed an experiment using a $F = 1$ condensate of ^{87}Rb, which undergoes a continuous quantum phase transition between a polar and a ferromagnetic phase. The competing parameters controlling this phase

transition are the spin-dependent mean-field interaction and a quadratic Zeeman interaction that can be tuned by an external magnetic field. The spinor gas was quenched across the transition by rapidly reducing the external magnetic field. After the quench, phase-contrast imaging, showed in Figure 1.2(b), revealed the spontaneous formation of ferromagnetic domains of variable size and the appearance of topological defects, identified as polar-core spin-vortices.

By trapping the ultracold gases in strong confining potentials it is possible to control the dimensionality of the system and experimentally study the dynamics in reduced dimensions. In particular, the realization of such systems allows us to investigate the relation between thermalization and integrability (see Sec. 1.3). A groundbreaking experiment in this sense was performed by Kinoshita et al. [30]. Arrays of tightly confined one-dimensional ultracold gases of ^{87}Rb were obtained by a deep two-dimensional optical lattice. To create a nonequilibrium momentum distribution, the array of tubes was placed in a superposition of states with opposite momentum. The gas was then allowed to evolve for variable durations before the momentum distribution was measured via absorption imaging (Figure 1.3). It was found no evidence of redistribution of momentum, so that the dephased distribution remains non-Gaussian even after thousands of collisions, signaling that the system did not thermalize on experimental time scales. This was in clear contrast to the case of a nonequilibrium momentum distribution created in a three-dimensional gas, where the system immediately relaxed to a thermal distribution. The lack of thermalization can be understood to be the consequence of the fact that this system is a very close experimental realization of the Lieb-Liniger gas with point-like interaction [31, 32], which is an integrable model. This remarkable result motivated the subsequent theoretical investigation on the interplay of integrability, quantum dynamics and thermalization in isolated systems.

1.2 Thermalization in quantum nonintegrable systems

For classical systems, the theory of thermalization is definitely related to the concept of ergodicity. A system is ergodic if the trajectories in phase space uniformly cover the constant-energy manifold for almost any initial condition. In this case, the time averages are equivalent to the phase space averages in the microcanonical ensemble. Hence, the details of the initial configuration are irrelevant at long times and the only parameters that matter are the integrals of motion, such as the total energy and the number of particles. However, if a system with n canonical degrees

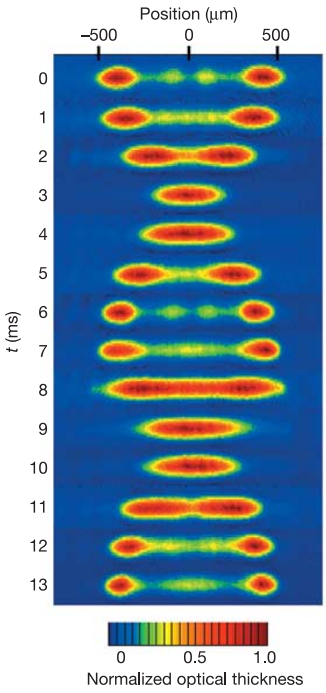

Figure 1.3: Absorption images of an ensemble of one-dimensional Bose gases evolving from an initial nonequilibrium momentum distribution. The non-Gaussian nature of the dephased momentum distribution clearly indicates an absence of thermalization. Figure adapted from [30].

of freedom has n independent constants of motion with vanishing Poisson brackets with the Hamiltonian and with each other, the evolution is confined to a highly restricted hypersurface of the energy manifold, so that microcanonical predictions fail and the system does not thermalize.

The generalization of the concept of ergodicity to the quantum case is not straightforward [33,34]. Indeed, let us consider a system described by a Hamiltonian with eigenstates $|\psi_\alpha\rangle$ and corresponding energies E_α. Denoting by $\mathcal{D}(E)$ the set of eigenstates with energies within the microcanonical shell $[E, E+\delta E]$, the quantum microcanonical density matrix can be defined as

$$\rho_{\rm mc} = \frac{1}{\mathcal{N}(E)} \sum_{\alpha \in \mathcal{D}(E)} |\psi_\alpha\rangle \langle\psi_\alpha| \,, \tag{1.1}$$

where $\mathcal{N}(E) = \sum_{\alpha\in\mathcal{D}(E)}$ is the number of states in that shell. Given a generic initial state $|\Psi_0\rangle$, superposition of eigenstates with different energies in the shell,

i.e.,

$$|\Psi_0\rangle = \sum_{\alpha \in \mathcal{D}(E)} c_\alpha \, |\psi_\alpha\rangle \,, \tag{1.2}$$

with $c_\alpha = \langle \psi_\alpha | \Psi_0 \rangle$, we want to compute the long time average of the density matrix of the system. Denoting as $|\Psi(t)\rangle$ the time evolution of $|\Psi_0\rangle$ and assuming the eigenstates not to be degenerate, we obtain

$$\lim_{T\to\infty} \frac{1}{T} \int_0^T \mathrm{d}t \; |\Psi(t)\rangle \langle \Psi(t)| \; = \sum_\alpha |c_\alpha|^2 \; |\psi_\alpha\rangle \langle \psi_\alpha| \equiv \rho_{\mathrm{diag}}, \tag{1.3}$$

where ρ_{diag} is the density matrix describing the so-called diagonal ensemble. We immediately notice that the most obvious definition of ergodicity, i.e., the requirement $\rho_{\mathrm{diag}} = \rho_{\mathrm{mc}}$, implies that $|c_\alpha|^2 = 1/\mathcal{N}(E)$ for any α, a condition almost never satisfied.

The apparent absence of thermalization is in stark contradiction to our common sense and expectations, which tell us that many quantum many-body systems behave thermally, unless some special conditions are met (e.g., integrability, see Sec. 1.3). The key for solving this paradox is the fact that the central role is not played by the evolving state but, instead, by the expectation value of local observables. A widely studied scenario, in this sense, is the eigenstate thermalization hypothesis (ETH), conjectured by Deutsch and Srednicki [35, 36] in the context of quantum chaotic systems [37]. The main idea is that thermalization is encoded in the eigenstates, i.e., the expectation value of a few-body observable $\mathcal{O}$ on an eigenstate $|\psi_\alpha\rangle$ of the Hamiltonian of a large, interacting many-body system is equal to the microcanonical average of $\mathcal{O}$ at the corresponding energy E_α. The expectation value $\langle \psi_\alpha | \mathcal{O} | \psi_\alpha \rangle$ is a smooth function of its energy E_α, being essentially constant on each microcanonical energy shell. This would lead to thermalization for every initial condition sufficiently narrow in energy. Although an experimental observation still lacks, the ETH has been numerically studied in many different systems, such as hard-core bosons [38–43], spinless fermions [43, 44], spin chains [45–47], and the Bose-Hubbard model [47].

As discussed in literature [48], even though the majority of the eigenstates leads to the microcanonical average, the possible existence of rare states for which this does not happen could prevent thermalization. As a consequence, two possible interpretations of the ETH were proposed: the strong one states that in the thermodynamic limit all states verify ETH [38]; the weak one states that initial conditions are spread in configuration space in such a way that in the thermodynamic limit rare states never give a contribution [48]. The weak version of the ETH does

not imply thermalization since the overlap of these rare nonthermal states with the initial condition could be large. Even if rare nonthermal states may be responsible of the lacking of thermalization in some known cases [49–51], what is the correct interpretations is not clear yet.

1.3 Integrable systems and the generalized Gibbs ensemble

In classical systems, the concept of integrability is well-defined by the existence of a full set of constants of motion which leads to nonergodic behavior and thus prevents thermalization.

The generalization of the notion of integrability to the quantum case is still a subject of debate. Among the different definitions applied in literature, there are the existence of a complete set of local conserved linearly or algebraically independent operators, the integrability by Bethe ansatz, or the occurrence of nondiffractive scattering [52, 53]. Even though a clear definition of integrability lacks, also for quantum systems described by a short-range interacting Hamiltonian the existence of an extensive number of local conserved quantities is expected to preclude thermalization.

Nonetheless, one may ask if expectation values of local observables relax to a well-defined steady state and, if so, how to predict such expectation values. As in the works by Jaynes on maximum entropy [54, 55], assuming that a relaxed state exists, it can be described by the density matrix of the generalized Gibbs ensemble (GGE) [56]

$$\rho_{\mathrm{GGE}} = \frac{1}{Z} \exp\left(- \sum_n \lambda_n \mathcal{I}_n \right), \tag{1.4}$$

where $\{\mathcal{I}_n\}$ is the full set of conserved quantities, $Z = \mathrm{Tr}\left[\exp\left(-\sum_n \lambda_n \mathcal{I}_n\right)\right]$ is the generalized partition function, and $\{\lambda_n\}$ are Lagrange multipliers fixed by requiring that

$$\langle \Psi_0 | \mathcal{I}_n | \Psi_0 \rangle = \mathrm{Tr}\left(\rho_{\mathrm{GGE}} \mathcal{I}_n\right), \tag{1.5}$$

being $|\Psi_0\rangle$ the initial state. The GGE is fundamentally different from thermal ensembles because it retains memory about the initial state through the values of the Lagrange multipliers.

Motivated by the aforementioned experiment on one-dimensional Bose gases [30], Rigol et al. [56] investigated the dynamics of hard-core bosons (the lattice analogue

of the Tonks-Girardeau gas [57]) through an ab initio numerical study. The authors found that the system can undergo relaxation to an equilibrium state, whose properties are well described by the GGE. Furthermore, they studied the time evolution of the momentum distribution initially split into four peaks, a setting very similar to that of the experiment. They showed that even after a very long propagation time, the characteristic peaks remained well resolved and interpreted this result as a consequence of the memory of the initial distribution stored in the GGE that prevents the peaks from overlapping.

GGE's predictions were mostly studied in models which can be mapped to free bosonic or fermionic theories [58–65], where the conserved charges are given by the mode occupation numbers. A paradigmatic example is the Luttinger model [66, 67], which exhibits bosonic quasiparticles. In Refs. [63, 64], the evolution of the correlations of this system after a sudden interaction switching was analytically studied. In the infinite-time limit, equal-time correlations relaxed algebraically towards a stationary state well described by GGE, which assigns a momentum-dependent temperature to each eigenmode.

More recently, also genuinely interacting integrable systems such as the Lieb-Liniger model [68–70], the Heisenberg XXZ spin chain [71–73], or field theories [74–76] were examined. In particular, Kormos et al. [70] provided exact analytical results for a quench in the Lieb-Liniger model from free bosons to hard-core bosons (which map to free fermions). Although the quench is between two free theories, the pre- and postquench mode operators are not linearly related. The authors computed the time evolution of the dynamical density-density correlation function: remarkably, its stationary value was still described by a GGE.

Some studies, however, question the validity of the GGE [77], and even indicate the failure of its predictions, especially in the interacting case [78–84]. For example, a quench in the spin-1/2 Heisenberg XXZ chain from a dimer product or Néel initial state was studied in Refs. [82, 83]. The long-time limit of various local spin-spin correlation functions was found to be significantly different from predictions based on the GGE, which therefore can not give a complete description, even of local observables.

1.4 Prethermalization

If we assume that an isolated quantum systems can thermalize, the next important question is how thermalization occurs. Indeed, the relaxation can be highly

nontrivial and require different stages related to different time scales: the system approaches an intermediate quasisteady state at short times, before decaying towards the thermal equilibrium state on much longer time scales. This phenomenon, called prethermalization, was predicted and experimentally studied in many different systems [19, 85–102].

The two-step mechanism was first suggested by Berges et al. [85] to describe the collision products in heavy-ion collisions, and later discussed in the context of low-energy physics. One of the first studies in this sense is that of Moeckel et al. [88], who investigated a sudden interaction-quench in a fermionic Hubbard model at half filling, starting in the ground state of the noninteracting system. The analysis, based on the flow equation method at second order in perturbation theory in the interaction strength, focused on the momentum distribution function and identified a short time regime, where quasiparticles were formed and the Fermi energy discontinuity in the momentum distribution reduced, followed by a quasisteady prethermalized state resembling a zero-temperature Fermi liquid, which had eventually to give up to a genuine thermal state if higher order corrections were kept into account. Evidences of a prethermalization regime were also found by Eckestein et al. [91], who numerically simulated through dynamical mean-field theory (DMFT) a sudden interaction-quench in the infinite-dimensional half-filled fermionic Hubbard model. In particular, at interaction values safely low to exclude any influence by the Mott transition, the authors found that the momentum distribution jump at the Fermi energy, after a plateau compatible with prethermalization of Ref. [88], started a steady decrease at longer times. Unfortunately, the affordable simulation time was too short to ascertain whether the jump indeed relaxed to zero as expected by thermalization. Studying the same problem, Stark et al. [97] employed the prethermalized state as initial condition to integrate a Boltzmann kinetic equation for the momentum distribution function, on the assumption that Wick's theorem holds for quasiparticles at sufficiently low interaction strength. The solution indeed flowed to a thermal distribution, which is unsurprising given those premises. Therefore, even though the general expectation is that thermalization should take place at sufficiently long times, there are not conclusive evidences in support. A recent attempt in this sense was done by Bertini et al. [101]. The authors focused on a one-dimensional spinless fermion model with weak interaction U and analyzed the system using equation of motion techniques. Tuning properly the value of the hopping amplitudes, they found a crossover between a prethermalized regime and a thermal steady state for local observables. The observed drift in time of the

single-particle Green's function towards thermal values was compatible with an exponential decay and characterized by a relaxation time proportional to U^{-2}. On short and intermediate time scales they benchmarked their method against t-DMRG computations and found it to be very accurate for weak interactions.

In the specific case of a quench that weakly breaks integrability, the phenomenon of prethermalization could establish a continuous connection between the relaxation behavior of integrable and nearly integrable systems, as proposed in Refs. [93, 99]. Indeed, nonthermal steady states attained by integrable systems and prethermalized states in which nearly integrable systems are trapped are both due to the existence of constants of motion, which are exact in the former case and approximate in the latter. These approximately conserved charges can be constructed through unitary perturbation theory [103, 104] and are employed to define the corresponding "deformed" GGE, which describes the prethermalization plateau. Thus, the relaxation dynamics of integrable and nearly integrable systems is described by the same statistical theory and nonthermal steady states of integrable theories can be regarded as prethermalized states that never decay. This interpretation can also be useful to explain why integrable models well describe the experimental systems, which are always nearly integrable realizations. Indeed, what is experimentally accessible is the prethermalization regime dominated by the integrable term of the Hamiltonian.

In this regard, let us go back to the aforementioned experimental observation of prethermalization [19–22]. The authors prepared and trapped a one-dimensional Bose gas of ^{87}Rb atoms in the quasicondensate regime. By rapidly transforming the initial radial harmonic confinement into a double well, this initial single gas was coherently split into two uncoupled gases with identical longitudinal phase profiles up to quantum noise; on the contrary, two independently created quasicondensates would have had different and uncorrelated phase profiles. The system was let evolve in the double well for a varying duration t_e before all trapping potentials were switched off and the gases allowed to expand. The resulting matter wave interference pattern was imaged (Figure 1.4(a)), revealing information about the fluctuating local relative phase field $\phi(z)$ between the two halves of the system. In order to quantitatively capture the dynamics of the relative phase and thus of the nonequilibrium system, they integrated the interference pattern longitudinally over a variable length L and extracted from the resultant line profile the integrated interference contrast $C(L, t_\mathrm{e})$. The mean squared contrast $\langle C^2(L, t_\mathrm{e})\rangle$ reported in Figure 1.4(a) is a direct measure of the integrated two-point correlation function of

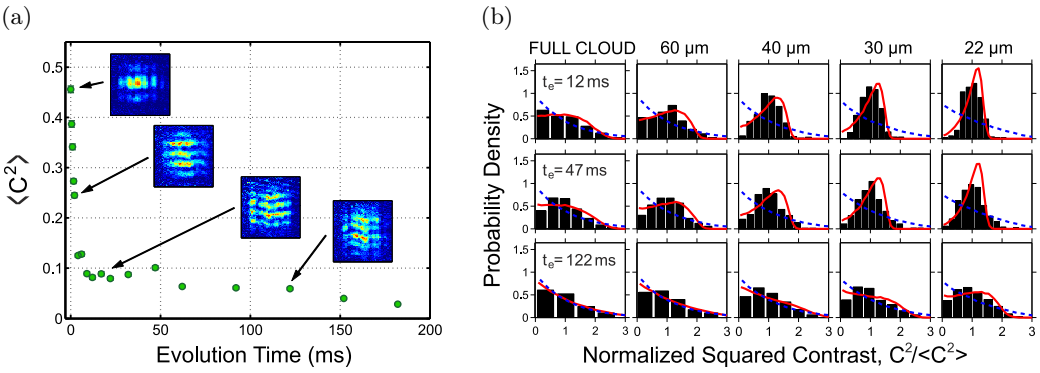

Figure 1.4: (a) Time evolution of the mean squared contrast for interference patterns integrated over the whole length of the system and some typical experimental images. Figure adapted from [22]. (b) Experimental nonequilibrium distributions of $C^2/\langle C^2\rangle$ at different evolution times (histograms), shown together with the respective best fitting equilibrium distributions at temperature T_{eff} (red solid lines). For comparison, the equilibrium distributions at the initial temperature $T = 78 \pm 10$ nK are added (blue dashed lines). Figure adapted from [22].

the relative phase. It exhibits an initial rapid decay on a time scale of ~ 10 ms, that is much faster than the one expected for thermalization, which should be very slow in one-dimensional Bose gases [30, 105]. After this rapid decay, a quasisteady state appears, which slowly evolves on a much slower time scale. To reveal the nature of such a quasisteady state, they measured the full probability distribution of the contrast, which contains information about all higher-order even relative-phase correlation functions. As shown in Figure 1.4(b), for long integration lengths the distributions exponentially decay, reflecting the decay of coherence, while for short integration lengths a peaked Gumbel-like distribution emerges, revealing that some coherence from the initial state still remains in the system. In contrast, for the thermal equilibrium case in the same temperature range of the system, the distributions exponentially decay for all length scales. From this strong difference, one can conclude that the quasisteady state is not the thermal equilibrium state of the system. However, it still shows thermal properties: after the initial decay, the authors found an excellent agreement between the experimental data and the theoretical equilibrium distribution at an effective temperature $T_{\text{eff}} \sim 14$ nK (slowly increasing in time), which is remarkably lower than the temperature of the unsplit gas ($T = 78 \pm 10$ nK).

The results of this experiment can be understood using the integrable Tomonaga-

Luttinger theory [102, 106], whose Hamiltominan reads

$$\mathcal{H} = \frac{\hbar c}{2} \int \left[\frac{K}{\pi} \left(\nabla \hat{\phi}(z) \right)^2 + \frac{\pi}{K} \hat{n}^2(z) \right] \mathrm{d}z, \tag{1.6}$$

where c is the sound velocity, K is the Luttinger parameter characterizing the strength of the interaction, and the operators $\hat{\phi}(z)$ and $\hat{n}(z)$ represent the relative phase and the relative density, respectively. The rapid evolution of the system in the first milliseconds corresponds to the dephasing between the different k-modes that diagonalize the Hamiltonian, due to their different k-dependent oscillation frequencies. The model also predicts a steady state to which the integrable system will relax and allows to assign an effective temperature to the system that is in good agreement with the experimental result. Thus, the experiment revealed the emergence of a prethermalized state, well described by the steady state of an integrable Hamiltonian. Moreover, a recent experiment [107] studied in detail higer-order correlation functions and obtained direct experimental signatures of the emergence of a GGE in the prethermalized state. Hamiltonian (1.6), however, can not describe the thermalization process, which would require to include interactions of particles that go beyond two-body scattering, such as three-body collisions. The experimental system is expected to reach full thermalization, but on time scales much longer than the dephasing. This fact allows the clear observation of the dynamics dominated by the integrable Hamiltonian.

Despite the fact that prethermalization was established to occur in several different models and, most notably, observed in experiments, there are still many open questions: even though this phenomenon seems to be characterized by the presence of different time scales, it is not clear in general which are the scales that control the various steps, neither under which conditions prethermalization takes place.

1.5 Dynamical phase transitions

One of the intriguing questions concerning nonequilibrium quantum dynamics is whether there exist universal phenomena generalizing the ones of equilibrium systems. Among the intriguing features related to the emergence of prethermalized states there is the opportunity to observe genuine dynamical critical effects such as dynamical phase transitions, i.e., transitions in the steady state where the relaxation behavior qualitatively changes.

This kind of transitions was first discussed by Eckstein et al. [91] who studied

the evolution of the half-filled fermionic Hubbard model using DMFT. The authors considered a sudden quench in the interaction strength U for a system initially prepared in the noninteracting ground state and studied the double occupation and the discontinuity of the momentum distribution at the Fermi energy. They established the existence of a prethermalized quasistationary state on intermediate time scales, both in the weak- and strong-coupling regime, and observed a sharp crossover at $U_c^{\mathrm{dyn}} = 0.8$ in units of the bandwidth, indicating a dynamical phase transition. In particular, for $U < U_c^{\mathrm{dyn}}$ the double occupation relaxed to its thermal value, while the Fermi surface discontinuity was trapped in a prethermalized plateau before starting a slow decrease. For $U > U_c^{\mathrm{dyn}}$, instead, both quantities exhibited damped collapse-and-revival oscillations not centered around the respective thermal values, revealing the presence of a prethermalization regime also at strong coupling. These two regimes were separated by a small region around $U_c^{\mathrm{dyn}} = 0.8$ characterized by fast thermalization.

This picture was confirmed by means of a variational approach based on a time-dependent Gutzwiller ansatz [108]. The authors distinguished two regimes in the real-time dynamics, depending on the final interaction strength, separated by a critical line at which mean-field dynamics exhibited exponential relaxation. Moreover, the long-time average of the double occupancy and of the quasiparticle residue had a singular behavior, vanishing as the inverse of a logarithm approaching the dynamical critical point. However, the suppression of quantum fluctuations, which is at the ground of this mean-field approach, prevented true relaxation. In order to investigate the role of quantum fluctuations on the nonequilibrium mean-field dynamics, Sandri et al. [109] developed a self-consistent treatment that goes beyond the Gaussian theory. They found that a dynamical transition was still present and that, as expected, approaching the critical region the dynamics of local observables was driven towards stationarity.

Evidences of dynamical phase transitions were later found by means of DMFT [110, 111], in a variety of mean-field models [112–115], and in field theories [116–119].

A recent attempt to go beyond mean-field was done by Sciolla et al. [117]. The authors studied the quantum $O(N)$ model in the large-N limit, retaining fluctuations at the leading order in the self-consistent $1/N$ expansion, and considered sudden quenches starting in the broken-symmetry phase. The numerical analysis of the subsequent evolution showed that the system always reached a steady state at long times, which was nonthermal since at the leading order in $1/N$ there is still an infinite number of conserved quantities preventing thermalization. They observed

the presence of a dynamical transition induced by the quench and signaled by a power-law vanishing asymptotic value of the order parameter, and the existence of diverging time and length scales approaching such transition. Studying the same model, Smacchia et al. [118] discussed a characterization of the dynamical phase transition based on the full statistics of excitations generated in a double quench. In particular, they suggested that the transition can be detected by studying qualitatively how the fluctuations in the number of excitations grow in time.

However, many aspects are still unclear: whether and how dynamical phase transitions are related to the existence of an underlying equilibrium phase transition [120, 121], what their nature is, and how to distinguish them from thermal critical phenomena are issues to be clarified.

1.6 Brief summary and plan of the Thesis

In the previous Sections we reviewed some of the issues concerning quantum nonequilibrium phenomena addressed in the recent literature. From this overview emerges that many problems are still open and controversial. In the following we investigate a few of them.

Chapter 2: Absence of thermalization in a Fermi liquid

In this Chapter we report two results that question the common expectation of thermalization in a Landau-Fermi liquid after an interaction quench. We first consider the perturbative expansion in the interaction strength of the long-wavelength structure factor $S(\mathbf{q})$ and show that it does not satisfy the hypothesis that steady-state averages correspond to thermal ones. In particular, $S(\mathbf{q})$ has an analytical component $\sim$ const. $+ O(q^2)$ for $\mathbf{q} \to \mathbf{0}$, compatible with thermalization, but it retains also a nonanalytic term $\sim |\mathbf{q}|$ characteristic of a Fermi liquid at zero-temperature. In real space, this nonanalyticity turns in a power-law decay of the density-density correlations, in contrast with the exponential decay associated to thermalization. We next analyze the low-density case, where one can obtain results valid at any order in interaction but at leading in the density, and find that in the steady state the momentum distribution jump at the Fermi surface is strictly finite, though smaller than at equilibrium.

This Chapter is based on

- A. Maraga, A. Silva, and M. Fabrizio, Phys. Rev. B **90**, 155131 (2014).

Chapter 3: Nonadiabatic stationary behavior in a driven Ising chain

In this Chapter we discuss the emergence of a nonadiabatic behavior in the dynamics of the order parameter in a low-dimensional system subject to a linear ramp of one of its parameters within a gapped phase, which should be the most favorable situation for an adiabatic evolution. We study in details the dynamics of the spontaneous magnetization $m^x(t)$ in a quantum Ising chain after a linear variation in time of the transverse field within the ordered phase. In particular, focusing on the value of the order parameter at the end of the ramp $m^x(\tau)$, we show that the smaller the switching rate of the transverse field is the closer $m^x(\tau)$ gets to its ground state value. Nonetheless, this apparently small correction to adiabaticity eventually leads to the disruption of the order exponentially fast in the subsequent time evolution, no matter how slowly the ramp is performed.

This Chapter is based on

- A. Maraga, P. Smacchia, M. Fabrizio, and A. Silva, Phys. Rev. B **90**, 041111 (2014).

Chapter 4: Aging and coarsening in isolated quantum systems after a quench

This Chapter analyzes the nonequilibrium dynamics of an isolated quantum system after a sudden quench to the dynamical critical point, where the emergence of scaling and universal exponents is expected, due to the absence of time and length scales. We explore these features for a bosonic interacting scalar field theory with $O(N)$ symmetry in the large-N limit, where the model is exactly solvable and the exponents and scaling forms of the relevant two-time correlation functions can be analytically calculated. Moreover, we provide evidence of the emergence of a dynamical scaling behavior also for quenches below the dynamical critical point, associated with coarsening. We find that the latter case is characterized by the same scaling functions as those describing the critical case, yet with different exponents.

This Chapter is based on

- A. Maraga, A. Chiocchetta, A. Mitra, and A. Gambassi, arXiv:1506.04528 (2015). Accepted for publication in Phys. Rev. E.

Chapter 5: Dynamical transitions and statistics of excitations

In this Chapter we study the dynamics of the $O(N)$ model (introduced in the previous Chapter) resulting from a different protocol: a linear ramp of one of its parameters. We find that the presence of a dynamical phase transition, as well as its critical properties, are robust against the change of the protocol. We show that a characterization based on the critical dimensions and exponents would suggest that the dynamical phase transition is analogous to the equilibrium thermal one. However, its nonequilibrium nature becomes evident analyzing the statistics of excitations produced in the ramp process. In particular, the critical properties are encoded in the fluctuations in the number of excitations, which display qualitatively different behaviors depending on the ramp being performed above, at, or below the dynamical critical point. These behaviors bear no dependence on the duration of the protocol.

This Chapter is based on a manuscript still in preparation.

Chapter 2

Absence of thermalization in a Fermi liquid

Landau's Fermi-liquid theory [122, 123], one of the milestones in the quantum theory of many-body systems, explains why interacting fermions almost always display thermodynamic and transport properties similar to those of noninteracting particles, which is, e.g., the reason of success of the Drude-Sommerfeld description of normal metals in terms of free electrons.

In the original paper [122], Landau developed semiphenomenologically his Fermi-liquid theory by postulating that the low-lying eigenstates of interacting fermions are in one-to-one correspondence to those of free fermions, namely that, if interaction is slowly turned on, the noninteracting low-energy eigenstates *adiabatically* evolve into the fully interacting ones. Since the former are Fock states labeled by occupation numbers $n_{\mathbf{k}\sigma}$ in momentum and spin space, the same labeling can be maintained also for the fully interacting eigenstates, in which case $n_{\mathbf{k}\sigma}$ refer to the so-called quasiparticles.

Such an adiabatic assumption might at first sight seem unjustified because of the absence of an energy gap in the spectrum. However, even though the single-particle spectrum of a normal Fermi gas is gapless, the density of states of particle-hole pairs, which are the only excitations generated in the process of switching interaction on, is actually power-law vanishing at low energy and in more than one dimension. This sort of pseudogapped behavior, though it does not rigorously prove the validity of adiabatic continuation, at least makes the latter less unlikely.

The past few years have witnessed a growing interest in quantum nonequilibrium phenomena. Among the issues under discussion, one of the most important is

whether a macroscopic but isolated quantum system can serve as its own dissipative bath. Imagine that such a system is initially supplied with an extensive excess energy and then let evolve until it relaxes to a steady state. As discussed in Sec. 1.2, should quantum ergodicity hold, the steady-state values of local observables would coincide with thermal averages at an effective temperature T_* such that the internal energy coincides with the initial one, which is conserved during the unitary evolution. The problem under discussion is when and how the above *thermalization hypothesis* holds.

In the specific case of a Landau-Fermi liquid, it is reasonable to expect that thermalization does take place because of the continuum of gapless excitations that can efficiently dissipate and redistribute the excess energy. It is, however, evident that thermalization after an interaction quench is not fully compatible with the aforementioned Landau's adiabatic assumption. In fact, if the interaction is turned on in a finite time τ, however long, the final-state energy differs from the ground state one by an extensive amount. Should thermalization indeed occur, such a finite energy density would translate into a finite temperature $T_* \neq 0$. A Landau-Fermi liquid is however very peculiar: it can be regarded as a *quantum critical state* where all equal-time correlation functions decay as a power-law in the distance at zero temperature and exponentially at any finite $T \neq 0$. This would imply that, no matter how large τ is, if thermalization holds the initial noninteracting Fermi sea will *never* evolve into the interacting ground state.

Therefore thermalization in a Landau-Fermi liquid is not as trivial as one could have envisaged, and indeed this issue is still open and controversial.

In this Chapter, we study an interaction quench in a three-dimensional Fermi gas. We first show that, under some general assumptions on time-dependent perturbation theory, the perturbative expansion of the long-wavelength structure factor $S(\mathbf{q})$ is not compatible with the hypothesis that steady-state averages correspond to thermal ones. In particular, $S(\mathbf{q})$ does develop an analytical component $\sim$ const. $+ O(q^2)$ at $\mathbf{q} \to \mathbf{0}$, as implied by thermalization, but, in contrast, it maintains a nonanalytic part $\sim |\mathbf{q}|$ characteristic of a Fermi liquid at zero-temperature. In real space, this nonanalyticity corresponds to persisting power-law decaying density-density correlations, whereas thermalization would predict only an exponential decay. We next consider the case of a dilute Fermi gas, where one can obtain nonperturbative results in the interaction strength but at leading order in the density. We find that in the steady state the momentum distribution jump at the Fermi surface remains finite, though smaller than in equilibrium, up to second order in $k_F f_0$,

where f_0 is the scattering length of two particles in the vacuum. Both results question the emergence of a finite length scale in the quench dynamics as expected by thermalization.

2.1 Consequences of thermalization for a weak quench

Let us start our analysis by formulating a general criterion to test the occurrence of thermalization. Hereafter, we shall deal with the specific example of a three-dimensional Fermi-Hubbard model $\mathcal{H}(t) = \mathcal{H}_0 + U(t)\,\mathcal{U}$, with

$$\mathcal{H}_0 = \sum_{\mathbf{k},\sigma} \epsilon_{\mathbf{k}}\, c^\dagger_{\mathbf{k}\sigma} c_{\mathbf{k}\sigma}, \tag{2.1}$$

$$\mathcal{U} = \frac{1}{V} \sum_{\mathbf{k},\mathbf{p},\mathbf{q}\neq\mathbf{0}} c^\dagger_{\mathbf{k}\uparrow} c^\dagger_{\mathbf{p}+\mathbf{q}\downarrow} c_{\mathbf{p}\downarrow} c_{\mathbf{k}+\mathbf{q}\uparrow}, \tag{2.2}$$

where V is the volume and we have removed from $\mathcal{U}$ the $\mathbf{q} = \mathbf{0}$ Hartree term, which refers to conserved quantities. We shall further assume a low electron density $n = N/V \ll 1$, where N is the number of particles, so that it is safe to approximate the dispersion relation with a quadratic form, $\epsilon_{\mathbf{k}} \propto |\mathbf{k}|^2$, and we will always take the thermodynamic limit before every other limit, $V \to \infty$ at constant density n.

The interaction is turned on as

$$U(t) = U\left(1 - \mathrm{e}^{-\varepsilon t}\right), \tag{2.3}$$

with $\varepsilon > 0$ and an interaction strength $U \ll T_F$, where T_F is the Fermi temperature. The expression (2.3) interpolates smoothly between the sudden quench, $\varepsilon \to \infty$, and the adiabatic switching, first send $t \to \infty$ and later $\varepsilon \to 0$.

Imagine that the system is prepared in the noninteracting Fermi sea $|0\rangle$, ground state of $\mathcal{H}_0$ with energy E_0, and let evolve with the full Hamiltonian $\mathcal{H}(t) = \mathcal{H}_0 + U(t)\,\mathcal{U}$, which corresponds to a time-dependent state $|\Psi(t)\rangle$ that satisfies ($\hbar = 1$)

$$i\,\frac{\partial\,|\Psi(t)\rangle}{\partial t} = \mathcal{H}(t)\,|\Psi(t)\rangle\,, \tag{2.4}$$

with $|\Psi(0)\rangle = |0\rangle$. The interaction switching protocol changes the total energy of the system according to

$$\begin{aligned} E_* - E_0 &= \int_0^\infty \mathrm{d}t\ \langle\Psi(t)|\,\frac{\partial\mathcal{H}(t)}{\partial t}\,|\Psi(t)\rangle \\ &\simeq -V\,\frac{U^2}{4}\int\frac{\mathrm{d}^3q}{(2\pi)^3}\iint_0\mathrm{d}\omega\,\mathrm{d}\omega'\ \rho_{\mathbf{q}}(\omega)\,\rho_{-\mathbf{q}}(\omega')\,\frac{\omega+\omega'}{(\omega+\omega')^2+\varepsilon^2}, \end{aligned} \tag{2.5}$$

where the last expression is the leading order correction and $\rho_{\mathbf{q}}(\omega)$ is the noninteracting density of states of particle-hole excitations at momentum transferred $\mathbf{q}$. We note that the energy decreases as always in second-order perturbation theory, which depends from our neglect of the Hartree term.

On the other hand, let us consider the asymptotic $t \to \infty$ Hamiltonian $\mathcal{H}_* = \mathcal{H}_0 + U\,\mathcal{U}$, and the equilibrium internal energy at temperature $T \ll T_F$ ($\beta = 1/T$ taking $k_B = 1$),

$$\begin{aligned} E(T) &= -\frac{\partial}{\partial\beta}\,\ln\left[\mathrm{Tr}\left(\mathrm{e}^{-\beta\mathcal{H}_*}\right)\right] \\ &\simeq E_0 + V\,\frac{\gamma_V}{2}\,T^2 - V\,\frac{U^2}{4}\int\frac{\mathrm{d}^3q}{(2\pi)^3}\iint_0 \mathrm{d}\omega\,\mathrm{d}\omega'\;\frac{\rho_{\mathbf{q}}(\omega)\,\rho_{-\mathbf{q}}(\omega')}{\omega+\omega'}, \end{aligned} \tag{2.6}$$

where γ_V is the specific heat coefficient at constant volume, and we expanded at leading order in $T \sim U \ll T_F$. According to the thermalization hypothesis, the steady state averages of the system should coincide with equilibrium thermal averages at a temperature T_* such that $E(T_*) = E_*$, which through Eqs. (2.5) and (2.6) leads, at leading order in U, to the expression

$$\begin{aligned} T_*(U)^2 &\simeq \frac{U^2}{2\gamma_V}\int\frac{\mathrm{d}^3q}{(2\pi)^3}\iint_0 \mathrm{d}\omega\,\mathrm{d}\omega'\;\rho_{\mathbf{q}}(\omega)\,\rho_{-\mathbf{q}}(\omega') \\ &\qquad\qquad \times\frac{\varepsilon^2}{(\omega+\omega')\left[(\omega+\omega')^2+\varepsilon^2\right]} + O\left(U^3\right) \\ &\equiv U^2\,g(\varepsilon)^2 + O\left(U^3\right), \end{aligned} \tag{2.7}$$

where $g(\varepsilon) \sim \varepsilon$ for small ε and tends to a constant for $\varepsilon \to \infty$. It follows that T_* starts linear in U [97] and vanishes in the adiabatic limit, $T_* \sim \varepsilon \to 0$, as in this case the system must evolve into the ground state of the fully interacting Hamiltonian $\mathcal{H}_*$.

2.1.1 An operating assumption

Let us then consider a generic observable $\mathcal{O}$ with time-dependent average $O(t,U) = \langle\Psi(t)|\,\mathcal{O}\,|\Psi(t)\rangle$. We shall denote as

$$O^{(m)}(t,U) = \frac{\partial^m O(t,U)}{\partial U^m}, \tag{2.8}$$

its Taylor coefficients. Similarly,

$$O_{\mathrm{eq}}(T,U) = \frac{\mathrm{Tr}\left(\mathrm{e}^{-\beta\mathcal{H}_*}\,\mathcal{O}\right)}{\mathrm{Tr}\left(\mathrm{e}^{-\beta\mathcal{H}_*}\right)}, \tag{2.9}$$

defines the thermal average of $\mathcal{O}$ with the asymptotic Hamiltonian $\mathcal{H}_*$ at temperature $T = \beta^{-1}$. If thermalization occurs, then

$$\lim_{t\to\infty} O(t,U) = O_{\rm eq}\left(T_*(U),U\right), \tag{2.10}$$

which also implies that

$$\lim_{U\to 0}\lim_{t\to\infty} O^{(m)}(t,U) = \left[\frac{\mathrm{d}^m O_{eq}\left(T_*(U),U\right)}{\mathrm{d}U^m}\right]_{U=0}, \tag{2.11}$$

where the derivative on the right-hand side (r.h.s.) acts both explicitly and implicitly through $T_*(U)$ of Eq. (2.7). We observe that, while the r.h.s. of Eq. (2.11), which we shall hereafter assume finite for the observable under investigation, can be readily evaluated by equilibrium perturbation theory, the left-hand side (l.h.s.) cannot unless it is possible to exchange the order of limits, i.e.,

$$\lim_{U\to 0}\lim_{t\to\infty} O^{(m)}(t,U) \stackrel{?}{=} \lim_{t\to\infty}\lim_{U\to 0} O^{(m)}(t,U), \tag{2.12}$$

since the r.h.s. is instead accessible by time-dependent perturbation theory. Should Eq. (2.12) be valid, we could evaluate independently both sides of Eq. (2.11) and check if they coincide, hence whether thermalization holds.

We first observe that for Eq. (2.12) to hold it is necessary that $O^{(m)}(t,0)$ does not grow indefinitely when $t\to\infty$. If the latter condition is fulfilled for any m, it is highly probable that Eq. (2.12) is valid, too. However, since it is practically unfeasible to check that $O^{(m)}(t\to\infty,0)$ is nonsingular whatever m is and, moreover, because we will be interested just in the second-order coefficient $m=2$, we shall make the following assumption.

Assumption 1. *If* $\lim_{t\to\infty} O^{(m\leq 2)}(t,0)$ *is finite, then Eq. (2.12) is valid at* $m=2$.

This is not a rigorous statement as singularities for $m>2$ would invalidate the results also at $m=2$. As a matter of fact, such an assumption is implicitly taken in any perturbative calculation, since nobody can ever guarantee that higher order terms are nonsingular making perturbation theory justified. In fact, Eq. (2.12) would be strictly valid should the time-dependent perturbation expansion be convergent or, if asymptotic, Borel summable [124], which is not unlikely to be the case for the Dyson's series of an interacting Fermi gas. In addition, the exchange of the two limits, $t\to\infty$ and $U\to 0$, is expected to hold in the adiabatic limit, i.e., if we subsequently send $\varepsilon\to 0$, which corresponds to the conventional equilibrium perturbation theory, which is believed to be convergent for a three-dimensional Fermi liquid. Therefore, if the exchange of the two limits were not possible but for $\varepsilon\to 0$, that should translate into a singular behavior in ε, which we do not find any trace of within time-dependent perturbation theory.

2.1.2 A clever observable

In order to test the consistency of the thermalization hypothesis, we shall focus on the charge structure factor $S(\mathbf{q})$, i.e., the Fourier transform of the static density-density correlation function $S(\mathbf{r}) = \langle n_{\mathbf{r}}\, n_{\mathbf{0}}\rangle - n^2$, where $n_{\mathbf{r}}$ is the density operator and n its average.

At equilibrium, a three-dimensional Landau-Fermi liquid at zero temperature has equal-time density-density correlations that decay as a power law,

$$S(\mathbf{r}, U, T = 0) \sim \frac{1}{r^4}, \tag{2.13}$$

being $r = |\mathbf{r}|$. However, at any finite temperature $T \neq 0$,

$$S(\mathbf{r}, U, T) \sim \exp\left(-\frac{2\pi T}{v_F}\, r\right), \tag{2.14}$$

decays exponentially, thus revealing the quantum-critical nature of the Fermi-liquid ground state that is spoiled as soon as temperature is turned on. We also mention that Eqs. (2.13) and (2.14) actually hold both in the absence and in the presence of the interaction U, which just affects the prefactors and the Fermi velocity v_F but not the exponent in Eq. (2.13) that is universal and depends only on the dimensionality d, equal 3 in our case. In the language of critical phenomena, we could say that a repulsive interaction is a marginally irrelevant perturbation to the quantum-critical noninteracting Fermi sea, whereas temperature is relevant.

Eqs. (2.13) and (2.14) can be readily derived in the absence of interaction. Here,

$$S_0(\mathbf{r}, T) = n\,\delta_{\mathbf{r},\mathbf{0}} - 2G_0(\mathbf{r}, T)^2, \tag{2.15}$$

with $G_0(\mathbf{r}, T) = \langle c^\dagger_{\mathbf{r}\sigma} c_{\mathbf{0}\sigma}\rangle_0$, which, for $k_F r \gg 1$ reads

$$\begin{aligned} G_0(\mathbf{r}, T) \simeq &- \frac{T k_F}{\pi v_F r \sinh\left(\pi T r / v_F\right)} \\ &\times \left[\cos\left(k_F r\right) - \frac{\pi T}{v_F k_F} \sin\left(k_F r\right) \coth\left(\frac{\pi T r}{v_F}\right)\right], \end{aligned} \tag{2.16}$$

being k_F the Fermi momentum. Thus, $G_0(\mathbf{r}, T)$ decays as r^{-2} at $T = 0$ but exponentially at any $T \neq 0$. As a consequence, the Fourier transform $S_0(\mathbf{q}, T)$ of $S_0(\mathbf{r}, T)$ is nonanalytic when $T = 0$ at $|\mathbf{q}| \to 0$ (as well as at $|\mathbf{q}| \sim 2k_F$),

$$S_0(\mathbf{q}, T = 0) = \frac{k_F^2\, |\mathbf{q}|}{6\pi^2}, \tag{2.17}$$

but turns analytic as soon as $T \neq 0$, specifically,

$$S_0(\mathbf{q} \to \mathbf{0}, T) = 2T\rho_0 + O\left(q^2\right), \tag{2.18}$$

with ρ_0 the single-particle density of states at the chemical potential. For the reasons discussed above, the same change of analytic behavior occurs even for the interacting charge structure factor $S(\mathbf{q}, U, T)$; interaction just modifies the single-particle density of states turning it into the quasiparticle one. In conclusion, the analytic properties of the charge structure factor for $|\mathbf{q}| \to 0$ neatly discriminate between power-law or exponentially decaying correlations in real space (see Appendix 2.A for more details).

Let us move back to our problem of interest. If thermalization indeed holds, according to the above discussion we must conclude that, while the structure factor $S(t, \mathbf{q}, U)$, i.e., the Fourier transform of $S(t, \mathbf{r}, U) = \langle \Psi(t)| \, n_{\mathbf{r}} \, n_{\mathbf{0}} \, |\Psi(t)\rangle - n^2$, initially is equal to $S_0(\mathbf{q}, 0)$, hence nonanalytic, in the steady state,

$$\lim_{t\to\infty} S(t, \mathbf{q}, U) \equiv S_*(\mathbf{q}, U) = S\left(\mathbf{q}, U, T_*(U)\right) \sim 2T_*(U)\rho_0 + O\left(q^2\right), \tag{2.19}$$

is instead analytic. In other words, the analytic properties of $S(t, \mathbf{q}, U)$ should totally change during the time evolution. Within perturbation theory, such an analyticity switch must show up as a singularity in the perturbative expansion. Indeed, if we first expand $S(\mathbf{q}, U, T)$ in U and $T = T_*(U) \sim U$, and only after we take $\mathbf{q} \to \mathbf{0}$, then we would find through Eq. (2.7) that for small $|\mathbf{q}|$,

$$\lim_{U\to 0} \frac{\mathrm{d}^2 S\left(\mathbf{q}, U, T_*(U)\right)}{\mathrm{d}U^2} \simeq \frac{32\pi^2\rho_0^2}{k_F^2} \frac{g(\epsilon)^2}{|\mathbf{q}|} = \lim_{U\to 0} \lim_{t\to\infty} \frac{\partial^2 S(t, \mathbf{q}, U)}{\partial U^2}. \tag{2.20}$$

It follows from Eq. (2.20) that the second-order Taylor coefficient of the steady-state structure factor must be singular as $|\mathbf{q}| \to 0$ if thermalization occurs. This is what we shall try to verify under Assumption 1, which specifically corresponds to approximate

$$S_*(\mathbf{q}, U) \overset{?}{\simeq} S_0(\mathbf{q}, 0) + U \lim_{t\to\infty} \lim_{U\to 0} \frac{\partial S(t, \mathbf{q}, U)}{\partial U} + \frac{U^2}{2} \lim_{t\to\infty} \lim_{U\to 0} \frac{\partial^2 S(t, \mathbf{q}, U)}{\partial U^2}, \tag{2.21}$$

which we caution once more it is not rigorous unless the two limits $U \to 0$ and $t \to \infty$ commute.

2.2 Second-order perturbation theory results

The occurrence of thermalization can thus be readily confirmed by verifying whether the second-order correction to $S(t \to \infty, \mathbf{q}, U)$ is singular as $|\mathbf{q}| \to 0$, a check that can be easily performed if Eq. (2.21) is taken to be valid. This is an elementary though lengthy calculation, which we thoroughly describe in Appendix 2.B. The

outcome is, however, totally unexpected. First of all, we find that the approach to the steady state is perfectly defined within perturbation theory and provided the thermodynamic limit is taken first. For instance, at first order and in the sudden quench limit, $\varepsilon \to \infty$, we find that

$$S(t, \mathbf{q}, U) \simeq S_0(\mathbf{q}, 0) - 4U \iint_0 \mathrm{d}\omega_1 \, \mathrm{d}\omega_2 \; \rho_{\mathbf{q}}(\omega_1) \, \rho_{\mathbf{q}}(\omega_2) \, \frac{1 - \cos\left((\omega_1 + \omega_2)\, t\right)}{\omega_1 + \omega_2}, \quad (2.22)$$

where hereafter momentum and energy are in units of the Fermi momentum k_F and the Fermi energy ϵ_F, respectively. Since for small $|\mathbf{q}|$ and $\omega \leq v_F|\mathbf{q}|$, the particle-hole density of states $\rho_{\mathbf{q}}(\omega) \sim \omega/(v_F|\mathbf{q}|)$, the structure factor remains $\propto |\mathbf{q}|$ at first order in U, and the time-dependent term in Eq. (2.22) vanishes as a power law in $1/t$ for large times. In addition, and more remarkably, we find that in the steady state the second-order corrections are not singular as predicted by thermalization. Specifically and still for $\varepsilon \to \infty$,

$$S_*(\mathbf{q}, U) \sim A(U) + B(U)\, |\mathbf{q}| + O\left(q^2\right), \quad (2.23)$$

where

$$A(U) = 8U^2 \int \frac{\mathrm{d}^3 p}{(2\pi)^3} \iint_0 \mathrm{d}\omega_1 \, \mathrm{d}\omega_2 \; \frac{\rho_{\mathbf{p}}(\omega_1) \, \rho_{\mathbf{p}}(\omega_2)}{(\omega_1 + \omega_2)^2}, \quad (2.24)$$

$$B(U) = \frac{1}{6\pi^2} + O\left(U\right), \quad (2.25)$$

so that in real-space $S_*(\mathbf{r}, U)$ still has a power-law decaying term that coexists with an exponentially vanishing one starting at order U^2. In other words, even though an exponential component arises as expected by thermalization, in contrast to it a power-law component persists in the steady state. We note that $S_*(\mathbf{q}, U) \sim A + B\,|\mathbf{q}|$ may also explains the contradictory one-dimensional results of Ref. [125].

We end by pointing out that the absence of singularities that we find up to second order, hence the apparent breakdown of thermalization, depends crucially on the vanishing particle-hole density of states at small frequency, $\rho_{\mathbf{q}}(\omega) \sim \omega$, which is also the reason why Landau's adiabatic assumption is not unlikely in spite of the gapless spectrum. We believe this is not at all accidental.

2.3 Out-of-equilibrium extension of Galitskii's low-density approach

Going beyond leading order is in general unfeasible but in limiting cases where a consistent re-summation of the perturbative series is possible in terms of expansion

parameters different from interaction. At equilibrium this occurs for instance in a dense Fermi gas with long-range Coulomb forces, or, alternatively, in the dilute limit with short-range interactions, where Galitskii [126] showed that replacing the full interaction vertex with the ladder diagrams in the particle-particle channel provides results valid at any order in interaction but at leading in the density. This was shown to actually correspond to diagonalizing the Hamiltonian in the subspace that includes, besides the Fermi sea, states with spin-singlet pairs of holes and particles, inside and outside the Fermi sphere, respectively [127]. This approximate scheme is in turn close to Anderson's treatment of quantum fluctuation corrections to the BCS mean-field theory of superconductivity [128], which we shall exploit to extend out-of-equilibrium Galitskii's theory. Indeed, let us suppose that quantum fluctuations brought by interaction do not spoil completely the noninteracting Fermi sphere, which we shall regard as the *vacuum* of the quantum fluctuations, hypothesis to be verified *a posteriori*. We observe that

$$\left[c^\dagger_{\mathbf{k}\uparrow}c^\dagger_{-\mathbf{k}+\mathbf{q}'\downarrow}, c_{-\mathbf{p}+\mathbf{q}\downarrow}c_{\mathbf{p}\uparrow}\right] = -\delta_{\mathbf{k},\mathbf{p}}c_{-\mathbf{k}+\mathbf{q}\downarrow}c^\dagger_{-\mathbf{k}+\mathbf{q}'\downarrow} + \delta_{-\mathbf{k}+\mathbf{q},-\mathbf{p}+\mathbf{q}'}c^\dagger_{\mathbf{k}\uparrow}c_{\mathbf{k}+\mathbf{q}'-\mathbf{q}\uparrow}, \quad (2.26)$$

has a finite value on the Fermi sea only if $\mathbf{k} = \mathbf{p}$ and $\mathbf{q} = \mathbf{q}'$, in which case is either $+1$ or -1 depending whether $\mathbf{k}$ and $-\mathbf{k}+\mathbf{q}$ are both inside or outside the Fermi sea, respectively. In the same spirit as, e.g., bosonization, we approximate the r.h.s. of Eq. (2.26) by its average value on the Fermi sphere. Therefore, we associate to the pair creation operator $c^\dagger_{\mathbf{k}\uparrow}c^\dagger_{-\mathbf{k}+\mathbf{q}\downarrow}$, where $\mathbf{k}$ and $-\mathbf{k}+\mathbf{q}$ are both outside the Fermi sphere, a hard-core boson creation operator $b^\dagger_{\mathbf{k},\mathbf{q}}$. Seemingly, we associate another independent hard-core boson operator $a^\dagger_{\mathbf{k},\mathbf{q}}$ to $c_{-\mathbf{k}+\mathbf{q}\downarrow}c_{\mathbf{k}\uparrow}$, where now both $\mathbf{k}$ and $-\mathbf{k}+\mathbf{q}$ are inside the Fermi sphere. Since

$$\left[\mathcal{H}_0,\, c^\dagger_{\mathbf{k}\uparrow}c^\dagger_{-\mathbf{k}+\mathbf{q}\downarrow}\right] = \left(\epsilon_{\mathbf{k}} + \epsilon_{-\mathbf{k}+\mathbf{q}}\right) c^\dagger_{\mathbf{k}\uparrow}c^\dagger_{-\mathbf{k}+\mathbf{q}\downarrow}, \quad (2.27)$$

the noninteracting dynamics of the hard-core bosons can be reproduced by mapping

$$\mathcal{H}_0 \to \sum_{\mathbf{q}}\sum_{\mathbf{k}} \omega_{\mathbf{k},\mathbf{q}} \left(a^\dagger_{\mathbf{k},\mathbf{q}}a_{\mathbf{k},\mathbf{q}} + b^\dagger_{\mathbf{k},\mathbf{q}}b_{\mathbf{k},\mathbf{q}}\right), \quad (2.28)$$

where $\omega_{\mathbf{k},\mathbf{q}} = |\epsilon_{\mathbf{k}} + \epsilon_{-\mathbf{k}+\mathbf{q}}| > 0$. In this scheme, the full Hamiltonian $\mathcal{H} = \mathcal{H}_0 + U\,\mathcal{U}$ is thus mapped onto [128]

$$\mathcal{H}_* = \sum_{\mathbf{q}} \mathcal{H}_{\mathbf{q}} = \sum_{\mathbf{q}} \left[\sum_{\mathbf{k}} \omega_{\mathbf{k},\mathbf{q}} \left(a^\dagger_{\mathbf{k},\mathbf{q}}a_{\mathbf{k},\mathbf{q}} + b^\dagger_{\mathbf{k},\mathbf{q}}b_{\mathbf{k},\mathbf{q}}\right) + \frac{U}{V}\sum_{\mathbf{k},\mathbf{p}} \left(b^\dagger_{\mathbf{k},\mathbf{q}} - a_{\mathbf{k},\mathbf{q}}\right)\left(b_{\mathbf{p},\mathbf{q}} - a^\dagger_{\mathbf{p},\mathbf{q}}\right) \right]. \quad (2.29)$$

The vacuum of the hard-core bosons is the Fermi sea, and the role of the interaction, second term on the r.h.s. of Eq. (2.29), is to create pairs of holes and particles out of the vacuum.

We observe that each $\mathcal{H}_{\mathbf{q}}$ in Eq. (2.29) resembles the Hamiltonian of hard-core bosons in the presence of a local potential. We thence foresee that $\langle a^\dagger_{\mathbf{k},\mathbf{q}} a_{\mathbf{k},\mathbf{q}} \rangle \sim \langle b^\dagger_{\mathbf{k},\mathbf{q}} b_{\mathbf{k},\mathbf{q}} \rangle \sim 1/V$. Consequently, we expect it is safe to relax the hard-core constraint, and regard $a_{\mathbf{k},\mathbf{q}}$ and $b_{\mathbf{k},\mathbf{q}}$ as conventional bosons. Within this approximation, which we verified *a posteriori*, it is relatively straightforward to diagonalize Eq. (2.29) (see Appendix 2.C).

The Hamiltonian (2.29) can be exploited to reproduce the dynamical behavior of certain electronic observables following a sudden quench. For instance, the time evolution of the momentum distribution, through the equation of motion $i\,\dot{n}_{\mathbf{k}} = [n_{\mathbf{k}}, \mathcal{H}]$, maps onto

$$n_{\mathbf{k}}(t) \simeq \begin{cases} 1 - \displaystyle\sum_{\mathbf{q}} \langle \Psi(t)|\, a^\dagger_{\mathbf{k},\mathbf{q}} a_{\mathbf{k},\mathbf{q}}\, |\Psi(t)\rangle & \text{if } |\mathbf{k}| \leq k_F, \\ \displaystyle\sum_{\mathbf{q}} \langle \Psi(t)|\, b^\dagger_{\mathbf{k},\mathbf{q}} b_{\mathbf{k},\mathbf{q}}\, |\Psi(t)\rangle & \text{if } |\mathbf{k}| > k_F, \end{cases} \tag{2.30}$$

so that the jump at the Fermi surface is

$$Z(t) \simeq 1 - \sum_{\mathbf{q}} \langle \Psi(t)|\, a^\dagger_{\mathbf{k},\mathbf{q}} a_{\mathbf{k},\mathbf{q}} + b^\dagger_{\mathbf{k},\mathbf{q}} b_{\mathbf{k},\mathbf{q}}\, |\Psi(t)\rangle\,, \tag{2.31}$$

where $|\mathbf{k}|$ is on the Fermi sphere and $|\Psi(t)\rangle$ is the boson vacuum evolved with the Hamiltonian (2.29). Through the exact diagonalization of the latter, assuming a spherical Fermi surface with energy dispersion $\epsilon_{\mathbf{k}} = |\mathbf{k}|^2$, which is indeed appropriate in the low-density limit, we obtain a steady state value of the jump at the Fermi surface $Z_* = Z_{\rm eq} + \delta Z_*$ (see Appendix 2.C), where

$$\delta Z_* = -\frac{(k_F a)^3}{8\pi^2} \int_0^2 q\,\mathrm{d}q \left[\int_0^{q(2-q)} \mathrm{d}\omega\, \left| T\left(-\omega + i0^+, \mathbf{q}\right)\right|^2 \int_0^{} \mathrm{d}\epsilon\, \frac{\mathcal{N}_{\rm OUT}(\epsilon, \mathbf{q})}{(\omega+\epsilon)^2} \right.$$
$$\left. + \int_0^{q(2+q)} \mathrm{d}\omega\, \left| T\left(\omega - i0^+, \mathbf{q}\right)\right|^2 \int_0^{} \mathrm{d}\epsilon\, \frac{\mathcal{N}_{\rm IN}(\epsilon, \mathbf{q})}{(\omega+\epsilon)^2} \right], \tag{2.32}$$

with a the lattice spacing, and $Z_{\rm eq}$ the equilibrium value at zero temperature [126]:

$$Z_{\rm eq} = 1 - \frac{(k_F a)^3}{8\pi^2} \int_0^2 q\,\mathrm{d}q \left[\int_0^{q(2-q)} \mathrm{d}\omega \int_0^{} \frac{\mathrm{d}\epsilon}{\pi}\, \frac{\Im\mathrm{m}\left[T\left(\epsilon - i0^+, \mathbf{q}\right)\right]}{(\omega+\epsilon)^2} \right.$$
$$\left. + \int_0^{q(2+q)} \mathrm{d}\omega \int_0^{} \frac{\mathrm{d}\epsilon}{\pi}\, \frac{\Im\mathrm{m}\left[T\left(-\epsilon + i0^+, \mathbf{q}\right)\right]}{(\omega+\epsilon)^2} \right]. \tag{2.33}$$

The function of complex variable $T(z)$, defined through

$$\begin{aligned} U\,T^{-1}(z,\mathbf{q}) &= 1 - U\,\chi(z,\mathbf{q}) \\ &= 1 + U\int_0 \mathrm{d}\epsilon\,\frac{\mathcal{N}_{\mathrm{IN}}(\epsilon,\mathbf{q})}{z+\epsilon} - U\int_0 \mathrm{d}\epsilon\,\frac{\mathcal{N}_{\mathrm{OUT}}(\epsilon,\mathbf{q})}{z-\epsilon}, \end{aligned} \tag{2.34}$$

is just the usual T matrix, with $\chi(z,\mathbf{q})$ the noninteracting Cooper bubble, $\mathcal{N}_{\mathrm{IN}}(\epsilon,\mathbf{q})$ and $\mathcal{N}_{\mathrm{OUT}}(\epsilon,\mathbf{q})$ the density of states of a pair of holes and particles, respectively, at total momentum $\mathbf{q}$. In particular, if we expand up to second order in U, we find that $1 - Z_* = 2\,(1 - Z_{\mathrm{eq}})$, in agreement with Ref. [88].

Following Galitskii, if $\chi_0(z,\mathbf{q})$ is the Cooper bubble of two electrons in the vacuum, then

$$T(z,\mathbf{q}) \simeq T_0(z,\mathbf{q}) + T_0(z,\mathbf{q})^2\,(\chi(z,\mathbf{q}) - \chi_0(z,\mathbf{q}))\,, \tag{2.35}$$

where $T_0(z,\mathbf{q})$ is the scattering T matrix in the vacuum. Using the first-order expansion of Eq. (2.35) in Eq. (2.32), one consistently obtains a value that is exact at any order in the interaction U, but valid up to second order in $T_0(z \to 0) \sim k_F f_0$, where f_0 is the scattering length of two particles in the vacuum [126].

We thus find that Z_* in the steady state remains strictly finite, though smaller than at equilibrium, at leading order in the density but infinite in U. The simplest interpretation of this result is that the momentum distribution jump does not thermalize at low density at any order in perturbation theory, which is consistent with the previous second-order calculation. Indeed, the discontinuity of $n_{\mathbf{k}}$ at the Fermi surface implies a Friedel-like behavior of the steady-state single-particle density matrix $G_*(\mathbf{r}) = \langle c^\dagger_{\mathbf{r}\sigma} c_{\mathbf{0}\sigma}\rangle_{t\to\infty} \sim \cos(k_F r)/r^2$, at odds with the thermalization prediction of an exponential decay.

Even though the above results are valid at any order in U, still an expansion in the small parameter $k_F f_0$ is assumed. Therefore also in this case in order for the results to be representative of the actual steady-state we have to assume like before that the two limits of $t \to \infty$ and $k_F f_0 \to 0$ commute for the Taylor coefficients of the expansion in powers of $k_F f_0$.

2.4 Concluding remarks

We have presented two separate calculations both of which show that the power-law decay of the equal-time correlations characteristic of a Fermi sea seems to survive the switching of a very weak interaction, even when not adiabatically slow. This contrasts the expectation that the excess energy supplied in the switching process,

when it is not adiabatic, should heat the system hence effectively rise its internal temperature. The common-sense reaction to those results would be they are not valid because time-dependent perturbation theory is unjustified as $t \to \infty$. The argument would be that, even if we have not encountered any singularity as the time $t \to \infty$ up to second order, it is certain that at some higher order a singularity arises invalidating also the second order calculation. We emphasize that should perturbation theory be indeed ill-defined, then a singularity should be accessible in perturbation theory simply because the effective temperature that corresponds to the injected energy is perturbative in the interaction. Therefore, if an exponential decay $\mathrm{e}^{-\gamma t}$ arises, which we do not find evidence for up to second order, the decay rate must be perturbative in the interaction, hence at some high order it must show up through a correction growing linearly with t. Evidently, we cannot exclude this is indeed the case, hence that our second-order calculation does not allow to conclude that thermalization is absent.

Even though a lot of reasonable arguments can be invoked to argue that thermalization must finally take place, nevertheless, there are also counterarguments that one can envisage, some of which we shall list here, which leave open this issue hence worth to be further investigated.

2.4.1 Fermi-liquid many-body spectrum

According to Landau [122, 123], a low excitation energy δE of a Fermi liquid can be parametrized in terms of the deviations $\delta n_{\mathbf{k}\sigma}$ from equilibrium of the quasiparticle occupation numbers at momentum $\mathbf{k}$ and spin σ, and Taylor expanded as

$$\delta E\left[\delta n\right] \simeq \sum_{\mathbf{k},\sigma} \epsilon_{\mathbf{k}\sigma}\, \delta n_{\mathbf{k}\sigma} + \frac{1}{2} \sum_{\mathbf{k},\mathbf{k}',\sigma,\sigma'} f_{\mathbf{k}\sigma,\mathbf{k}'\sigma'}\, \delta n_{\mathbf{k}\sigma}\, \delta n_{\mathbf{k}'\sigma'} + O\left(\delta n^3\right). \tag{2.36}$$

Because of the correspondence between noninteracting and interacting low-energy many-body eigenstates, the entropy of a nonequilibrium quasiparticle population coincides with that of noninteracting particles, which, together with Eq. (2.36), allow to calculate finite temperature properties, which it is well known reproduce the correct thermodynamic behavior of a Fermi liquid for temperature $T \lesssim T_F$. This implies that Eq. (2.36) describes the many-body eigenvalue spectrum over a macroscopic energy interval above the ground state, $\Delta E \lesssim V\, T_F$. Unsurprisingly, the level statistics that corresponds to the energy functional (2.36) has a Poisson distribution [129, 130] characteristic of an integrable system, even though a three-dimensional interacting Fermi gas is supposedly not integrable. It was suggested in

Ref. [131] that a nonintegrable model whose low-energy properties can be described by an integrable effective Hamiltonian, which is the case of a Landau-Fermi liquid, will posses Poisson's level statistics of the low-energy many-body spectrum, while the full many-body spectrum will obviously have a Wigner-Dyson's distribution. If that conjecture were true, it would imply no equipartition of the low-energy density $\ll T_F$ that is injected during the switching process, which might explain our results.

2.4.2 Locality of observables and thermalization

Rigorously speaking, thermalization can be justified only when the Hamiltonian density is local and in reference to local observables. In this situation, one reasonably expects that the reduced density matrix of a subsystem, with the rest of the system playing the role of a dissipative bath, will evolve towards a Maxwell-Boltzmann distribution in the steady state, so that any subsystem observable will indeed thermalize.

On the contrary, long-range correlations are nonlocal observables hence it is not guaranteed they are going to thermalize. Indeed, while the interaction

$$U\,\mathcal{U} = U \sum_{\mathbf{R}} n_{\mathbf{R}\uparrow}\, n_{\mathbf{R}\downarrow}, \tag{2.37}$$

is local in real space, it is infinitely long-ranged in momentum space,

$$U\,\mathcal{U} = \frac{U}{V} \sum_{\mathbf{k},\mathbf{p},\mathbf{q}} c^{\dagger}_{\mathbf{k}\uparrow} c^{\dagger}_{\mathbf{p}+\mathbf{q}\downarrow} c_{\mathbf{p}\downarrow} c_{\mathbf{k}+\mathbf{q}\uparrow}. \tag{2.38}$$

Therefore it is not evident that an observable local in momentum space may thermalize.

Note that the restriction of the notion of thermalization to observables that are local in real space would have no contradiction with our findings and no inconsistency as well with the adiabatic assumption at the basis of Landau's Fermi-liquid theory, since the latter mainly concerns long-wavelength properties. Indeed, the long-wavelength limit of the static structure factor or the momentum distribution close to k_F are, rigorously speaking, not "local observable".

2.4.3 Relevance/irrelevance of interaction at the Fermi-liquid quantum critical point

We mentioned several times that a Fermi sea can be regarded as a quantum critical state of matter. At zero temperature, all equal-time correlations decay as

a power-law in the distance, with universal exponents that depend only on the dimensionality d, while at any finite temperature the decay turns exponential in the distance. From the viewpoint of criticality, a repulsive interaction in $d > 1$ plays the role of a marginally irrelevant perturbation that only changes the prefactors of correlation functions but does not affect the exponent of their power-law decay.

In the language of critical phenomena, one could be tempted to conclude that the noninteracting Fermi sea critical state is stable towards switching a weak repulsion or, more generally, that the Landau-Fermi liquid critical state survives weak changes of the repulsion strength. If thermalization occurred, that statement would be incorrect, since no matter how weak and slow the change of interaction is, a finite temperature will be eventually generated driving the system away from criticality.

The above question whether the irrelevant character of a perturbation with respect to a quantum critical point remains unaltered also when the switching process is not adiabatic is to our knowledge still open [132, 133]. Therefore we cannot exclude that the power-law decay of correlations in a Fermi sea does survive the turning on of a weak repulsion, hence that our results are correct.

Appendix

2.A Remarks on the long-wavelength structure factor

Here we recall the connection between the analytic properties of the long-wavelength structure factor $S(\mathbf{q})$ and the behavior in real space of its inverse Fourier transform, $S(\mathbf{r})$. In three dimensions and assuming space isotropy $S(\mathbf{r}) = S(r)$, we find

$$S(\mathbf{q}) = S(q) = \int \mathrm{d}^3 r \; S(\mathbf{r})\, \mathrm{e}^{-i\,\mathbf{q}\cdot\mathbf{r}} = \frac{4\pi}{q} \int_0^\infty r\,\mathrm{d}r \; S(r) \sin(qr)\,. \tag{2.39}$$

Even though $q = |\mathbf{q}|$ is by definition positive, if we extend artificially the domain of $S(q)$ also to $q \leq 0$, we readily note that $S(q) = S(-q)$ in an even function. Therefore the Taylor expansion of $S(q)$ near $q = 0$ must contain even powers, q^{2n}, and/or odd powers but of the absolute value, $|q|^{2n+1}$. In the latter case, the function $S(q)$, $q \in [-\infty, +\infty]$, is not analytic at the origin (and presumably also at $q = \pm 2k_F$).

Through Eq. (2.39), we observe that, if $S(r)$ vanishes faster than any power of $1/r$ for $r \to \infty$, then only even-order derivatives of $S(q)$ are finite for $q \to 0$; the function is analytic. On the contrary, if $S(r) \sim 1/r^{2m}$ for large r and $m \geq 2$, then the derivative of order $2m-3$ will be finite at $q = 0$, i.e., $S(q)$ will have a nonanalytic behavior $S(q) \sim |q|^{2m-3}$ at small q. In particular, if

$$S(r \to \infty) \sim A\,\mathrm{e}^{-r/\xi} + \frac{B}{r^4}, \tag{2.40}$$

then

$$S(q \to 0) \sim 8\pi\,\xi^3 A - \pi^2 B\,|q| + O\left(q^2\right), \tag{2.41}$$

where A and B are constants. Therefore, even though the term linear in q is subleading with respect to the constant, its inverse Fourier transform corresponds to a power-law decaying contribution, which dominates over the exponentially

vanishing one that derives from the leading constant-in-q term $8\pi\,\xi^3 A$. In other words, what discriminates between a power law with respect to an exponential decay of $S(r)$ for large r is just the finiteness of odd-order derivatives of $S(q)$ at $q = 0$.

2.B Second-order perturbation theory

We consider a Hamiltonian

$$\mathcal{H} = \mathcal{H}_0 + U(t)\,\mathcal{U}, \tag{2.42}$$

where the unperturbed $\mathcal{H}_0$ has eigenstates $|n\rangle$ with eigenvalues E_n, measured with respect to the ground-state energy. We shall assume that $\langle n|\,\mathcal{U}\,|n\rangle = 0$, for any $|n\rangle$, and, in addition, that the Hamiltonian as well as the eigenvalues are real.

We shall here consider a very general turning on of the interaction,

$$U(t) = U\left(1 - \mathrm{e}^{-\varepsilon t}\right), \tag{2.43}$$

with $\varepsilon > 0$, which interpolates between the sudden switch, $\varepsilon \to \infty$, and the adiabatic one, send first $t \to \infty$ and only later $\varepsilon \to 0$. The reason is that, as we shall see, there is not a dramatic difference between the adiabatic $\varepsilon \to 0$ limit and the general case of finite ε, at least up to second order. Since the former is known not to lead to singularities as $t \to \infty$, this suggests the same holds for any $\varepsilon \neq 0$.

We assume that the system is initially in the ground state $|0\rangle$ of $\mathcal{H}_0$, and evolves at positive times with the interacting Hamiltonian (2.42). We study the time evolution by second-order perturbation theory applied directly to the Schrœdinger equation in the interaction representation. Namely, we write the wave function as ($\hbar = 1$)

$$|\Psi(t)\rangle = \mathrm{e}^{-i\mathcal{H}_0 t}\,|\Phi(t)\rangle\,, \tag{2.44}$$

where $|\Phi(0)\rangle = |0\rangle$, and set

$$|\Phi(t)\rangle = \sum_{m\geq 0} U^m\,|\phi_m(t)\rangle\,, \tag{2.45}$$

where m is the order in perturbation theory, being $|\phi_0(t)\rangle = |0\rangle$ and, for any $m > 0$, $|\phi_m(0)\rangle = 0$. It readily follows that

$$i\,\frac{\partial\,|\phi_m(t)\rangle}{\partial t} = \frac{U(t)}{U}\,\mathrm{e}^{i\mathcal{H}_0 t}\,\mathcal{U}\,\mathrm{e}^{-i\mathcal{H}_0 t}\,|\phi_{m-1}(t)\rangle\,, \tag{2.46}$$

which leads to

$$\begin{aligned}
\mathrm{e}^{-i\mathcal{H}_0 t}\,|\phi_1(t)\rangle &= \sum_{n\neq 0}\left(\frac{\mathrm{e}^{-iE_n t}-1}{E_n}-\frac{\mathrm{e}^{-iE_n t}-\mathrm{e}^{-\varepsilon t}}{E_n+i\,\varepsilon}\right)W_{n0}\,|n\rangle \\
&\equiv \sum_{n\neq 0}\Lambda_\varepsilon(E_n;t)\,W_{n0}\,|n\rangle\,, \qquad (2.47)\\
\mathrm{e}^{-i\mathcal{H}_0 t}\,|\phi_2(t)\rangle &= \Bigg\{\sum_{n\neq 0}\Bigg[\frac{1}{E_n^2+\varepsilon^2}-\frac{1}{E_n^2}+\frac{\mathrm{e}^{-iE_n t}}{E_n}\left(\frac{1}{E_n}-\frac{1}{E_n+i\,\varepsilon}\right) \\
&\quad -\frac{\mathrm{e}^{-iE_n t-\varepsilon t}}{E_n-i\,\varepsilon}\left(\frac{1}{E_n}-\frac{1}{E_n+i\,\varepsilon}\right)+\frac{i}{E_n}\left(t-\frac{1-\mathrm{e}^{-\varepsilon t}}{\varepsilon}\right) \\
&\quad -\frac{i}{E_n+i\,\varepsilon}\,\frac{(1-\mathrm{e}^{-\varepsilon t})^2}{2\varepsilon}\Bigg]|W_{n,0}|^2\Bigg\}\,|0\rangle \\
&\quad +\sum_{m\neq 0}\sum_{n\neq 0,m}\Bigg[\frac{1}{E_n}\left(\frac{\mathrm{e}^{-iE_m t}-\mathrm{e}^{-iE_n t}}{E_m-E_n}-\frac{\mathrm{e}^{-iE_m t}-\mathrm{e}^{-iE_n t-\varepsilon t}}{E_m-E_n+i\,\varepsilon}\right) \\
&\quad -\frac{1}{E_n}\left(\frac{\mathrm{e}^{-iE_m t}-1}{E_m}-\frac{\mathrm{e}^{-iE_m t}-\mathrm{e}^{-\varepsilon t}}{E_m+i\,\varepsilon}\right) \\
&\quad -\frac{1}{E_n+i\,\varepsilon}\left(\frac{\mathrm{e}^{-iE_m t}-\mathrm{e}^{-iE_n t}}{E_m-E_n}-\frac{\mathrm{e}^{-iE_m t}-\mathrm{e}^{-iE_n t-\varepsilon t}}{E_m-E_n+i\,\varepsilon}\right) \\
&\quad +\frac{1}{E_n+i\,\varepsilon}\left(\frac{\mathrm{e}^{-iE_m t}-\mathrm{e}^{-\varepsilon t}}{E_m+i\,\varepsilon}-\frac{\mathrm{e}^{-iE_m t}-\mathrm{e}^{-2\varepsilon t}}{E_m+2\,i\,\varepsilon}\right)\Bigg]W_{mn}\,W_{n0}\,|m\rangle \\
&\equiv (A(t)-1)\,|0\rangle+\sum_{m\neq 0}\sum_{n\neq 0,m}\Xi_\varepsilon(E_m,E_n;t)\,W_{mn}\,W_{n0}\,|m\rangle\,, \qquad (2.48)
\end{aligned}$$

with $W_{nm}=\langle n|\,\mathcal{U}\,|m\rangle$.

In the specific case of the Hubbard interaction,

$$\begin{aligned}
\mathcal{H} &= \sum_{\mathbf{k},\sigma}\epsilon_{\mathbf{k}}\,c^\dagger_{\mathbf{k}\sigma}c_{\mathbf{k}\sigma}+\frac{U(t)}{V}\sum_{\mathbf{k},\mathbf{p}}\sum_{\mathbf{Q}\neq\mathbf{0}}c^\dagger_{\mathbf{k}\uparrow}c^\dagger_{\mathbf{p}+\mathbf{Q}\downarrow}c_{\mathbf{p}\downarrow}c_{\mathbf{k}+\mathbf{Q}\uparrow} \\
&= \mathcal{H}_0+U(t)\,\mathcal{U}, \qquad (2.49)
\end{aligned}$$

where the $\mathbf{Q}=\mathbf{0}$ term is not included so to fulfill $W_{nn}=\langle n|\,\mathcal{U}\,|n\rangle=0$, for any $|n\rangle$, the matrix element W_{n0}, where $|0\rangle$ is the unperturbed Fermi sea, is finite only if

$$|n\rangle = c^\dagger_{\mathbf{k}\uparrow}c^\dagger_{\mathbf{p}+\mathbf{Q}\downarrow}c_{\mathbf{p}\downarrow}c_{\mathbf{k}+\mathbf{Q}\uparrow}\,|0\rangle\,, \qquad (2.50)$$

where $|\mathbf{k}|>k_F$ and $|\mathbf{p}+\mathbf{Q}|>k_F$, hence refer to particles, while $|\mathbf{k}+\mathbf{Q}|\leq k_F$ and $|\mathbf{p}|\leq k_F$, hence refer to holes. The energy of this state is $E_n=\omega_{\mathbf{k},\mathbf{k}+\mathbf{Q}}+\omega_{\mathbf{p}+\mathbf{Q},\mathbf{p}}=(\epsilon_{\mathbf{k}}-\epsilon_{\mathbf{k}+\mathbf{Q}})+(\epsilon_{\mathbf{p}+\mathbf{Q}}-\epsilon_{\mathbf{p}})>0$, where energies are measured with respect

to the chemical potential. The matrix element is $W_{n0} = 1/V$. At second order we must account also for states with three and four particle-hole pairs besides those with two.

We write the wave function up to second order as

$$|\Psi(t)\rangle = A(t)\,|0\rangle + |\psi_1(t)\rangle + |\psi_2(t)\rangle\,, \tag{2.51}$$

where $A(t) = 1 + O\left(U^2\right)$, $\langle 0|\psi_1(t)\rangle = \langle 0|\psi_2(t)\rangle = 0$, and

$$|A(t)|^2 + \langle\psi_1(t)|\psi_1(t)\rangle = 1 + O(U^3). \tag{2.52}$$

We are interested in calculating up to second order the average of the structure-factor operator $\mathcal{S}_{\mathbf{q}} = n_{\mathbf{q}} n_{-\mathbf{q}}/V$ at $\mathbf{q} \neq \mathbf{0}$, which reads, through Eqs. (2.47), (2.48), and (2.52),

$$\begin{aligned} S(\mathbf{q},t) \simeq\; & S_0(\mathbf{q}) + (\,\langle\psi_1(t)|\mathcal{S}_{\mathbf{q}}|0\rangle + c.c.\,) + (\,\langle\psi_2(t)|\mathcal{S}_{\mathbf{q}}|0\rangle + c.c.\,) \\ & + \langle\psi_1(t)|\mathcal{S}_{\mathbf{q}} - S_0(\mathbf{q})|\psi_1(t)\rangle \\ =\; & S_0(\mathbf{q}) + U\sum_{n\neq 0} (\,\Lambda^{\star}_{\varepsilon}(E_n;t)\,W_{0n}\,\langle n|\mathcal{S}_{\mathbf{q}}|0\rangle + c.c.\,) \\ & + U^2 \sum_{m\neq 0}\sum_{n\neq 0,m} (\,\Xi^{\star}_{\varepsilon}(E_m,E_n;t)\,W_{0n}\,W_{nm}\,\langle m|\mathcal{S}_{\mathbf{q}}|0\rangle + c.c.\,) \\ & + U^2 \sum_{n,m\neq 0} \Lambda^{\star}_{\varepsilon}(E_m;t)\,\Lambda_{\varepsilon}(E_n;t)\,W_{0m}\,W_{n0}\,\langle m|\mathcal{S}_{\mathbf{q}} - S_0(\mathbf{q})|n\rangle\,, \end{aligned} \tag{2.53}$$

where $S_0(\mathbf{q}) = \langle 0|\mathcal{S}_{\mathbf{q}}|0\rangle$ is the structure factor of the Fermi sea.

The equilibrium perturbation theory can be recovered in the adiabatic limit, which amounts in Eqs. (2.47) and (2.48) to set first $\varepsilon t \to \infty$ and then send $\varepsilon \to 0$. Indeed, in this limit we obtain

$$\Lambda_{\varepsilon\to 0}(E_n; t \gg 1/\varepsilon) = -\frac{1}{E_n}, \tag{2.54}$$

$$\Xi_{\varepsilon\to 0}(E_m, E_n; t \gg 1/\varepsilon) = \frac{1}{E_n\,E_m}, \tag{2.55}$$

which are the well known expansion coefficients at second order and at equilibrium.

Therefore the equilibrium perturbative expansion of the structure factor is

$$\begin{aligned} S_{\rm eq}(\mathbf{q}) &= \lim_{\varepsilon\to 0} S(\mathbf{q}, t \gg 1/\varepsilon) \\ &= S_0(\mathbf{q}) - U \sum_{n\neq 0} \left(\frac{W_{0n}}{E_n} \langle n|\mathcal{S}_{\mathbf{q}}|0\rangle + c.c. \right) \\ &\quad + U^2 \sum_{m\neq 0} \sum_{n\neq 0,m} \left(\frac{W_{0n}\, W_{nm}}{E_n\, E_m} \langle m|\mathcal{S}_{\mathbf{q}}|0\rangle + c.c. \right) \\ &\quad + U^2 \sum_{n,m\neq 0} \frac{W_{0m}\, W_{n0}}{E_m\, E_n} \langle m|\mathcal{S}_{\mathbf{q}} - S_0(\mathbf{q})|n\rangle \,, \end{aligned} \tag{2.56}$$

and we know it does not contain any singular term.

However, we are actually interested in the opposite limit of a sudden switch, which amounts to send $\varepsilon \to \infty$ so that

$$\Lambda_{\varepsilon\to\infty}(E_n; t) = -\frac{1 - \mathrm{e}^{-iE_n t}}{E_n}, \tag{2.57}$$

$$\Xi_{\varepsilon\to\infty}(E_m, E_n; t) = \frac{1}{E_n} \frac{\mathrm{e}^{-iE_m t} - \mathrm{e}^{-iE_n t}}{E_m - E_n} - \frac{1}{E_n} \frac{\mathrm{e}^{-iE_m t} - 1}{E_m}. \tag{2.58}$$

By means of Eqs. (2.53) and (2.56), and observing that all matrix elements are real, we can write the structure factor in the sudden limit as

$$\begin{aligned} S(\mathbf{q}, t) &= S_{\rm eq}(\mathbf{q}) + U \sum_{n\neq 0} \left[\left(\Lambda^{\star}_{\varepsilon\to\infty}(E_n; t) - \Lambda^{\star}_{\varepsilon\to 0}(E_n; t) \right) W_{0n} \langle n|\mathcal{S}_{\mathbf{q}}|0\rangle + c.c. \right] \\ &\quad + U^2 \sum_{m\neq 0} \sum_{n\neq 0,m} \left[\left(\Xi^{\star}_{\varepsilon\to\infty}(E_m, E_n; t) - \Xi^{\star}_{\varepsilon\to 0}(E_m, E_n; t) \right) \right. \\ &\qquad \left. \times W_{0n}\, W_{nm} \langle m|\mathcal{S}_{\mathbf{q}}|0\rangle + c.c. \right] \\ &\quad + U^2 \sum_{n,m\neq 0} \left(\Lambda^{\star}_{\varepsilon\to\infty}(E_m; t)\, \Lambda_{\varepsilon\to\infty}(E_n; t) - \Lambda^{\star}_{\varepsilon\to 0}(E_m; t)\, \Lambda_{\varepsilon\to 0}(E_n; t) \right) \\ &\qquad \times W_{0m}\, W_{n0} \langle m|\mathcal{S}_{\mathbf{q}} - S_0(\mathbf{q})|n\rangle \\ &= S_{\rm eq}(\mathbf{q}) + 2U \sum_{n\neq 0} \frac{\cos(E_n t)}{E_n} W_{0n} \langle n|\mathcal{S}_{\mathbf{q}}|0\rangle \qquad \text{(2.59a)} \\ &\quad + 2U^2 \sum_{m\neq 0} \sum_{n\neq 0,m} \left[\frac{\cos(E_m t) - \cos(E_n t)}{E_n\,(E_m - E_n)} - \frac{\cos(E_m t)}{E_n\, E_m} \right] \\ &\qquad \times W_{0n}\, W_{nm} \langle m|\mathcal{S}_{\mathbf{q}}|0\rangle \qquad \text{(2.59b)} \\ &\quad + U^2 \sum_{n,m\neq 0} \frac{\cos((E_m - E_n)\, t) - \cos(E_m t) - \cos(E_n t)}{E_m\, E_n} \\ &\qquad \times W_{0m}\, W_{n0} \langle m|\mathcal{S}_{\mathbf{q}} - S_0(\mathbf{q})|n\rangle \,. \qquad \text{(2.59c)} \end{aligned}$$

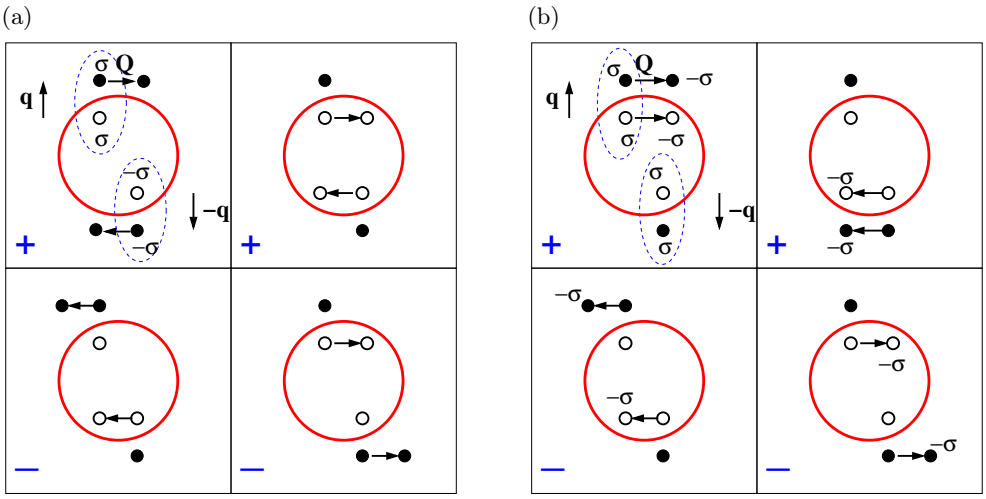

Figure 2.1: (a) Scattering processes that refer to Eq. (2.59b). The circle represents the Fermi sphere, open dots holes and solid ones particles. The initial particle-hole pairs in $|m\rangle$ are encircled and have opposite spins. The scattering process, i.e., the motion of particles/holes, indicated by the arrows, leads to a new state $|n\rangle$. The sign of the process is indicated. (b) Same as Figure 2.1(a) but for initial pairs that have the same spin.

In the thermodynamic limit the second term in Eq. (2.59a) can be written as

$$\delta S^{(1)}(\mathbf{q},t) = 4U \iint_0 \mathrm{d}\omega_1\, \mathrm{d}\omega_2\; \rho_{\mathbf{q}}(\omega_1)\, \rho_{\mathbf{q}}(\omega_2)\, \frac{\cos\left((\omega_1+\omega_2)\, t\right)}{\omega_1+\omega_2}, \tag{2.60}$$

where $\rho_{\mathbf{q}}(\omega)$ is the density of states of a particle-hole excitation at momentum transferred $\mathbf{q}$. The denominator vanishes at small frequencies but this singularity is canceled by the numerator since, for $\omega \ll v_F|\mathbf{q}|$, $\rho_{\mathbf{q}}(\omega) \sim \theta(2k_F - |\mathbf{q}|)\, \omega/(v_F|\mathbf{q}|)$. As a result, in the long time limit Eq. (2.60) vanishes with a power law in $1/t$, so that the steady-state $S_*(\mathbf{q})$ after a sudden quench coincides with the equilibrium $S_{\mathrm{eq}}(\mathbf{q})$ up to first order.

The explicit evaluation of Eqs. (2.59b) and (2.59c) as well as their final expressions are simple though quite lengthy. Therefore we prefer to show graphically all terms that contribute. Their matrix elements have all the same absolute value, equal to $1/V^3$, apart from a sign that is indicated in the Figures.

Let us first consider the term in Eq. (2.59b). The state $|m\rangle$ includes two particle-hole (p-h) pairs at momentum transferred $\mathbf{q}$ and $-\mathbf{q}$ and spin σ and σ'. The intermediate state $|n\rangle$ can be reached by the interaction both from $|m\rangle$ and from $|0\rangle$, hence it contains two p-h pairs with opposite spin and transferred momenta.

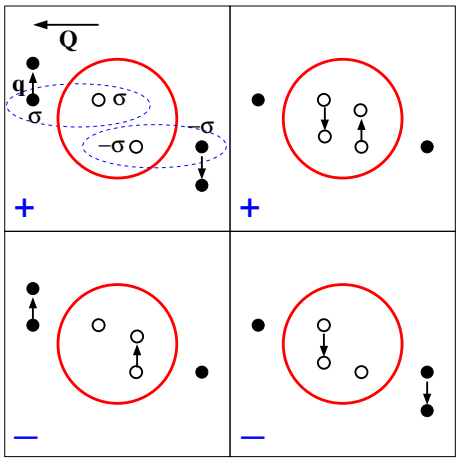

Figure 2.2: Scattering processes that refer to Eq. (2.59c) and are produced by $n_{\mathbf{q}\sigma}n_{-\mathbf{q}-\sigma}$. The initial particle-hole pairs in $|n\rangle$ are encircled and the sign of the process is indicated.

If $\sigma' = -\sigma$, the processes that bring $|m\rangle$ to $|n\rangle$ are shown in Figure 2.1(a). In the figure $|n\rangle$ contains two opposite-spin p-h pairs at momenta $\mathbf{q}+\mathbf{Q}$ and $-\mathbf{q}-\mathbf{Q}$.

If $\sigma = \sigma'$, the interaction must also flip two spins so to lead to two opposite-spin p-h pairs. The processes are shown in Figure 2.1(b) with their signs.

The term in Eq. (2.59c) has contributions whenever two states $|n\rangle$ and $|m\rangle$, each that contains two p-h pairs with opposite spin and momentum, can be connected by $\mathcal{S}_{\mathbf{q}}$. In particular, the processes generated by $n_{\mathbf{q}\sigma}n_{-\mathbf{q}-\sigma}$ are shown in Figure 2.2, where the states $|n\rangle$ and $|m\rangle$ have two p-h pairs at opposite momenta $\pm\mathbf{Q}$ and $\pm(\mathbf{Q}+\mathbf{q})$, respectively.

All processes that are produced by $n_{\mathbf{q}\sigma}n_{-\mathbf{q}\sigma}$ are instead drawn in Figures 2.3(a) and 2.3(b). In particular, the two lower panels of Figure 2.3(a) refer to the case in which $|n\rangle$ has two p-h pairs already at momenta $\pm\mathbf{q}$; the interaction simply shifts rigidly one of the pair in momentum space, in the figure the momentum shift is $\mathbf{K}$.

Finally, Figure 2.3(b) refers to the case in which $|m\rangle = |n\rangle$. Here, for instance, a particle is shifted by $\mathbf{q}$ and then comes back to the initial position.

Since all states that contribute to Eqs. (2.59b) and (2.59c) have two p-h pairs, their linearly vanishing densities of states at low energy compensate the singularity of the denominators. Therefore the sums, which become integral over a continuous spectrum of degrees of freedom, are all convergent. Even more, all terms but one vanish as a power in $1/t$ for large times. In fact, even though in the sense of

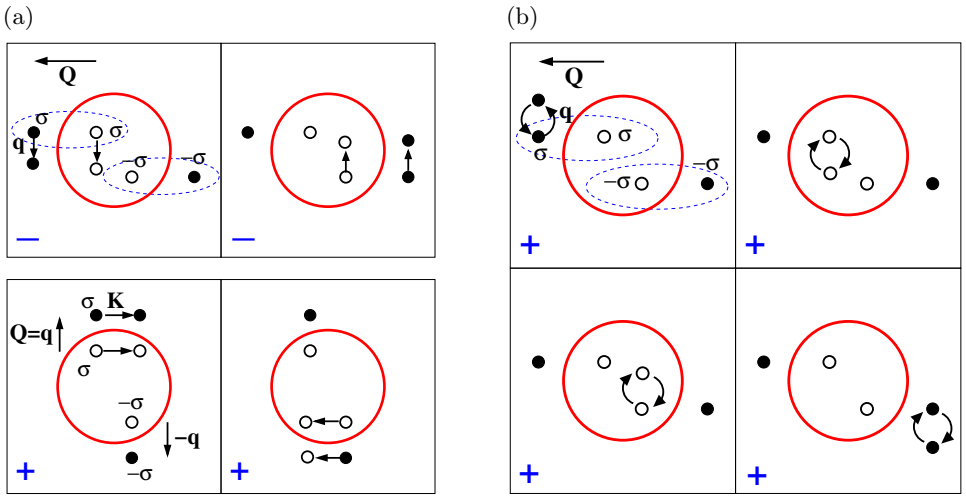

Figure 2.3: (a) Scattering processes that refer to Eq. (2.59c) and are produced by $n_{\mathbf{q}\sigma}n_{-\mathbf{q}\sigma}$. The initial particle-hole pairs in $|n\rangle$ are encircled and the sign of the process is indicated. (b) Same as Figure 2.3(a) but in the case in which $|n\rangle = |m\rangle$.

distributions,

$$\frac{\cos(Et) - \cos(E't)}{E'(E-E')} \xrightarrow{t\to\infty} -\delta(E)\,\delta(E'-E) + O\left(\frac{1}{t}\right), \tag{2.61}$$

$$\frac{\cos((E-E')\,t)}{EE'} \xrightarrow{t\to\infty} \delta(E)\,\delta(E') + O\left(\frac{1}{t}\right), \tag{2.62}$$

those singularities are killed by the vanishing density of states of p-h excitations, leading to a null result for $t \to \infty$.

The only term that actually survives is the one shown in Figure 2.3(b), which corresponds to the case $|n\rangle = |m\rangle$ in Eq. (2.59c). We observe that, if we send $|\mathbf{q}| \to 0$ before taking the limit $t \to \infty$, this term would be canceled by those shown in the upper panels of Figure 2.3(a). This simply reflects the trivial fact the $S(\mathbf{q}=\mathbf{0},t) = 0$. The correct procedure is instead to first reach the steady-state $t \to \infty$, and only after send $|\mathbf{q}| \to 0$. In this way we do find a finite steady-state contribution from Eqs. (2.59b) and (2.59c), which reads

$$\delta S^{(2)}_{*}(\mathbf{q}) = \frac{4U^2}{V^3} \sum_{\mathbf{k},\mathbf{p},\mathbf{Q}} n_{\mathbf{k}}\,\bar{n}_{\mathbf{k}+\mathbf{Q}}\,n_{\mathbf{p}+\mathbf{Q}}\,\bar{n}_{\mathbf{p}} \left[\frac{\bar{n}_{\mathbf{k}+\mathbf{Q}+\mathbf{q}}}{(\omega_{\mathbf{k}+\mathbf{Q},\mathbf{k}} + \omega_{\mathbf{p},\mathbf{p}+\mathbf{Q}})(\omega_{\mathbf{k}+\mathbf{Q}+\mathbf{q},\mathbf{k}} + \omega_{\mathbf{p},\mathbf{p}+\mathbf{Q}})} + \frac{n_{\mathbf{k}-\mathbf{q}}}{(\omega_{\mathbf{k}+\mathbf{Q},\mathbf{k}} + \omega_{\mathbf{p},\mathbf{p}+\mathbf{Q}})(\omega_{\mathbf{k}+\mathbf{Q},\mathbf{k}-\mathbf{q}} + \omega_{\mathbf{p},\mathbf{p}+\mathbf{Q}})} \right], \tag{2.63}$$

where $n_{\mathbf{k}} = \theta(k_F - |\mathbf{k}|)$ is the momentum distribution of the Fermi sea and $\bar{n}_{\mathbf{k}} = 1 - n_{\mathbf{k}}$. If we now take the limit $\mathbf{q} \to \mathbf{0}$, we find a term $\delta S_*^{(2)}(\mathbf{0})$ that is finite plus a correction that starts linear in $|\mathbf{q}|$. Specifically, since $n_{\mathbf{k}}^2 = n_{\mathbf{k}}$,

$$\begin{aligned}\delta S_*^{(2)}(\mathbf{0}) &= \frac{8U^2}{V^3} \sum_{\mathbf{k},\mathbf{p},\mathbf{Q}} \frac{n_{\mathbf{k}}\, \bar{n}_{\mathbf{k}+\mathbf{Q}}\, n_{\mathbf{p}+\mathbf{Q}}\, \bar{n}_{\mathbf{p}}}{(\omega_{\mathbf{k}+\mathbf{Q},\mathbf{k}} + \omega_{\mathbf{p},\mathbf{p}+\mathbf{Q}})^2} \\ &= 8U^2 \int \frac{\mathrm{d}^3 Q}{(2\pi)^3} \iint_0 \mathrm{d}\omega_1\, \mathrm{d}\omega_2\, \frac{\rho_{\mathbf{Q}}(\omega_1)\, \rho_{\mathbf{Q}}(\omega_2)}{(\omega_1 + \omega_2)^2}, \end{aligned} \tag{2.64}$$

and is finite, i.e., not singular. The leading correction to $\delta S_*^{(2)}(\mathbf{0})$ reads

$$\begin{aligned}\delta S_*^{(2)}(\mathbf{q}) - \delta S_*^{(2)}(\mathbf{0}) &= \frac{8U^2}{V^3} \sum_{\mathbf{k},\mathbf{p},\mathbf{Q}} \frac{n_{\mathbf{k}}\, \bar{n}_{\mathbf{k}+\mathbf{Q}}\, n_{\mathbf{p}+\mathbf{Q}}\, \bar{n}_{\mathbf{p}}\, \bar{n}_{\mathbf{k}-\mathbf{q}}}{(\omega_{\mathbf{k}+\mathbf{Q},\mathbf{k}} + \omega_{\mathbf{p},\mathbf{p}+\mathbf{Q}})(\omega_{\mathbf{k}+\mathbf{Q},\mathbf{k}-\mathbf{q}} + \omega_{\mathbf{p},\mathbf{p}+\mathbf{Q}})} \\ &\simeq -|\mathbf{q}|\, \frac{U^2}{4} \int \frac{\mathrm{d}^3 Q}{(2\pi)^3}\, \frac{1}{Q} \\ &\quad \times \int_{\mathrm{Max}[0,Q(Q-2)]}^{Q(2+Q)} \mathrm{d}\omega_1 \int_0 \mathrm{d}\omega_2\, \frac{\rho_{\mathbf{Q}}(\omega_2)}{(\omega_1 + \omega_2)^2} + O\left(q^2\right). \end{aligned} \tag{2.65}$$

Therefore the second-order correction to the coefficient of the nonanalytic term $\propto |\mathbf{q}|$ in the steady-state differs from that at equilibrium.

2.C Diagonalization of the effective Hamiltonian for the p-p and h-h excitations in the low-density limit

In this section, we explicitly diagonalize the Hamiltonian

$$\begin{aligned}\mathcal{H}_* = \sum_{\mathbf{Q}} \mathcal{H}_{\mathbf{Q}} = \sum_{\mathbf{Q}} \Bigg[&\sum_{\mathbf{k}} \omega_{\mathbf{k},\mathbf{Q}} \left(a_{\mathbf{k},\mathbf{Q}}^\dagger a_{\mathbf{k},\mathbf{Q}} + b_{\mathbf{k},\mathbf{Q}}^\dagger b_{\mathbf{k},\mathbf{Q}} \right) \\ &+ \frac{U}{V} \sum_{\mathbf{k},\mathbf{p}} \left(b_{\mathbf{k},\mathbf{Q}}^\dagger - a_{\mathbf{k},\mathbf{Q}} \right) \left(b_{\mathbf{p},\mathbf{Q}} - a_{\mathbf{p},\mathbf{Q}}^\dagger \right) \Bigg], \end{aligned} \tag{2.66}$$

relaxing the hard-core constraint. In Eq. (2.66), $b_{\mathbf{k},\mathbf{Q}}^\dagger$ creates two particles outside the Fermi sea with momenta $\mathbf{k}$, spin $\uparrow$ and $-\mathbf{k} + \mathbf{Q}$, spin $\downarrow$, i.e., $\mathbf{Q}$ is the total momentum of the pair. On the contrary, $a_{\mathbf{k},\mathbf{Q}}^\dagger$ creates two holes within the Fermi sea, one at momentum $\mathbf{k}$, spin $\uparrow$, and the other at momentum $-\mathbf{k} + \mathbf{Q}$, spin $\downarrow$. We recall that $\mathcal{H}_*$ describes the excitations of the Fermi sea brought by the interaction in the dilute limit. Hereafter, we shall use dimensionless units in which momentum is in units of k_F, energy in units of $\epsilon_F = \hbar^2 k_F^2/(2m)$, and time in units of $\hbar/\epsilon_F$. In

addition, the constraint of being outside or inside the Fermi sea will be implicitly hidden in the definition of $b_{\mathbf{k},\mathbf{Q}}$ and $a_{\mathbf{k},\mathbf{Q}}$, respectively.

We start by noting that a pair of holes requires $|\mathbf{Q}| \leq 2$, so that

$$\begin{aligned} H_* = & \sum_{\mathbf{k},\mathbf{Q}:|\mathbf{Q}|\leq 2} \omega_{\mathbf{k},\mathbf{Q}} \left(a^\dagger_{\mathbf{k},\mathbf{Q}} a_{\mathbf{k},\mathbf{Q}} + b^\dagger_{\mathbf{k},\mathbf{Q}} b_{\mathbf{k},\mathbf{Q}} \right) \\ & + \frac{U}{V} \sum_{\mathbf{k},\mathbf{p},\mathbf{Q}:|\mathbf{Q}|\leq 2} \left(b^\dagger_{\mathbf{k},\mathbf{Q}} - a_{\mathbf{k},\mathbf{Q}} \right) \left(b_{\mathbf{p},\mathbf{Q}} - a^\dagger_{\mathbf{p},\mathbf{Q}} \right) \\ & + \sum_{\mathbf{k},\mathbf{Q}:|\mathbf{Q}|>2} \omega_{\mathbf{k},\mathbf{Q}}\, b^\dagger_{\mathbf{k},\mathbf{Q}} b_{\mathbf{k},\mathbf{Q}} + \frac{U}{V} \sum_{\mathbf{k},\mathbf{p},\mathbf{Q}:|\mathbf{Q}|>2} b^\dagger_{\mathbf{k},\mathbf{Q}} b_{\mathbf{p},\mathbf{Q}}. \end{aligned} \tag{2.67}$$

The last two terms are diagonalized by a simple unitary transformation, while the former two by a generalized canonical transformation, which we shall focus on first.

Let us therefore diagonalize H_* in a subspace at fixed $\mathbf{Q}$ such that $Q \leq 2$. For simplicity, we shall drop the label $\mathbf{Q}$. We define the canonical transformation

$$a_{\mathbf{k}} = \sum_{\epsilon} U_{\mathbf{k}\epsilon}\, \alpha_\epsilon + \sum_{\bar{\epsilon}} V_{\mathbf{k}\bar{\epsilon}}\, \beta^\dagger_{\bar{\epsilon}}, \tag{2.68}$$

$$b^\dagger_{\mathbf{k}} = \sum_{\bar{\epsilon}} Z_{\mathbf{k}\bar{\epsilon}}\, \beta^\dagger_{\bar{\epsilon}} + \sum_{\epsilon} W_{\mathbf{k}\epsilon}\, \alpha_\epsilon, \tag{2.69}$$

where $\hat{U}$ and $\hat{Z}$ are square real matrices, while $\hat{V}$ and $\hat{W}$ are still real but, in general, rectangular —the number of holes being much smaller than the number of particles in the low-density limit— satisfying

$$\begin{aligned} U\,U^T - V\,V^T &= I, \qquad & U^T U - W^T W &= I, \\ Z\,Z^T - W\,W^T &= I, \qquad & Z^T Z - V^T V &= I, \\ U\,W^T - V\,Z^T &= 0, \qquad & U^T V - W^T Z &= 0. \end{aligned} \tag{2.70}$$

The inverse transformation then reads

$$\alpha_\epsilon = \sum_{\mathbf{k}} U_{\mathbf{k}\epsilon}\, a_{\mathbf{k}} - \sum_{\mathbf{k}} W_{\mathbf{k}\epsilon}\, b^\dagger_{\mathbf{k}}, \tag{2.71}$$

$$\beta^\dagger_{\bar{\epsilon}} = \sum_{\mathbf{k}} Z_{\mathbf{k}\bar{\epsilon}}\, b^\dagger_{\mathbf{k}} - \sum_{\mathbf{k}} V_{\mathbf{k}\bar{\epsilon}}\, a_{\mathbf{k}}. \tag{2.72}$$

We define the matrix A with elements

$$A_{\mathbf{kp}} = \omega_{\mathbf{k}}\, \delta_{\mathbf{k},\mathbf{p}} + \frac{U}{V}, \tag{2.73}$$

for $|\mathbf{k}| \leq 1$ and $|-\mathbf{k}+\mathbf{Q}| \leq 1$, the matrix B with elements

$$B_{\mathbf{kp}} = \omega_{\mathbf{k}}\, \delta_{\mathbf{k},\mathbf{p}} + \frac{U}{V}, \tag{2.74}$$

for $|\mathbf{k}| > 1$ and $|-\mathbf{k}+\mathbf{Q}| > 1$, and finally the matrix D with elements

$$D_{\mathbf{kp}} = -\frac{U}{V}, \tag{2.75}$$

which couples the interior to the exterior of the Fermi sphere. The interaction U is also measured in units of ϵ_F. With the above definitions, the diagonalization of the Hamiltonian corresponds to the eigenvalue equation

$$\begin{pmatrix} A & D \\ -D^T & -B \end{pmatrix} \begin{pmatrix} U & V \\ W & Z \end{pmatrix} = \begin{pmatrix} U & V \\ W & Z \end{pmatrix} \begin{pmatrix} \epsilon & 0 \\ 0 & -\overline{\epsilon} \end{pmatrix}. \tag{2.76}$$

The solution can be readily found. Specifically, the eigenvalues satisfy

$$1 = \frac{U}{V} \sum_{\mathbf{k}}^{\text{IN}} \frac{1}{\epsilon - \omega_{\mathbf{k}}} - \frac{U}{V} \sum_{\mathbf{k}}^{\text{OUT}} \frac{1}{\epsilon + \omega_{\mathbf{k}}} \equiv U\,\chi(-\epsilon), \tag{2.77}$$

$$1 = \frac{U}{V} \sum_{\mathbf{k}}^{\text{OUT}} \frac{1}{\overline{\epsilon} - \omega_{\mathbf{k}}} - \frac{U}{V} \sum_{\mathbf{k}}^{\text{IN}} \frac{1}{\overline{\epsilon} + \omega_{\mathbf{k}}} \equiv U\,\chi(\overline{\epsilon}), \tag{2.78}$$

where the suffix IN means $|\mathbf{k}| \leq 1$ and $|-\mathbf{k}+\mathbf{Q}| \leq 1$, while OUT refers to $|\mathbf{k}| > 1$ and $|-\mathbf{k}+\mathbf{Q}| > 1$. In fact, one can solve for any $x \lessgtr 0$,

$$U\,\chi(x) = \frac{U}{V} \sum_{\mathbf{k}}^{\text{OUT}} \frac{1}{x - \omega_{\mathbf{k}}} - \frac{U}{V} \sum_{\mathbf{k}}^{\text{IN}} \frac{1}{x + \omega_{\mathbf{k}}} = 1, \tag{2.79}$$

and set the positive solutions to $\overline{\epsilon}$ and the negative ones to $-\epsilon$. The coefficients of the canonical transformation read

$$\begin{aligned} U_{\mathbf{k}\epsilon} &= \sqrt{\frac{U}{V}}\, N_\epsilon \frac{1}{\epsilon - \omega_{\mathbf{k}}}, \qquad & W_{\mathbf{k}\epsilon} &= \sqrt{\frac{U}{V}}\, N_\epsilon \frac{1}{\epsilon + \omega_{\mathbf{k}}}, \\ Z_{\mathbf{k}\overline{\epsilon}} &= \sqrt{\frac{U}{V}}\, N_{\overline{\epsilon}} \frac{1}{\overline{\epsilon} - \omega_{\mathbf{k}}}, \qquad & V_{\mathbf{k}\overline{\epsilon}} &= \sqrt{\frac{U}{V}}\, N_{\overline{\epsilon}} \frac{1}{\overline{\epsilon} + \omega_{\mathbf{k}}}, \end{aligned} \tag{2.80}$$

with the parameters N_ϵ and $N_{\overline{\epsilon}}$ that should be determined by imposing the transformation to be indeed canonical, i.e.,

$$1 = N_\epsilon^2 \frac{U}{V} \sum_{\mathbf{k}}^{\text{IN}} \frac{1}{(\epsilon - \omega_{\mathbf{k}})^2} - N_\epsilon^2 \frac{U}{V} \sum_{\mathbf{k}}^{\text{OUT}} \frac{1}{(\epsilon + \omega_{\mathbf{k}})^2}, \tag{2.81}$$

$$1 = N_{\overline{\epsilon}}^2 \frac{U}{V} \sum_{\mathbf{k}}^{\text{OUT}} \frac{1}{(\overline{\epsilon} - \omega_{\mathbf{k}})^2} - N_{\overline{\epsilon}}^2 \frac{U}{V} \sum_{\mathbf{k}}^{\text{IN}} \frac{1}{(\overline{\epsilon} + \omega_{\mathbf{k}})^2}, \tag{2.82}$$

$$0 = N_\epsilon\, N_{\overline{\epsilon}} \sum_{\mathbf{k}}^{\text{IN}} \frac{1}{(\epsilon - \omega_{\mathbf{k}})(\overline{\epsilon} + \omega_{\mathbf{k}})} - N_\epsilon\, N_{\overline{\epsilon}} \sum_{\mathbf{k}}^{\text{OUT}} \frac{1}{(\overline{\epsilon} - \omega_{\mathbf{k}})(\epsilon + \omega_{\mathbf{k}})}. \tag{2.83}$$

We observe that the last condition is also equivalent to

$$0 = N_\epsilon N_{\bar\epsilon} \sum_{\mathbf{k}}^{\text{IN}} \frac{1}{(\epsilon - \omega_{\mathbf{k}})(\bar\epsilon + \omega_{\mathbf{k}})} - N_\epsilon N_{\bar\epsilon} \sum_{\mathbf{k}}^{\text{OUT}} \frac{1}{(\bar\epsilon - \omega_{\mathbf{k}})(\epsilon + \omega_{\mathbf{k}})}$$
$$= V \frac{N_\epsilon N_{\bar\epsilon}}{\epsilon + \bar\epsilon} \left(\chi(-\epsilon) - \chi(\bar\epsilon)\right), \tag{2.84}$$

hence is automatically satisfied because of the eigenvalue equations (2.77) and (2.78).

We conclude by noting that the same calculation can be carried out also for $Q > 2$. In this case, there are no a bosons, and one only needs to find the unitary transformation $Z_{\mathbf{k}\bar\epsilon}$, i.e., one has to solve

$$1 = \frac{U}{V} \sum_{\mathbf{k}}^{\text{OUT}} \frac{1}{\bar\epsilon - \omega_{\mathbf{k}}}, \tag{2.85}$$

and define

$$Z_{\mathbf{k}\bar\epsilon} = \sqrt{\frac{U}{V}}\, N_{\bar\epsilon} \frac{1}{\bar\epsilon - \omega_{\mathbf{k}}}, \tag{2.86}$$

where

$$N_{\bar\epsilon}^{-2} = \frac{U}{V} \sum_{\mathbf{k}}^{\text{OUT}} \frac{1}{(\bar\epsilon - \omega_{\mathbf{k}})^2}. \tag{2.87}$$

2.C.1 Continuum limit

A proper definition of a steady state requires to take first the thermodynamic limit, hence to turn all finite sums into integrals over a continuum of degrees of freedom, and only afterward send the time $t \to \infty$.

In order to understand what the above formulas mean in the continuum limit, we may follow the different route to solve the problem at equilibrium within the Matsubara technique. We would find, for instance, that the imaginary-time Fourier transforms of $G_b(\tau, \mathbf{k}) = -\langle \mathcal{T}_\tau[b_{\mathbf{k}}(\tau) b_{\mathbf{k}}^\dagger]\rangle$ and $G_a(\tau, \mathbf{k}) = -\langle \mathcal{T}_\tau[a_{\mathbf{k}}(\tau) a_{\mathbf{k}}^\dagger]\rangle$, where $\mathcal{T}_\tau[...]$ denotes the time-ordered product, read

$$G_b(i\Omega, \mathbf{k}) = \frac{1}{i\Omega - \omega_{\mathbf{k}}} + \frac{1}{V} \frac{T(i\Omega)}{(i\Omega - \omega_{\mathbf{k}})^2}, \tag{2.88}$$

$$G_a(i\Omega, \mathbf{k}) = \frac{1}{i\Omega - \omega_{\mathbf{k}}} + \frac{1}{V} \frac{T(-i\Omega)}{\left(i\Omega - \omega_{\mathbf{k}}\right)^2}, \tag{2.89}$$

where

$$T(i\Omega) = \frac{U}{1 - U\,\chi(i\Omega)}, \tag{2.90}$$

is the usual definition of the T matrix, with $\chi(z)$ the Cooper bubble that actually corresponds to the same function defined in Eq. (2.79) continued in the complex frequency plane. In the continuum limit, $\chi(z)$ has a branch cut on the real axis, specifically,

$$\begin{aligned}\chi(\epsilon+i0^+)-\chi(\epsilon-i0^+) &= 2\pi i\,\frac{1}{V}\sum_{\mathbf{k}}^{\text{IN}}\delta(\epsilon+\omega_{\mathbf{k}})-2\pi i\,\frac{1}{V}\sum_{\mathbf{k}}^{\text{OUT}}\delta(\epsilon-\omega_{\mathbf{k}})\\ &\equiv 2\pi i\,\mathcal{N}_{\text{IN}}(-\epsilon)-2\pi i\,\mathcal{N}_{\text{OUT}}(\epsilon),\end{aligned} \tag{2.91}$$

where $\mathcal{N}_{\text{IN}}(x)$ and $\mathcal{N}_{\text{OUT}}(x)$ are defined only for $x>0$ and correspond to the density of states of pairs of holes and particles, respectively, at total momentum $\mathbf{Q}$. Introducing back the dependence on $\mathbf{Q}$ and in dimensionless units,

$$\begin{aligned}\frac{\mathcal{N}_{\text{IN}}(\epsilon,\mathbf{Q})}{(k_Fa)^3} &= \theta(\epsilon-Q(2-Q))\,\theta((2+Q)(2-Q)-2\epsilon)\,\frac{\sqrt{4-2\epsilon-Q^2}}{16\pi^2}\\ &\quad+\theta(Q(2-Q)-\epsilon)\,\frac{\epsilon}{16\pi^2Q},\end{aligned} \tag{2.92}$$

$$\begin{aligned}\frac{\mathcal{N}_{\text{OUT}}(\epsilon,|\mathbf{Q}|\le 2)}{(k_Fa)^3} &= \theta(\epsilon-Q(2+Q))\,\frac{\sqrt{4+2\epsilon-Q^2}}{16\pi^2}\\ &\quad+\theta(Q(2+Q)-\epsilon)\,\frac{\epsilon}{16\pi^2Q},\end{aligned} \tag{2.93}$$

$$\begin{aligned}\frac{\mathcal{N}_{\text{OUT}}(\epsilon,|\mathbf{Q}|>2)}{(k_Fa)^3} &= \theta(2\epsilon-(2+Q)(Q-2))\,\theta(Q(Q-2)-\epsilon)\,\frac{\sqrt{4+2\epsilon-Q^2}}{16\pi^2}\\ &\quad+\theta(\epsilon-Q(2+Q))\,\frac{\sqrt{4+2\epsilon-Q^2}}{16\pi^2}\\ &\quad+\theta(Q(2+Q)-\epsilon)\,\frac{\epsilon}{16\pi^2Q},\end{aligned} \tag{2.94}$$

where a is the lattice spacing.

We then note that, in the limit of zero temperature,

$$\begin{aligned}\langle b^\dagger_{\mathbf{k}}b_{\mathbf{k}}\rangle &= -T\sum_{\Omega}\mathrm{e}^{i\Omega0^+}G_b(i\Omega,\mathbf{k})\\ &= \frac{U}{V}\int_0^\infty \mathrm{d}\epsilon\;\frac{1}{(\epsilon+\omega_{\mathbf{k}})^2}\,\frac{U\,\mathcal{N}_{\text{IN}}(\epsilon)}{(1-U\,\chi'(-\epsilon))^2+(\pi\,U\,\mathcal{N}_{\text{IN}}(\epsilon))^2},\end{aligned} \tag{2.95}$$

$$\begin{aligned}\langle a^\dagger_{\mathbf{k}}a_{\mathbf{k}}\rangle &= -T\sum_{\Omega}\mathrm{e}^{i\Omega0^+}G_a(i\Omega,\mathbf{k})\\ &= \frac{U}{V}\int_0^\infty \mathrm{d}\epsilon\;\frac{1}{(\epsilon+\omega_{\mathbf{k}})^2}\,\frac{U\,\mathcal{N}_{\text{OUT}}(\epsilon)}{(1-U\,\chi'(\epsilon))^2+(\pi\,U\,\mathcal{N}_{\text{OUT}}(\epsilon))^2},\end{aligned} \tag{2.96}$$

where $\chi'(\epsilon)=\Re\mathrm{e}\,[\chi(\epsilon-i0^+)]$. On the other hand, if we calculate the above average

values directly via exact diagonalization, we find

$$\langle b^\dagger_{\mathbf{k}} b_{\mathbf{k}}\rangle = \frac{U}{V}\sum_{\epsilon} N^2_{\epsilon}\,\frac{1}{(\epsilon+\omega_{\mathbf{k}})^2}, \tag{2.97}$$

$$\langle a^\dagger_{\mathbf{k}} a_{\mathbf{k}}\rangle = \frac{U}{V}\sum_{\bar\epsilon} N^2_{\bar\epsilon}\,\frac{1}{(\bar\epsilon+\omega_{\mathbf{k}})^2}, \tag{2.98}$$

showing that, in the continuum limit,

$$\sum_{\epsilon} \to \int_0 \mathrm{d}\epsilon, \tag{2.99}$$

$$U\,N^2_{\epsilon} \to \frac{1}{\pi}\,\Im\mathrm{m}\left[T(-\epsilon+i0^+)\right] \equiv N_{\mathrm{IN}}(\epsilon), \tag{2.100}$$

$$U\,N^2_{\bar\epsilon} \to \frac{1}{\pi}\,\Im\mathrm{m}\left[T(\bar\epsilon-i0^+)\right] \equiv N_{\mathrm{OUT}}(\bar\epsilon). \tag{2.101}$$

2.C.2 Time-dependent averages

The advantage of the exact diagonalization is to allow calculating the out-of-equilibrium evolution after suddenly switching on U at time $t=0$, without solving any integral equation. The initial state is thence the vacuum of the original bosons, but the operators are time-evolved with the $U\neq 0$ Hamiltonian. By means of the exact diagonalization, we find that, for $|\mathbf{Q}|\leq 2$,

$$\langle \alpha^\dagger_{\epsilon}(t)\alpha_{\epsilon'}(t)\rangle = N_{\epsilon}\,N_{\epsilon'}\,\mathrm{e}^{i(\epsilon-\epsilon')t}\,\frac{U}{V}\sum_{\mathbf{p}}^{\mathrm{OUT}}\frac{1}{(\epsilon+\omega_{\mathbf{p}})(\epsilon'+\omega_{\mathbf{p}})}, \tag{2.102}$$

$$\langle \beta^\dagger_{\bar\epsilon}(t)\beta_{\bar\epsilon'}(t)\rangle = N_{\bar\epsilon}\,N_{\bar\epsilon'}\,\mathrm{e}^{i(\bar\epsilon-\bar\epsilon')t}\,\frac{U}{V}\sum_{\mathbf{p}}^{\mathrm{IN}}\frac{1}{(\bar\epsilon+\omega_{\mathbf{p}})(\bar\epsilon'+\omega_{\mathbf{p}})}, \tag{2.103}$$

$$\langle \alpha^\dagger_{\epsilon}(t)\beta^\dagger_{\bar\epsilon}(t)\rangle = -N_{\epsilon}\,N_{\bar\epsilon}\,\mathrm{e}^{i(\epsilon+\bar\epsilon)t}\,\frac{U}{V}\sum_{\mathbf{p}}^{\mathrm{OUT}}\frac{1}{(\epsilon+\omega_{\mathbf{p}})(\bar\epsilon-\omega_{\mathbf{p}})}, \tag{2.104}$$

$$\langle \beta^\dagger_{\bar\epsilon}(t)\alpha^\dagger_{\epsilon}(t)\rangle = -N_{\epsilon}\,N_{\bar\epsilon}\,\mathrm{e}^{i(\epsilon+\bar\epsilon)t}\,\frac{U}{V}\sum_{\mathbf{p}}^{\mathrm{IN}}\frac{1}{(\epsilon-\omega_{\mathbf{p}})(\bar\epsilon+\omega_{\mathbf{p}})}. \tag{2.105}$$

All other averages can be obtained by the above ones as, for instance,

$$\langle \alpha_{\epsilon'}(t)\alpha^\dagger_{\epsilon}(t)\rangle = \delta_{\epsilon,\epsilon'} + \langle \alpha^\dagger_{\epsilon}(t)\alpha_{\epsilon'}(t)\rangle\,, \tag{2.106}$$

or

$$\langle \alpha_{\epsilon}(t)\beta_{\bar\epsilon}(t)\rangle = \langle \beta^\dagger_{\bar\epsilon}(t)\alpha^\dagger_{\epsilon}(t)\rangle^\star\,. \tag{2.107}$$

For $|\mathbf{Q}|>2$, the boson vacuum remains instead unaffected, only the excitation energies are modified by interaction.

It follows therefore that, for $|\mathbf{Q}| \leq 2$,

$$\begin{aligned}
\langle a^\dagger_{\mathbf{k}}(t) a_{\mathbf{k}}(t)\rangle = & \frac{U}{V}\sum_{\overline{\epsilon}} \frac{N^2_{\overline{\epsilon}}}{(\overline{\epsilon}+\omega_{\mathbf{k}})^2} \\
& + \frac{U^2}{V^2}\sum_{\epsilon,\epsilon'} \frac{N^2_{\epsilon}\, N^2_{\epsilon'}\, \cos\left((\epsilon-\epsilon')\, t\right)}{(\epsilon-\omega_{\mathbf{k}})(\epsilon'-\omega_{\mathbf{k}})} \sum_{\mathbf{p}}^{\mathrm{OUT}} \frac{1}{(\epsilon+\omega_{\mathbf{p}})(\epsilon'+\omega_{\mathbf{p}})} \\
& + \frac{U^2}{V^2}\sum_{\overline{\epsilon},\overline{\epsilon}'} \frac{N^2_{\overline{\epsilon}}\, N^2_{\overline{\epsilon}'}\, \cos\left((\overline{\epsilon}-\overline{\epsilon}')\, t\right)}{(\overline{\epsilon}+\omega_{\mathbf{k}})(\overline{\epsilon}'+\omega_{\mathbf{k}})} \sum_{\mathbf{p}}^{\mathrm{IN}} \frac{1}{(\overline{\epsilon}+\omega_{\mathbf{p}})(\overline{\epsilon}'+\omega_{\mathbf{p}})} \\
& - \frac{2U^2}{V^2}\sum_{\epsilon,\overline{\epsilon}} \frac{N^2_{\epsilon}\, N^2_{\overline{\epsilon}}\, \cos\left((\epsilon+\overline{\epsilon})\, t\right)}{(\epsilon-\omega_{\mathbf{k}})(\overline{\epsilon}+\omega_{\mathbf{k}})} \sum_{\mathbf{p}}^{\mathrm{OUT}} \frac{1}{(\epsilon+\omega_{\mathbf{p}})(\overline{\epsilon}-\omega_{\mathbf{p}})}, \qquad (2.108) \\
\langle b^\dagger_{\mathbf{k}}(t) b_{\mathbf{k}}(t)\rangle = & \frac{U}{V}\sum_{\epsilon} \frac{N^2_{\epsilon}}{(\epsilon+\omega_{\mathbf{k}})^2} \\
& + \frac{U^2}{V^2}\sum_{\overline{\epsilon},\overline{\epsilon}'} \frac{N^2_{\overline{\epsilon}}\, N^2_{\overline{\epsilon}'}\, \cos\left((\overline{\epsilon}-\overline{\epsilon}')\, t\right)}{(\overline{\epsilon}-\omega_{\mathbf{k}})(\overline{\epsilon}'-\omega_{\mathbf{k}})} \sum_{\mathbf{p}}^{\mathrm{IN}} \frac{1}{(\overline{\epsilon}+\omega_{\mathbf{p}})(\overline{\epsilon}'+\omega_{\mathbf{p}})} \\
& + \frac{U^2}{V^2}\sum_{\epsilon,\epsilon'} \frac{N^2_{\epsilon}\, N^2_{\epsilon'}\, \cos\left((\epsilon-\epsilon')\, t\right)}{(\epsilon+\omega_{\mathbf{k}})(\epsilon'+\omega_{\mathbf{k}})} \sum_{\mathbf{p}}^{\mathrm{OUT}} \frac{1}{(\epsilon+\omega_{\mathbf{p}})(\epsilon'+\omega_{\mathbf{p}})} \\
& - \frac{2U^2}{V^2}\sum_{\epsilon,\overline{\epsilon}} \frac{N^2_{\epsilon}\, N^2_{\overline{\epsilon}}\, \cos\left((\epsilon+\overline{\epsilon})\, t\right)}{(\overline{\epsilon}-\omega_{\mathbf{k}})(\epsilon+\omega_{\mathbf{k}})} \sum_{\mathbf{p}}^{\mathrm{IN}} \frac{1}{(\overline{\epsilon}+\omega_{\mathbf{p}})(\epsilon-\omega_{\mathbf{p}})}, \qquad (2.109)
\end{aligned}$$

while, for $|\mathbf{Q}| > 2$, $\langle b^\dagger_{\mathbf{k}}(t) b_{\mathbf{k}}(t)\rangle = 0$.

The first terms on the right hand sides of Eqs. (2.108) and (2.109) are the equilibrium values, hence all the rest is due to the sudden quench. We observe that, because of the eigenvalue equations (2.77) and (2.78),

$$\begin{aligned}
& \frac{U}{V}\sum_{\mathbf{p}}^{\mathrm{IN}} \frac{1}{(\epsilon-\omega_{\mathbf{p}})(\overline{\epsilon}+\omega_{\mathbf{p}})} = \frac{U}{V}\sum_{\mathbf{p}}^{\mathrm{OUT}} \frac{1}{(\overline{\epsilon}-\omega_{\mathbf{p}})(\epsilon+\omega_{\mathbf{p}})} \\
& = \frac{1}{\epsilon+\overline{\epsilon}}\left(1 + \frac{U}{V}\sum_{\mathbf{p}}^{\mathrm{IN}} \frac{1}{\overline{\epsilon}+\omega_{\mathbf{p}}} + \frac{U}{V}\sum_{\mathbf{p}}^{\mathrm{OUT}} \frac{1}{\epsilon+\omega_{\mathbf{p}}}\right), \qquad (2.110)
\end{aligned}$$

which therefore brings no singularity when $\overline{\epsilon} = \omega_{\mathbf{p}}$.

Since before the continuum limit is taken $T(\omega_{\mathbf{k}}) = 0$, if we consider a contour

that run anti-clockwise closely around the positive real axis, then

$$\begin{aligned}\overline{\mathcal{I}} &= U^2 \sum_{\overline{\epsilon},\overline{\epsilon}'} N_{\overline{\epsilon}}^2\, N_{\overline{\epsilon}'}^2\, \frac{\cos\left((\overline{\epsilon}-\overline{\epsilon}')\,t\right)}{(\overline{\epsilon}-\omega_{\mathbf{k}})(\overline{\epsilon}'-\omega_{\mathbf{k}})}\, F(\overline{\epsilon},\overline{\epsilon}') \\ &= \oint\!\!\oint \frac{\mathrm{d}z\,\mathrm{d}z'}{(2\pi i)^2}\, T(z)\,T(z')\, \frac{\cos\left((z-z')\,t\right)}{(z-\omega_{\mathbf{k}})(z'-\omega_{\mathbf{k}})}\, F(z,z'), \end{aligned} \tag{2.111}$$

where $F(z,z') = F(z',z)$ is assumed analytic. We can now take the continuum limit and find that

$$\begin{aligned}\overline{\mathcal{I}} \to{}& \fint_0 \mathrm{d}\epsilon\,\mathrm{d}\epsilon'\, N_{\mathrm{OUT}}(\epsilon)\, N_{\mathrm{OUT}}(\epsilon')\, \frac{\cos\left((\epsilon-\epsilon')\,t\right)}{(\epsilon-\omega_{\mathbf{k}})(\epsilon'-\omega_{\mathbf{k}})}\, F(\epsilon,\epsilon') \\ &- 2T'(\omega_{\mathbf{k}}) \fint_0 \mathrm{d}\epsilon\, N_{\mathrm{OUT}}(\epsilon)\, \frac{\cos\left((\epsilon-\omega_{\mathbf{k}})\,t\right)}{\epsilon-\omega_{\mathbf{k}}}\, F(\epsilon,\omega_{\mathbf{k}}) + T'(\omega_{\mathbf{k}})^2 F(\omega_{\mathbf{k}},\omega_{\mathbf{k}}), \end{aligned} \tag{2.112}$$

where $\fint \ldots$ is the Cauchy principal value integration and $T'(\epsilon) = \Re\mathrm{e}\,[T(\epsilon - i0^+)]$. Seemingly,

$$\begin{aligned}\mathcal{I} &= U^2 \sum_{\epsilon,\epsilon'} N_{\epsilon}^2\, N_{\epsilon'}^2\, \frac{\cos\left((\epsilon-\epsilon')\,t\right)}{(\epsilon-\omega_{\mathbf{k}})(\epsilon'-\omega_{\mathbf{k}})}\, F(\epsilon,\epsilon') \\ &= \oint\!\!\oint \frac{\mathrm{d}z\,\mathrm{d}z'}{(2\pi i)^2}\, T(-z)\,T(-z')\, \frac{\cos\left((z-z')\,t\right)}{(z-\omega_{\mathbf{k}})(z'-\omega_{\mathbf{k}})}\, F(z,z') \\ &\to \fint_0 \mathrm{d}\epsilon\,\mathrm{d}\epsilon'\, N_{\mathrm{IN}}(\epsilon)\, N_{\mathrm{IN}}(\epsilon')\, \frac{\cos\left((\epsilon-\epsilon')\,t\right)}{(\epsilon-\omega_{\mathbf{k}})(\epsilon'-\omega_{\mathbf{k}})}\, F(\epsilon,\epsilon') \\ &- 2T'(-\omega_{\mathbf{k}}) \fint_0 \mathrm{d}\epsilon\, N_{\mathrm{IN}}(\epsilon)\, \frac{\cos\left((\epsilon-\omega_{\mathbf{k}})\,t\right)}{\epsilon-\omega_{\mathbf{k}}}\, F(\epsilon,\omega_{\mathbf{k}}) + T'(-\omega_{\mathbf{k}})^2 F(\omega_{\mathbf{k}},\omega_{\mathbf{k}}). \end{aligned} \tag{2.113}$$

We are actually interested in the large-t limit. We observe that

$$\lim_{t\to\infty} \frac{\sin\left((\epsilon-\omega_{\mathbf{k}})\,t\right)}{\epsilon-\omega_{\mathbf{k}}} = \pi\delta(\epsilon-\omega_{\mathbf{k}}), \tag{2.114}$$

so that

$$\begin{aligned}\lim_{t\to\infty} \overline{\mathcal{I}} &= \left(T'(\omega_{\mathbf{k}})^2 + \pi^2 N_{\mathrm{OUT}}(\omega_{\mathbf{k}})^2\right) F(\omega_{\mathbf{k}},\omega_{\mathbf{k}}) \\ &= |T(\omega_{\mathbf{k}} - i0^+)|^2\, F(\omega_{\mathbf{k}},\omega_{\mathbf{k}}), \end{aligned} \tag{2.115}$$

and

$$\begin{aligned}\lim_{t\to\infty} \mathcal{I} &= \left(T'(-\omega_{\mathbf{k}})^2 + \pi^2 N_{\mathrm{IN}}(\omega_{\mathbf{k}})^2\right) F(\omega_{\mathbf{k}},\omega_{\mathbf{k}}) \\ &= |T(-\omega_{\mathbf{k}} + i0^+)|^2\, F(\omega_{\mathbf{k}},\omega_{\mathbf{k}}). \end{aligned} \tag{2.116}$$

2.C.3 Steady-state values

We are now in the position to evaluate the steady state value of the Fermi distribution jump $Z(t)$ defined by

$$Z(t) \simeq 1 - \sum_{\mathbf{Q}} \langle \Psi(t)| \, a^\dagger_{\mathbf{k},\mathbf{Q}} a_{\mathbf{k},\mathbf{Q}} + b^\dagger_{\mathbf{k},\mathbf{Q}} b_{\mathbf{k},\mathbf{Q}} \, |\Psi(t)\rangle \,, \tag{2.117}$$

where $|\mathbf{k}| = k_F$ and $|\Psi(t)\rangle$ is the boson vacuum evolved with the Hamiltonian (2.66). Once we set $|\mathbf{k}| = k_F$ and integrate over $\mathbf{Q}$, the only terms in Eqs. (2.108) and (2.109) than could survive in the $t \to \infty$ limit are, apart from the equilibrium values, the second ones. By the formulas above, we thence find, inserting back the total momentum label $\mathbf{Q}$, that

$$\begin{aligned} \langle a^\dagger_{\mathbf{k},\mathbf{Q}}(t) a_{\mathbf{k},\mathbf{Q}}(t) \rangle_{t\to\infty} \to & \frac{1}{V} \int_0 \frac{\mathrm{d}\epsilon}{\pi} \, \frac{\Im\mathrm{m}\left[T\left(\epsilon - i0^+, \mathbf{Q}\right)\right]}{(\omega_{\mathbf{k},\mathbf{Q}} + \epsilon)^2} \\ & + \frac{1}{V} \left| T\left(-\omega_{\mathbf{k},\mathbf{Q}} + i0^+, \mathbf{Q}\right)\right|^2 \int_0 \mathrm{d}\epsilon \, \frac{\mathcal{N}_{\mathrm{OUT}}(\epsilon, \mathbf{Q})}{(\omega_{\mathbf{k},\mathbf{Q}} + \epsilon)^2}, \end{aligned} \tag{2.118}$$

$$\begin{aligned} \langle b^\dagger_{\mathbf{k},\mathbf{Q}}(t) b_{\mathbf{k},\mathbf{Q}}(t) \rangle_{t\to\infty} \to & \frac{1}{V} \int_0 \frac{\mathrm{d}\epsilon}{\pi} \, \frac{\Im\mathrm{m}\left[T\left(-\epsilon - i0^+, \mathbf{Q}\right)\right]}{(\omega_{\mathbf{k},\mathbf{Q}} + \epsilon)^2} \\ & + \frac{1}{V} \left| T\left(\omega_{\mathbf{k},\mathbf{Q}} + i0^+, \mathbf{Q}\right)\right|^2 \int_0 \mathrm{d}\epsilon \, \frac{\mathcal{N}_{\mathrm{IN}}(\epsilon, \mathbf{Q})}{(\omega_{\mathbf{k},\mathbf{Q}} + \epsilon)^2}. \end{aligned} \tag{2.119}$$

As anticipated, the boson occupation numbers are $\sim 1/V$, thus justifying our discarding the hard-core constraint.

Through Eqs. (2.117)–(2.119) above, and by means of Eqs. (2.124) and (2.127) below, we find that the steady state value $Z_* = Z(t \to \infty)$ reads

$$\begin{aligned} Z_* = Z_{\mathrm{eq}} - \frac{(k_F a)^3}{8\pi^2} \int_0^2 Q \, \mathrm{d}Q \Bigg[& \int_0^{Q(2-Q)} \mathrm{d}\omega \, \left| T\left(-\omega + i0^+, \mathbf{Q}\right)\right|^2 \int_0 \mathrm{d}\epsilon \, \frac{\mathcal{N}_{\mathrm{OUT}}(\epsilon, \mathbf{Q})}{(\omega + \epsilon)^2} \\ & + \int_0^{Q(2+Q)} \mathrm{d}\omega \, \left| T\left(\omega - i0^+, \mathbf{Q}\right)\right|^2 \int_0 \mathrm{d}\epsilon \, \frac{\mathcal{N}_{\mathrm{IN}}(\epsilon, \mathbf{Q})}{(\omega + \epsilon)^2} \Bigg], \end{aligned} \tag{2.120}$$

where

$$\begin{aligned} Z_{\mathrm{eq}} = 1 - \frac{(k_F a)^3}{8\pi^2} \int_0^2 Q \, \mathrm{d}Q \Bigg[& \int_0^{Q(2-Q)} \mathrm{d}\omega \int_0 \frac{\mathrm{d}\epsilon}{\pi} \, \frac{\Im\mathrm{m}\left[T\left(\epsilon - i0^+, \mathbf{Q}\right)\right]}{(\omega + \epsilon)^2} \\ & + \int_0^{Q(2+Q)} \mathrm{d}\omega \int_0 \frac{\mathrm{d}\epsilon}{\pi} \, \frac{\Im\mathrm{m}\left[T\left(-\epsilon + i0^+, \mathbf{Q}\right)\right]}{(\omega + \epsilon)^2} \Bigg], \end{aligned} \tag{2.121}$$

is the equilibrium value at zero temperature.

2.C.4 Useful formulas

Let us consider a function $F(Q,\omega_{\mathbf{k},\mathbf{Q}})$ and define as $n_{\mathbf{k}}$ the noninteracting momentum distribution. Because of momentum isotropy

$$f_{\rm IN}(\mathbf{k}) = \frac{1}{V}\sum_{\mathbf{Q}} F(Q,\omega_{\mathbf{k},\mathbf{Q}})\, n_{\mathbf{k}}\, n_{-\mathbf{k}+\mathbf{Q}}, \tag{2.122}$$

only depends on $|\mathbf{k}| = k$. Therefore

$$\begin{aligned} f_{\rm IN}(k_F) &= \rho_0^{-1}\,\frac{1}{V}\sum_{\mathbf{k}} f(\mathbf{k})\,\delta(\epsilon_{\mathbf{k}}) \\ &= \rho_0^{-1}\,\frac{1}{V}\sum_{\mathbf{Q}}\frac{1}{V}\sum_{\mathbf{k}} \delta(\epsilon_{\mathbf{k}})\, F(Q,\omega_{\mathbf{k},\mathbf{Q}})\, n_{\mathbf{k}}\, n_{-\mathbf{k}+\mathbf{Q}} \\ &= \rho_0^{-1}\,\frac{1}{V}\sum_{\mathbf{Q}}\int_0 \mathrm{d}\omega\ \rho_{\rm IN}(\omega,\mathbf{Q})\, F(Q,\omega), \end{aligned} \tag{2.123}$$

where ρ_0 is the noninteracting density of states at the Fermi energy and

$$\begin{aligned} \rho_{\rm IN}(\omega,\mathbf{Q}) &= \frac{1}{V}\sum_{\mathbf{k}} \delta(\epsilon_{\mathbf{k}})\,\delta(\omega-\delta(\omega-\omega_{\mathbf{k},\mathbf{Q}})\, n_{\mathbf{k}}\, n_{-\mathbf{k}+\mathbf{Q}} \\ &= \frac{\rho_0}{4Q}\,\theta(Q(2-Q)-\omega)\,\theta(2-Q). \end{aligned} \tag{2.124}$$

Seemingly, if

$$f_{\rm OUT}(\mathbf{k}) = \frac{1}{V}\sum_{\mathbf{Q}} F(Q,\omega_{\mathbf{k},\mathbf{Q}})\,(1-n_{\mathbf{k}})\,(1-n_{-\mathbf{k}+\mathbf{Q}}), \tag{2.125}$$

then

$$f_{\rm OUT}(k_F) = \rho_0^{-1}\,\frac{1}{V}\sum_{\mathbf{Q}}\int_0 \mathrm{d}\omega\ \rho_{\rm OUT}(\omega,\mathbf{Q})\, F(Q,\omega), \tag{2.126}$$

where

$$\begin{aligned} \rho_{\rm OUT}(\omega,\mathbf{Q}) &= \frac{1}{V}\sum_{\mathbf{k}} \delta(\epsilon_{\mathbf{k}})\,\delta(\omega-\omega_{\mathbf{k},\mathbf{Q}})\,(1-n_{\mathbf{k}})\,(1-n_{-\mathbf{k}+\mathbf{Q}}) \\ &= \frac{\rho_0}{4Q}\,\theta(Q(2+Q)-\omega). \end{aligned} \tag{2.127}$$

The above expressions are useful to evaluate the momentum distribution jump at k_F.

Chapter 3

Nonadiabatic stationary behavior in a driven Ising chain

In all intriguing issues addressed in the recent literature, such as the meaning and occurrence of thermalization in isolated quantum systems, or the quest for "universal" behavior out of equilibrium, a recurring theme has been the characterization of the response of a many-body system to the variation of the Hamiltonian parameters. In particular, the main focus has been on the two extremes of instantaneous changes (sudden quenches) and slow ones (slow quenches). The latter has been mostly studied for systems driven across a quantum critical point, where a generalization of the classical Kibble-Zurek theory led to the prediction of a universal scaling of the excitation density with the speed at which the critical point is crossed [134, 135], successively extended also to quenches within gapless phases [136, 137], where even full violation of adiabaticity may occur [138]. Specifically, universality is expected whenever the scaling dimension of the fidelity susceptibility [139] (or its generalization for non linear protocols) is negative, and extends to other quantities besides the excitation density, such as the excess energy.

Intuitive quantum mechanical arguments, rooted ultimately on the adiabatic theorem [140], suggest that the case of quenches within a *gapped* phase is much less interesting. Indeed, in this case the scaling dimension of the fidelity susceptibility is always positive, implying that the density of excitations and the excess energy always tends to zero with the square of the switching rate for linear ramps (generalization to power-law protocols is straightforward). This also suggests that other thermodynamic quantities share the same property [136], i.e., corrections with respect to their equilibrium value are quadratic in the rate [1]. However, intuition

indicates a different scenario when considering the *order parameter* in a phase with spontaneous symmetry breaking. Since even when performing a variation of the Hamiltonian within a gapped phase an extensive amount of energy is injected, one expects to be in a situation similar to the case of finite temperature. In certain instances, for example in low-dimensional systems, the effect of temperature is the complete disruption of long-range order [141], an effect which is very far from being a small correction.

This Chapter addresses this apparent contradiction by studying the dynamics of the order parameter $m^x(t)$ in a one-dimensional quantum Ising chain after a linear variation in time of the transverse field within the ferromagnetic, ordered phase. In particular, we focus on the asymptotic value of the order parameter $m^x(t \to \infty)$ as a function of the duration τ of the linear ramp. We show that, even though the bigger τ is the closer $m^x(\tau)$ gets to its ground state value m_1^x, nevertheless, however small $|m^x(\tau) - m_1^x|$ is —actually it is proportional to $1/\tau$— it is enough to completely disrupt the order exponentially fast in the subsequent time evolution, $m^x(t \to \infty) \to 0$. In particular, in the stationary state the inverse correlation length depends quadratically on the ramp rate for large τ. These quadratic corrections persist also in the limit of small τ, where the reference value is that of the sudden limit $\tau = 0$. For protocols of intermediate durations, in turn, the inverse correlation length displays an oscillatory behavior. These results show that in low-dimensional many-body systems an apparently small correction to adiabaticity can lead to major consequences for certain observables, even in a gapped phase.

3.1 Model and quench protocol

Let us start our analysis by introducing the Hamiltonian of the transverse field Ising chain

$$\mathcal{H} = -\sum_{j=1}^{L} \left(\sigma_j^x \sigma_{j+1}^x + h\, \sigma_j^z \right), \tag{3.1}$$

where σ_j^α are the Pauli matrices at site j, obeying the usual commutation relations $[\sigma_j^\alpha, \sigma_l^\beta] = 2i\, \delta_{j,l}\, \epsilon^{\alpha\beta\gamma}\, \sigma_j^\gamma$, being $\epsilon^{\alpha\beta\gamma}$ the completely antisymmetric tensor, and satisfying periodic boundary conditions $\sigma_{j+L}^\alpha = \sigma_j^\alpha$, $h > 0$ is the transverse field and L is the number of sites in the chain, assumed to be even in the following. The Hamiltonian (3.1) exhibits a $\mathbb{Z}_2$ symmetry for rotations by π around the z-axis in spin space, i.e., it is invariant under the transformation

$$\sigma_j^z \to \sigma_j^z, \qquad \sigma_j^\alpha \to -\sigma_j^\alpha,\ \alpha = x, y. \tag{3.2}$$

In the thermodynamic limit and at zero temperature, this model undergoes a prototypical quantum phase transition [142], whose critical point $h_c = 1$ separates two gapped phases: for $h > h_c$ the system is paramagnetic, whereas for $h < h_c$ the $\mathbb{Z}_2$ symmetry is spontaneously broken and a ferromagnetic ordering appears. At any finite temperature, instead, the system is in a paramagnetic phase. The order parameter for the quantum phase transition is the spontaneous magnetization along the x-axis, defined as

$$m^x = \frac{1}{L}\sum_{j=1}^{L} \langle \sigma_j^x \rangle \,, \tag{3.3}$$

which is finite in the ferromagnetic phase and vanishes in the paramagnetic one.

In the following, we shall focus on the case of a system driven out of equilibrium by linearly varying the transverse field in time within the ferromagnetic phase, according to

$$h(t) = \begin{cases} h_0 & \text{if } t \leq 0, \\ h_0 + \dfrac{h_1 - h_0}{\tau}\, t & \text{if } 0 \leq t \leq \tau, \\ h_1 & \text{if } t \geq \tau, \end{cases} \tag{3.4}$$

with $h_0, h_1 < 1$ and the ramp duration $\tau > 0$. We assume that the system is initially prepared in its ground state for $h(t) = h_0$.

3.1.1 Fermionic representation and diagonalization

The transverse field Ising chain can be mapped to a model of spinless fermions by performing a Jordan-Wigner transformation [143],

$$\begin{aligned} \sigma_j^x &= \prod_{m<j} \left(1 - 2c_m^\dagger c_m\right) \left(c_j + c_j^\dagger\right), \\ \sigma_j^z &= 1 - 2c_j^\dagger c_j, \end{aligned} \tag{3.5}$$

with the fermionic operators satisfying anticommutation relations $\{c_m, c_n^\dagger\} = \delta_{m,n}$ and $\{c_m, c_n\} = 0$. Since the Hamiltonian conserves the fermion parity, it can be split in two parts acting on different fermion-parity subspaces [144], even (+) and odd (−),

$$\mathcal{H}(t) = \mathcal{P}^+\mathcal{H}^+(t)\mathcal{P}^+ + \mathcal{P}^-\mathcal{H}^-(t)\mathcal{P}^-, \tag{3.6}$$

where

$$\mathcal{P}^\pm = \frac{1}{2}\left(1 \pm \prod_{j=1}^{L} \sigma_j^z\right) \tag{3.7}$$

are the projectors in each subspace and

$$\mathcal{H}^{\pm}(t) = -\sum_{j=1}^{L}\left[\left(c_j^{\dagger}c_{j+1} + c_j^{\dagger}c_{j+1}^{\dagger} + h.c.\right) + h(t)\left(1 - 2c_j^{\dagger}c_j\right)\right], \tag{3.8}$$

with the c_j's obeying antiperiodic boundary conditions $c_{L+1} = -c_1$ in the even sector and periodic boundary conditions $c_{L+1} = c_1$ in the odd one.

For finite chains, the ground state is always in the even sector and the order parameter is strictly zero, since σ_j^x changes the parity of the fermion number. However, in the thermodynamic limit and in the ferromagnetic phase the energy gap between the lowest energy states within each sector, $|\Omega_+\rangle$ and $|\Omega_-\rangle$, vanishes exponentially and the states become degenerate, revealing the spontaneous breaking of the $\mathbb{Z}_2$ symmetry.

One can nonetheless recognize spontaneous symmetry breaking even within each separate sector through the long-distance behavior of the correlation function $R^{xx}(r) = \langle\Omega_{\pm}|\sigma_j^x\,\sigma_{j+r}^x|\Omega_{\pm}\rangle$, which is independent of j. Indeed, in the ferromagnetic phase, $\lim_{r\to\infty} R^{xx}(r) = (m^x)^2 > 0$, signaling the established long-range order. We shall thence focus on the even sector, where the finite-size ground state lies, and study the time evolution of

$$R^{xx}(r,t) = \lim_{L\to\infty}\langle\Psi_+(t)|\sigma_j^x\,\sigma_{j+r}^x|\Psi_+(t)\rangle\,, \tag{3.9}$$

where $|\Psi_+(t)\rangle = \mathcal{U}(t)\,|\Omega_+\rangle$, being $\mathcal{U}(t)$ the evolution operator and $|\Omega_+\rangle$ the initial state assumed to be the ground state for $h(t) = h_0$.

The Hamiltonian (3.8) is diagonalized performing a Fourier transform, followed by a Bogoliubov transformation. Introducing the operator c_k in Fourier space through the transformation

$$c_j = \frac{\mathrm{e}^{i\pi/4}}{\sqrt{L}}\sum_k \mathrm{e}^{ikj}c_k, \tag{3.10}$$

with

$$k = \frac{\pi}{L}\,(2n+1)\,, \quad n = -\frac{L}{2},\ldots,\frac{L}{2}-1, \tag{3.11}$$

so to implement the antiperiodic boundary conditions in the even sector, we can write $\mathcal{H}^+(t)$ as a sum of independent terms

$$\mathcal{H}^+(t) = 2\sum_{k>0}\begin{pmatrix}c_k^{\dagger} & c_{-k}\end{pmatrix}\mathcal{H}_k(t)\begin{pmatrix}c_k\\ c_{-k}^{\dagger}\end{pmatrix}, \tag{3.12}$$

where

$$\mathcal{H}_k(t) = \begin{pmatrix} h(t) - \cos(k) & -\sin(k) \\ -\sin(k) & \cos(k) - h(t) \end{pmatrix}. \tag{3.13}$$

The operators γ_k^t that instantaneously diagonalize the Hamiltonian at time t are related to the fermionic operators through a Bogoliubov rotation

$$\begin{pmatrix} c_k \\ c_{-k}^\dagger \end{pmatrix} = \begin{pmatrix} u_k(t) & -v_k(t) \\ v_k(t) & u_k(t) \end{pmatrix} \begin{pmatrix} \gamma_k^t \\ \gamma_{-k}^{t\,\dagger} \end{pmatrix}, \tag{3.14}$$

with real coefficients

$$u_k(t) = \frac{1}{\sqrt{2}} \sqrt{1 + \frac{h(t) - \cos(k)}{\epsilon_k(t)}}, \tag{3.15}$$

$$v_k(t) = -\operatorname{sign}(k) \frac{1}{\sqrt{2}} \sqrt{1 - \frac{h(t) - \cos(k)}{\epsilon_k(t)}}, \tag{3.16}$$

and

$$\epsilon_k(t) = \sqrt{1 + h(t)^2 - 2h(t)\cos(k)}, \tag{3.17}$$

After this transformation, the Hamiltonian takes the diagonal form

$$\mathcal{H}^+(t) = \sum_{k>0} 2\epsilon_k(t) \left(\gamma_k^{t\,\dagger} \gamma_k^t + \gamma_{-k}^{t\,\dagger} \gamma_{-k}^t - 1 \right) \tag{3.18}$$

and its instantaneous ground state $|\Omega_+\rangle_t$, defined by the condition $\gamma_k^t |\Omega_+\rangle_t = 0$, for any k, factorizes into the product

$$|\Omega_+\rangle_t = \prod_{k>0} \left(u_k(t) + v_k(t)\, c_{-k}^\dagger c_k^\dagger \right) |0\rangle , \tag{3.19}$$

with $c_k |0\rangle = 0$, for any k, and $|0\rangle = \bigotimes_{k>0} |0\rangle_k$.

3.1.2 Evolution equations

Let us now derive the equations describing the dynamics of the system induced by the linear ramp $h(t)$. In order to compute the correlation function $R^{xx}(r,t)$, it is convenient to write the fermionic operators in Heisenberg representation in terms of the ones diagonalizing the initial Hamiltonian. To this purpose, we introduce a time-dependent operator $\tilde{\gamma}_k(t)$ annihilating the evolved state $|\Psi_+(t)\rangle = \mathcal{U}(t) |\Omega_+\rangle$, i.e.,

$$\tilde{\gamma}_k(t) |\Psi_+(t)\rangle = 0, \quad \forall\, k. \tag{3.20}$$

This operator is characterized by being time independent in Heisenberg representation. Indeed, taking the time derivative of Eq. (3.20), we find

$$\left(i\,\frac{\partial\,\tilde{\gamma}_k(t)}{\partial t} + \left[\tilde{\gamma}_k(t), \mathcal{H}^+(t)\right] \right) |\Psi_+(t)\rangle = 0, \tag{3.21}$$

which implies that, in the subspace spanned by $|\Psi_+(t)\rangle$,

$$i\,\frac{\mathrm{d}}{\mathrm{d}t}\,\tilde{\gamma}_k^H(t) = 0, \tag{3.22}$$

where $\tilde{\gamma}_k^H(t) = \mathcal{U}(t)^\dagger\,\tilde{\gamma}_k(t)\,\mathcal{U}(t)$ denotes the Heisenberg version of the operator $\tilde{\gamma}_k(t)$. Therefore, we can set $\tilde{\gamma}_k^H(t) = \tilde{\gamma}_k^H(0) \equiv \gamma_k^0\ , \forall\, t$.

Keeping in mind our final goal, we make the following ansatz in order to express the fermionic operators in Heisenberg representation $c_k(t)$ (in this case we shall drop the superscript H) in terms of the time independent operators $\tilde{\gamma}_k^H(t) \equiv \gamma_k^0$

$$\begin{pmatrix} c_k(t) \\ c_{-k}^\dagger(t) \end{pmatrix} = \begin{pmatrix} \alpha_k(t) & -\beta_k^\star(t) \\ \beta_k(t) & \alpha_k^\star(t) \end{pmatrix} \begin{pmatrix} \gamma_k^0 \\ \gamma_{-k}^{0\,\dagger} \end{pmatrix}, \tag{3.23}$$

and then we look for the evolution equations of the complex coefficients $\alpha_k(t)$ and $\beta_k(t)$. To this end, we write the Heisenberg equations of motion for the fermionic operators $c_k(t)$, which can be easily computed taking the commutator with the Hamiltonian (3.12):

$$i\,\frac{\mathrm{d}}{\mathrm{d}t}\begin{pmatrix} c_k(t) \\ c_{-k}^\dagger(t) \end{pmatrix} = 2\begin{pmatrix} h(t) - \cos(k) & -\sin(k) \\ -\sin(k) & \cos(k) - h(t) \end{pmatrix}\begin{pmatrix} c_k(t) \\ c_{-k}^\dagger(t) \end{pmatrix}. \tag{3.24}$$

Finally, through Eqs. (3.23) and (3.24), the equations of motion for the coefficients read

$$\begin{cases} i\,\dfrac{\mathrm{d}}{\mathrm{d}t}\,\alpha_k(t) = 2\,(h(t) - \cos(k))\,\alpha_k(t) - 2\sin(k)\,\beta_k(t) \\ i\,\dfrac{\mathrm{d}}{\mathrm{d}t}\,\beta_k(t) = -2\,(h(t) - \cos(k))\,\beta_k(t) - 2\sin(k)\,\alpha_k(t), \end{cases} \tag{3.25}$$

with initial conditions

$$\begin{cases} \alpha_k(0) = u_k(0) \\ \beta_k(0) = v_k(0) \end{cases} \tag{3.26}$$

given by the Bogoliubov transformation (3.14).

By requiring $|\Psi_+(t)\rangle$ to be annihilated by the time-dependent operator $\tilde{\gamma}_k(t) = \alpha_k^\star(t)\,c_k + \beta_k^\star(t)\,c_{-k}^\dagger$, we obtain the following expression for the evolved state:

$$|\Psi_+(t)\rangle = \prod_{k>0}\left(\alpha_k^\star(t) + \beta_k^\star(t)\,c_{-k}^\dagger c_k^\dagger\right)|0\rangle\,. \tag{3.27}$$

We note that the complex coefficients of the ansatz (3.23) must satisfy the condition $|\alpha_k(t)|^2 + |\beta_k(t)|^2 = 1$. Therefore, Eq. (3.25) can be rewritten in terms of three real functions, defined as

$$f_{1,k}(t) = |\alpha_k(t)|^2 - |\beta_k(t)|^2, \tag{3.28}$$

$$f_{2,k}(t) = 2\,\Re\mathrm{e}\,[\alpha_k(t)\beta_k^\star(t)], \tag{3.29}$$

$$f_{3,k}(t) = 2\,\Im\mathrm{m}\,[\alpha_k(t)\beta_k^\star(t)]. \tag{3.30}$$

Thus, an equivalent description of the evolution of the system is given by

$$\begin{cases} \dfrac{\mathrm{d}}{\mathrm{d}t} f_{1,k}(t) = 4\sin(k)\, f_{3,k}(t) \\ \dfrac{\mathrm{d}}{\mathrm{d}t} f_{2,k}(t) = 4\,(h(t) - \cos(k))\, f_{3,k}(t) \\ \dfrac{\mathrm{d}}{\mathrm{d}t} f_{3,k}(t) = -4\,(h(t) - \cos(k))\, f_{2,k}(t) - 4\sin(k)\, f_{1,k}(t), \end{cases} \tag{3.31}$$

with initial conditions

$$\begin{cases} f_{1,k}(0) = \dfrac{h_0 - \cos(k)}{\epsilon_{0k}} \\ f_{2,k}(0) = -\dfrac{\sin(k)}{\epsilon_{0k}} \\ f_{3,k}(0) = 0, \end{cases} \tag{3.32}$$

where $\epsilon_{0k} = \epsilon_k(0) = \sqrt{1 + h_0^2 - 2h_0\cos(k)}$.

We observe that the description of the dynamics in terms of the functions $f_{n,k}(t)$ is analogous to a description through the density matrix of the model $\rho_+(t) = |\Psi_+(t)\rangle\langle\Psi_+(t)|$, which, since the k-modes are decoupled one from each other, takes the form $\rho_+(t) = \bigotimes_{k>0}\rho_k(t)$. Each $\rho_k(t)$ is a 2×2 Hermitian matrix with unit trace, so it is a function of only three independent real parameters. Indeed, in the basis $\{|0\rangle_k\,, c_{-k}^\dagger c_k^\dagger\,|0\rangle_k\}$ and in terms of the functions $f_{n,k}(t)$, it reads

$$\rho_k(t) = \frac{1}{2}\begin{pmatrix} 1 + f_{1,k}(t) & f_{2,k}(t) + i\, f_{3,k}(t) \\ f_{2,k}(t) - i\, f_{3,k}(t) & 1 - f_{1,k}(t) \end{pmatrix}. \tag{3.33}$$

3.2 Correlation function

We can address now our problem of interest: studying the time evolution of the correlation function $R^{xx}(r,t)$. Indeed, by means of the Jordan-Wigner transforma-

tion (3.5),

$$R^{xx}(r,t) = \lim_{L\to\infty} \langle \Psi_+(t)|\sigma_j^x\, \sigma_{j+r}^x|\Psi_+(t)\rangle$$
$$= \lim_{L\to\infty} \langle (c_j^\dagger(t) - c_j(t)) \prod_{j<m<j+r} (1 - 2c_m^\dagger(t)c_m(t))\, (c_{j+r}^\dagger(t) + c_{j+r}(t))\rangle_0, \quad (3.34)$$

where $\langle \ldots \rangle_0$ denotes the average over the initial state. We observe that $1 - 2c_m^\dagger(t)c_m(t) = (c_m^\dagger(t) + c_m(t))(c_m^\dagger(t) - c_m(t))$ and we define the operators

$$A_m(t) = c_m^\dagger(t) + c_m(t), \quad (3.35)$$
$$B_m(t) = c_m^\dagger(t) - c_m(t), \quad (3.36)$$

satisfying the anticommutation relations $\{A_m(t), A_n(t)\} = 2\delta_{m,n}$, $\{B_m(t), B_n(t)\} = -2\delta_{m,n}$, and $\{A_m(t), B_n(t)\} = 0$. Thus, the correlation function reads [145]

$$R^{xx}(r,t) = \lim_{L\to\infty} \langle B_j(t)A_{j+1}(t)B_{j+1}(t)\ldots A_{j+r-1}(t)B_{j+r-1}(t)A_{j+r}(t)\rangle_0. \quad (3.37)$$

Applying the Wick's theorem, Eq. (3.37) can be expressed in terms of the contractions of the $A_j(t)$'s and $B_j(t)$'s. By means of Eqs. (3.10) and (3.23), we finally obtain

$$\langle A_m(t)A_n(t)\rangle_0 = \delta_{m,n} - \frac{1}{L}\sum_k \mathrm{e}^{ik(m-n)} f_{3,k}(t), \quad (3.38)$$
$$\langle B_m(t)B_n(t)\rangle_0 = -\delta_{m,n} - \frac{1}{L}\sum_k \mathrm{e}^{ik(m-n)} f_{3,k}(t), \quad (3.39)$$
$$\langle B_m(t)A_n(t)\rangle_0 = -\frac{1}{L}\sum_k \mathrm{e}^{ik(m-n)} \left(f_{1,k}(t) + i\, f_{2,k}(t)\right). \quad (3.40)$$

We readily note that these equations differ from those at equilibrium [145], where the first two contractions have no contribution other than the delta and Eq. (3.37) can be written as a Toeplitz determinant involving only $\langle B_m(t)A_n(t)\rangle_0$. However, we shall see that a similar situation is recovered when considering the stationary state.

3.3 Stationary state behavior

Let us study the behavior of the system in the stationary state, that is, for $t \to \infty$ after taking the thermodynamic limit, i.e., replacing discrete sums over k with integrals.

For $t > \tau$, $h(t) = h_1$ is constant, so Eqs. (3.31) can be readily integrated in terms of the boundary values $f_{1,k}(\tau)$, $f_{2,k}(\tau)$, and $f_{3,k}(\tau)$, leading to

$$\begin{aligned} f_{1,k}(t) = {} & \frac{h_1 - \cos(k)}{\epsilon_{1k}} \left(\frac{h_1 - \cos(k)}{\epsilon_{1k}} f_{1,k}(\tau) - \frac{\sin(k)}{\epsilon_{1k}} f_{2,k}(\tau) \right) \\ & + \frac{\sin(k)}{\epsilon_{1k}} \left(\frac{\sin(k)}{\epsilon_{1k}} f_{1,k}(\tau) + \frac{h_1 - \cos(k)}{\epsilon_{1k}} f_{2,k}(\tau) \right) \cos\left(4\epsilon_{1k}(t-\tau)\right) \\ & + \frac{\sin(k)}{\epsilon_{1k}} f_{3,k}(\tau) \sin\left(4\epsilon_{1k}(t-\tau)\right), \end{aligned} \tag{3.41}$$

$$\begin{aligned} f_{2,k}(t) = {} & \frac{\sin(k)}{\epsilon_{1k}} \left(\frac{\sin(k)}{\epsilon_{1k}} f_{2,k}(\tau) - \frac{h_1 - \cos(k)}{\epsilon_{1k}} f_{1,k}(\tau) \right) \\ & + \frac{h_1 - \cos(k)}{\epsilon_{1k}} \left(\frac{h_1 - \cos(k)}{\epsilon_{1k}} f_{2,k}(\tau) + \frac{\sin(k)}{\epsilon_{1k}} f_{1,k}(\tau) \right) \cos\left(4\epsilon_{1k}(t-\tau)\right) \\ & + \frac{h_1 - \cos(k)}{\epsilon_{1k}} f_{3,k}(\tau) \sin\left(4\epsilon_{1k}(t-\tau)\right), \end{aligned} \tag{3.42}$$

$$\begin{aligned} f_{3,k}(t) = {} & f_{3,k}(\tau) \cos\left(4\epsilon_{1k}(t-\tau)\right) \\ & - \left(\frac{h_1 - \cos(k)}{\epsilon_{1k}} f_{2,k}(\tau) + \frac{\sin(k)}{\epsilon_{1k}} f_{1,k}(\tau) \right) \sin\left(4\epsilon_{1k}(t-\tau)\right), \end{aligned} \tag{3.43}$$

where $\epsilon_{1k} = \epsilon_k(\tau) = \sqrt{1 + h_1^2 - 2h_1\cos(k)}$.

We observe that the solutions consist in a stationary part plus oscillatory terms with frequency $4\epsilon_{1k}$, which vanish in the thermodynamic limit for $t \to \infty$ once integrated over k. Therefore, we find

$$\langle A_m(t) A_n(t) \rangle_0 \xrightarrow{t\to\infty} \delta_{m,n}, \tag{3.44}$$

$$\langle B_m(t) B_n(t) \rangle_0 \xrightarrow{t\to\infty} -\delta_{m,n}, \tag{3.45}$$

$$\langle B_m(t) A_n(t) \rangle_0 \xrightarrow{t\to\infty} C(m-n+1), \tag{3.46}$$

with

$$C(r) = \int_{-\pi}^{\pi} \frac{\mathrm{d}k}{2\pi} \, \frac{\cos(kr) - h_1 \cos\left(k(r-1)\right)}{\sqrt{1 + h_1^2 - 2h_1\cos(k)}} \, (1 - 2n_k), \tag{3.47}$$

being $n_k = \langle \Psi_+(t) | {\gamma_k^\tau}^\dagger \gamma_k^\tau \, | \Psi_+(t) \rangle$ the occupation numbers in the evolved state, which are actually time independent for $t > \tau$ and read

$$1 - 2n_k = \frac{\left(h_1 - \cos(k)\right) f_{1,k}(\tau) - \sin(k) \, f_{2,k}(\tau)}{\sqrt{1 + h_1^2 - 2h_1\cos(k)}}. \tag{3.48}$$

We note that disregarding the oscillatory terms is equivalent to stating that the stationary value, being the correlation a local observable, can be computed in the diagonal ensemble, which is completely determined by the occupation numbers n_k.

As in equilibrium, the conditions in Eqs. (3.44)–(3.46) allow to express the correlation function in the stationary state $R^{xx}_*(r) \equiv \lim_{t\to\infty} R^{xx}(r,t)$ as a $r \times r$ Toeplitz determinant,

$$R^{xx}_*(r) = \begin{vmatrix} C(0) & C(-1) & \dots & C(-r+1) \\ C(1) & C(0) & \dots & C(-r+2) \\ \vdots & \vdots & \ddots & \vdots \\ C(r-1) & C(r-2) & \dots & C(0) \end{vmatrix}, \tag{3.49}$$

whose asymptotic behavior in the limit $r \to \infty$ has to be determined. To this end, we first note that

$$C(r) = \int_{-\pi}^{\pi} \frac{\mathrm{d}k}{2\pi}\, \tilde{C}(k)\, \mathrm{e}^{-ikr}, \tag{3.50}$$

with

$$\tilde{C}(k) = \left(\frac{1 - h_1\, \mathrm{e}^{ik}}{1 - h_1\, \mathrm{e}^{-ik}} \right)^{1/2} (1 - 2n_k). \tag{3.51}$$

In terms of the complex variable $z = \mathrm{e}^{ik}$, the function $\tilde{C}(z)$ has zero index about the origin $z = 0$ and is nonvanishing on the unit circle $|z| = 1$ as long as $n_k < 1/2$, $\forall k$, a condition that has been verified numerically and perturbatively, and is equivalent to say that the effective temperature of all the modes is less than infinity. Under these conditions, the asymptotic behavior of $R^{xx}_*(r)$ can be found applying the strong Szegő lemma [146], which states that

$$R^{xx}_*(r) \sim \mathrm{e}^{-r/\xi}, \tag{3.52}$$

with inverse correlation length

$$\xi^{-1} = -\int_{-\pi}^{\pi} \frac{\mathrm{d}k}{2\pi}\, \ln\left(1 - 2n_k\right). \tag{3.53}$$

Therefore, whenever $n_k \neq 0$, the correlation length is finite, implying that $R^{xx}_*(r)$ decays to zero exponentially hence that the order parameter m^x is zero. Such a condition is verified for any finite duration of the linear ramp, implying that adiabaticity is broken for the order parameter. From Eq. (3.53), we observe that a tiny deviation of the occupation numbers with respect to their equilibrium value ($n_k = 0$) translates into a comparably small inverse correlation length. Nonetheless, such small quantitative corrections lead to a completely different behavior of the correlation function $R^{xx}_*(r)$ and of the order parameter.

Figure 3.1 shows the correlation length as a function of τ, computed by numerically solving Eqs. (3.31) and evaluating Eq. (3.53): for long ramps the correlation

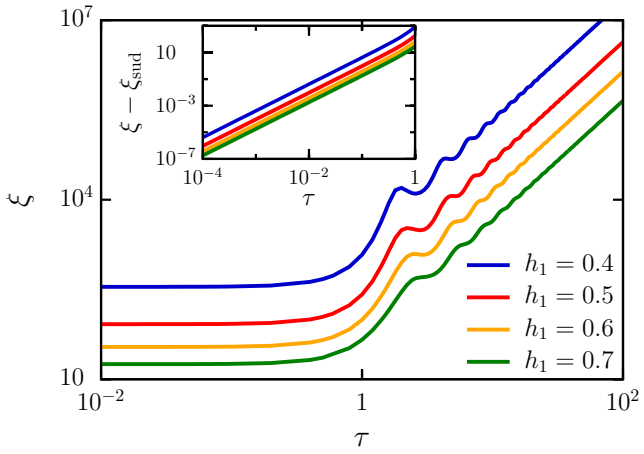

Figure 3.1: Main plot: correlation length ξ as a function of the duration of the linear ramp τ for $h_0 = 0.3$ and different final values of h_1. Inset: difference between the correlation length ξ and its value $\xi_{\rm sud}$ for a sudden quench from h_0 to h_1 as a function of the duration of the linear ramp in the small-τ regime.

length grows as τ^2, while for $\tau \sim 1$ oscillations are displayed. The inset of the figure focuses on the small-τ regime, showing that ξ departs quadratically in τ from its sudden-quench value $\xi_{\rm sud}$.

The two limiting cases of sudden and slow quenches can be captured by two different perturbative expansions.

For small τ, the result of the perturbative expansion of Eqs. (3.31) at the leading order leads to

$$\xi(\tau) = -\frac{1}{\ln\left[\left(1+h_0h_1+\sqrt{(1-h_1^2)(1-h_0^2)}\right)/2\right]} + \frac{2(h_1-h_0)^2\left(1+h_0h_1-\sqrt{(1-h_1^2)(1-h_0^2)}\right)}{3(h_0+h_1)^2\ln^2\left[\left(1+h_0h_1+\sqrt{(1-h_1^2)(1-h_0^2)}\right)/2\right]}\tau^2 + O\left(\tau^4\right), \quad (3.54)$$

where the first term is the result for a sudden quench from h_0 to h_1 ($\xi_{\rm sud}$). Higher order in the power series can be straightforwardly computed (see Appendix 3.A). In particular we notice that only even powers of τ appears in the expansion, and all the corrections we computed are even under $h_0 \leftrightarrow h_1$, i.e., inversion of the ramp. Figure 3.2(a) compares the perturbative and the numerical results: the agreement is excellent up to $\tau \simeq 1$ provided that corrections up to eighth order in τ are taken into account.

For long ramps, instead, we applied the adiabatic perturbation theory (APT)

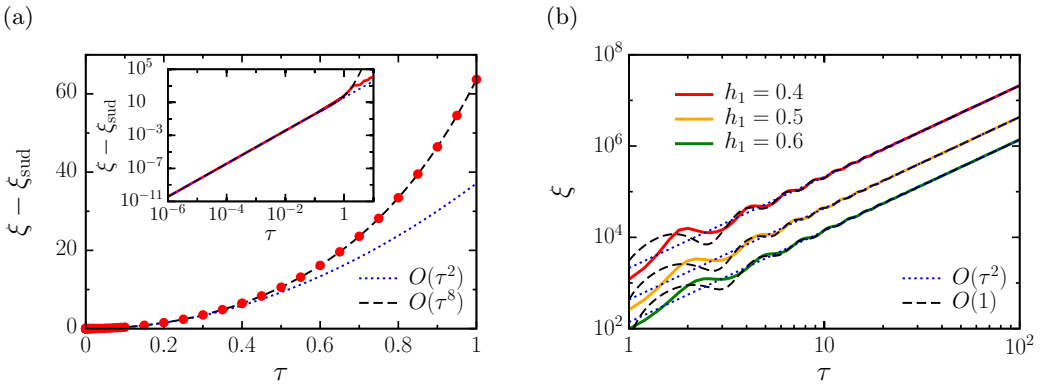

Figure 3.2: (a) Main plot: difference between the correlation length ξ and its value $\xi_{\rm sud}$ for a sudden quench from $h_0 = 0.3$ to $h_1 = 0.6$ as a function of the duration of the linear ramp in the small-τ regime. Numerical results (red dots) are compared with the perturbative expansion up to second (see Eq. (3.54)) and eighth order (dashed lines). Inset: same plot in log-log scale. (b) Correlation length ξ as a function of the duration of the linear ramp in the large-τ regime for $h_0 = 0.3$ and different values of h_1. Numerical results (solid lines) are compared with the predictions of adiabatic perturbation theory up to $O(\tau^2)$ and $O(1)$ (see Eq. (3.55)) (dashed lines).

described in Ref [147], which predicts that for large τ the occupation numbers n_k vanish as $1/\tau^2$ in an oscillating fashion. This is actually the source of oscillations observed in ξ. Indeed, the result of the perturbative expansion for large τ is

$$\xi(\tau) = \frac{64\left(1-h_0^2\right)^3\left(1-h_1^2\right)^3}{\left(h_1-h_0\right)^2\left[\left(1-h_0^2\right)^3+\left(1-h_1^2\right)^3\right]}\tau^2 + \Xi(\tau)\sqrt{\tau} + \Lambda + O\left(\tau^{-1/2}\right), \quad (3.55)$$

where $\Xi(\tau)$ is an oscillating function and Λ is a constant (see Appendix 3.B). As a consequence, the relative oscillations of the correlation length goes to zero as $\tau^{-3/2}$. Also in this case all the corrections are invariant under the transformation $h_0 \leftrightarrow h_1$. Figure 3.2(b) shows a comparison between the prediction of APT and numerical data: by including correction up to $O(1)$ there is quite good agreement for $\tau \gtrsim 10$.

3.4 Approaching the stationary state

Let us now address the question of how the stationary state described in the previous section is reached. For a generic time t, Eqs. (3.44)–(3.46) are no more valid, so that the correlation function can not be represented as a Toeplitz determinant.

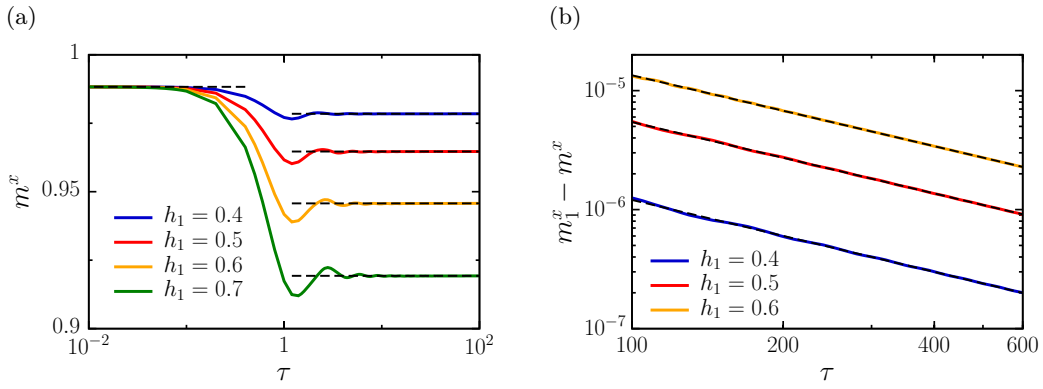

Figure 3.3: (a) Spontaneous magnetization m^x measured at the end of the ramp as a function of its duration τ for $h_0 = 0.3$ and different values of h_1. (b) Difference between the equilibrium value of the spontaneous magnetization m_1^x corresponding to the ground state of the final Hamiltonian and its value m^x measured at the end of the ramp as a function of its duration τ for $h_0 = 0.3$ and different values of h_1. Black dashed lines are fits $\propto 1/\tau$.

Instead, Eq. (3.37) can be expressed as the Pfaffian of a $2r \times 2r$ antisymmetric matrix [148], i.e.,

$$R^{xx}(r,t) = \mathrm{pf}\left[\Gamma(t)\right], \tag{3.56}$$

where $\Gamma(t)$ is

$$\Gamma(t) = \begin{bmatrix} \Gamma_0(t) & \Gamma_{-1}(t) & \dots & \Gamma_{-r+1}(t) \\ \Gamma_1(t) & \Gamma_0(t) & \dots & \Gamma_{-r+2}(t) \\ \vdots & \vdots & \ddots & \vdots \\ \Gamma_{r-1}(t) & \Gamma_{r-2}(t) & \dots & \Gamma_0(t) \end{bmatrix}, \quad \Gamma_n(t) = \begin{pmatrix} -F_n(t) & G_n(t) \\ -G_{-n}(t) & F_n(t) \end{pmatrix}, \tag{3.57}$$

with

$$F_n(t) = i\,\langle A_m(t) A_{n+m}(t)\rangle_0 - i\,\delta_{n,0}, \tag{3.58}$$

$$G_n(t) = \langle B_{n+m-1}(t) A_m(t)\rangle_0. \tag{3.59}$$

Since for an antisymmetric matrix $\mathcal{M}$ the identity $\left(\mathrm{pf}\left[\mathcal{M}\right]\right)^2 = \det\left[\mathcal{M}\right]$ holds, the time evolution of the order parameter can be expressed as

$$m^x(t) = \left(\lim_{r\to\infty} \det\left[\Gamma(t)\right] \right)^{1/4}. \tag{3.60}$$

In Figure 3.3(a) the value of the spontaneous magnetization measured right after the end of the ramp, i.e. for $t = \tau$, is reported: in the limit of small and

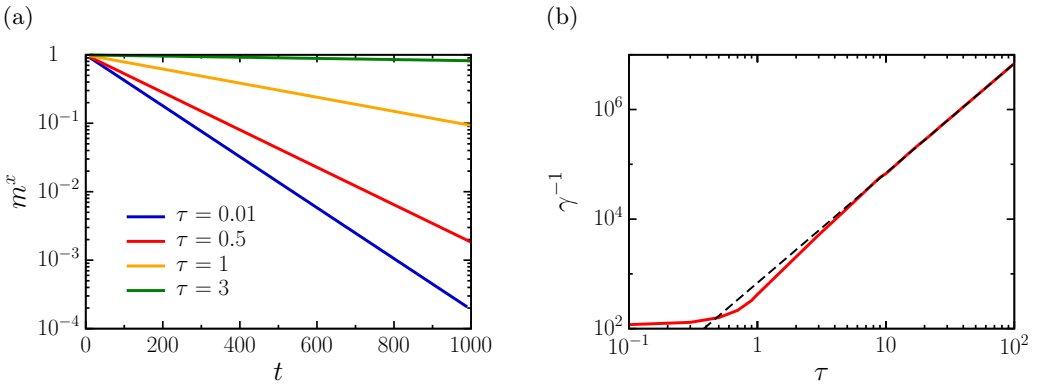

Figure 3.4: (a) Spontaneous magnetization m^x as a function of the time t elapsed after the end of the ramp for different ramp durations τ and for $h_0 = 0.5$ and $h_1 = 0.2$. Black dashed lines indicates the equilibrium values m_0^x and m_1^x. (b) Inverse decay rate γ^{-1} as a function of the duration of the ramp τ for $h_0 = 0.5$ and $h_1 = 0.2$. The black dashed line is a fit $\propto \tau^2$.

large τ it approaches its equilibrium values m_0^x and m_1^x, corresponding to those it would have in the ground state of the initial ($h(t) = h_0$) and final ($h(t) = h_1$) Hamiltonian respectively.

Figure 3.3(b) shows the behavior of the magnetization at the end of the ramp in the limit of large τ: in this case the order parameter is

$$m^x(\tau) = m_1^x + \delta m^x(\tau), \tag{3.61}$$

where $\delta m^x(\tau)$ is a correction $\propto 1/\tau$. As expected, the larger the duration of the ramp is, the closer $m^x(\tau)$ gets to its equilibrium value. However, the order parameter is not a conserved quantity and unlike classical systems, where the small correction $\delta m^x(\tau)$ would lead to a small precession of the magnetization around its equilibrium value, in quantum low-dimensional systems this state is dynamically very fragile, and the subsequent time evolution produces a collapse of the magnetization, as shown in the previous section.

Indeed, by solving the dynamics for $t > \tau$, we find that the magnetization always decays to zero exponentially in time, as reported in Figure 3.4(a), i.e.,

$$m^x(t) \sim \mathrm{e}^{-\gamma t}, \tag{3.62}$$

with a decay rate γ that scales as $1/\tau^2$ for large ramp durations (Figure 3.4(b)).

3.5 Concluding remarks

In this Chapter, we have shown that the stationary value of the order parameter of a one-dimensional quantum Ising model does not behave in an adiabatic way within the ferromagnetic phase, however small the switching rate of the transverse field is. This occurs in spite of the fact that the Hamiltonian is gapped, which in principle is the most favorable situation for an adiabatic evolution. Such a behavior of the order parameter has to be expected whenever the system has a phase transition only at zero temperature and it is driven within the ordered phase. Indeed a finite density of excitations $n_{ex} \sim 1/\tau^2$ will always be generated and in this situation will be always sufficient to destroy order. From this, one can estimate also the behavior of the correlation length, which, following the same reasoning as the Kibble-Zurek argument, will be $\xi \sim 1/n_{ex}^{1/d} \sim \tau^{2/d}$, with d being the dimension of the system. A natural question that comes up is what happens instead in an analogous system where the transition survives at finite temperature. One possibility is that there is a transition in the value of the order parameter as a function of τ, namely, for sufficiently slow ramps its asymptotic value is finite, while it goes to zero for fast ramps. If this is really the case, and, if so, when the value of the order parameter is finite or not remain interesting questions.

Appendix

3.A Small τ expansion

In this section we show the derivation of the series expansion in powers of τ of the correlation length, valid for small durations of the ramp.

Introducing the dimensionless variable $s = t/\tau$, with $0 \leq s \leq 1$, we write the functions $f_{n,k}(t)$ as power series of τ, i.e.,

$$f_{1,k}(s) = \sum_{n\geq 0} a_k^{(n)}(s)\,\tau^n, \tag{3.63}$$

$$f_{2,k}(s) = \sum_{n\geq 0} b_k^{(n)}(s)\,\tau^n, \tag{3.64}$$

$$f_{3,k}(s) = \sum_{n\geq 0} c_k^{(n)}(s)\,\tau^n, \tag{3.65}$$

with the coefficients satisfying initial conditions $a_k^{(0)}(0) = f_{1,k}(0)$, $b_k^{(0)}(0) = f_{2,k}(0)$, $c_k^{(0)}(0) = 0$, and, for any $n > 0$, $a_k^{(n)}(0) = b_k^{(n)}(0) = c_k^{(n)}(0) = 0$. Replacing the expansions in Eq. (3.31), we find the evolution equations of the coefficients,

$$\begin{cases} \dfrac{\mathrm{d}}{\mathrm{d}s}\, a_k^{(n)}(s) = 4\sin(k)\, c_k^{(n-1)}(s) \\ \dfrac{\mathrm{d}}{\mathrm{d}s}\, b_k^{(n)}(s) = 4\left[h_0 - \cos(k) + (h_1 - h_0)s\right] c_k^{(n-1)}(s) \\ \dfrac{\mathrm{d}}{\mathrm{d}s}\, c_k^{(n)}(s) = -4\left[h_0 - \cos(k) + (h_1 - h_0)s\right] b_k^{(n-1)}(s) - 4\sin(k)\, a_k^{(n-1)}(s). \end{cases} \tag{3.66}$$

These equations can be readily integrated, obtaining an iterative procedure to compute $f_{1,k}(s)$, $f_{2,k}(s)$, and $f_{3,k}(s)$ at the desired order in τ. We readily note that, since $c_k^{(0)} = 0$, we have $a_k^{(2n+1)} = b_k^{(2n+1)} = c_k^{(2n)} = 0$, $\forall n$. This in turn implies that the corrections to n_k, and so to the correlation length ξ, with respect to the sudden quench value are given by even powers of τ.

Let us compute the first non-vanishing correction. From the last equation of (3.66) we find

$$c_k^{(1)}(s) = \frac{2(h_1 - h_0)\sin k}{\epsilon_{0k}}\, s^2, \tag{3.67}$$

and then, replacing this expression in the first two equations,

$$a_k^{(2)}(s) = \frac{8(h_1 - h_0)\sin^2(k)}{3\epsilon_{0k}}\, s^3, \tag{3.68}$$

$$b_k^{(2)}(s) = \frac{8(h_1 - h_0)\sin(k)\,(h_0 - \cos(k))}{3\epsilon_{0k}}\, s^3 + \frac{2(h_1 - h_0)^2\sin(k)}{\epsilon_{0k}}\, s^4. \tag{3.69}$$

Through Eq. (3.48), we can calculate the occupation numbers:

$$1-2n_k(\tau) = \frac{1 + h_0h_1 - (h_0 + h_1)\cos(k)}{\epsilon_{0k}\,\epsilon_{1k}} + \frac{2(h_1 - h_0)^2\sin^2(k)}{3\,\epsilon_{0k}\,\epsilon_{1k}}\,\tau^2 + O\left(\tau^4\right). \tag{3.70}$$

Then, by means of Eq. (3.53), we find the expansion of the inverse of the correlation length up to second order in τ, which reads

$$\begin{aligned}\xi^{-1}(\tau) = &-\ln\left(\frac{1 + h_0h_1 + \sqrt{(1-h_1^2)(1-h_0^2)}}{2}\right)\\ &- \frac{3(h_0 + h_1)^2}{2(h_1 - h_0)^2\left(1 + h_0h_1 - \sqrt{(1-h_1^2)(1-h_0^2)}\right)}\,\tau^2 + O\left(\tau^4\right),\end{aligned} \tag{3.71}$$

Finally, by inverting the previous expression, we recover Eq. (3.54).

This procedure can be straightforwardly repeated for computing higher order corrections, and it is easily implementable on a computer. We performed the calculations up to the eighth order in τ and we notice that all contributions are even if we exchange h_0 and h_1, that is if we either ramp up or down the transverse field.

3.B Large τ expansion

In this section we provide details on the derivation of the perturbative expansion in powers of τ of the correlation length, valid for large τ. First, we find an approximate expression of the evolved state by applying the adiabatic perturbation theory (APT) [147]. Then we perform a power series expansion of the occupation numbers $n_k = \langle\Psi_+(t)|\gamma_k^{\tau\,\dagger}\gamma_k^{\tau}\,|\Psi_+(t)\rangle$ in terms of the small parameter $1/\tau$ and we finally use it to compute the correlation length.

3.B.1 Adiabatic Perturbation Theory

Our problem can be reduced to a two-level problem, greatly simplifying the general results of Ref. [147]. Indeed, because of the momentum conservation, the instantaneous excited states are obtained by applying products ${\gamma^t_{-k}}^\dagger {\gamma^t_k}^\dagger$ to the instantaneous ground state $|\Omega_+\rangle_t$. Since excitations to different k-modes are independent one from each other, we can consider the problem as a sum of independent two-level systems. Again, it is convenient to rescale the time as $s = t/\tau$, $0 \leq s \leq 1$. The instantaneous eigenstates of the two-level system are $|-(s)\rangle_k = (u_k(s), v_k(s))^T$ and $|+(s)\rangle_k = (v_k(s), -u_k(s))^T$, with corresponding eigenvalues $E_\pm(s) = \pm 2\epsilon_k(s)$. Using the same notation as in Ref. [147], we write the k-mode evolved state as a power series in terms of $1/\tau$

$$|\Psi(s)\rangle_k = \sum_{p\geq 0} \frac{1}{\tau^p} |\psi^{(p)}(s)\rangle_k \,, \tag{3.72}$$

and we set

$$|\psi^{(p)}(s)\rangle_k = \sum_{m,n=-,+} \mathrm{e}^{-i\tau\omega_m(s)}\, b^{(p)}_{nm}(s)\, |n(s)\rangle_k \,, \tag{3.73}$$

where

$$\omega_+(s) = -\omega_-(s) = \int_0^s \mathrm{d}s'\, 2\epsilon_k(s') \equiv \omega_k(s), \tag{3.74}$$

while $b^{(p)}_{nm}(s)$ are k-dependent coefficients, whose explicit expressions are given below. Since the initial state is the ground state of the two-level system, the initial conditions are $|\psi^{(0)}(0)\rangle_k = |-(0)\rangle_k$ and, for any $p > 0$, $|\psi^{(p)}(0)\rangle_k = 0$. Requiring the adiabatic approximation to be the zeroth order term in the power series expansion of APT, we obtain

$$|\psi^{(0)}(s)\rangle_k = \mathrm{e}^{i\omega_k(s)\tau} |-(s)\rangle_k \,. \tag{3.75}$$

The first order correction to the adiabatic approximation is

$$\begin{aligned} |\psi^{(1)}(s)\rangle_k = {} & \mathrm{e}^{i\omega_k(s)\tau}\, b^{(1)}_{--}(s)\, |-(s)\rangle_k \\ & + \left(\mathrm{e}^{-i\omega_k(s)\tau}\, b^{(1)}_{++}(s) + e^{i\omega_k(s)\tau}\, b^{(1)}_{+-}(s)\right) |+(s)\rangle_k \,, \end{aligned} \tag{3.76}$$

while the second order correction is

$$\begin{aligned} |\psi^{(2)}(s)\rangle_k = {} & \left(\mathrm{e}^{-i\omega_k(s)\tau}\, b^{(2)}_{-+}(s) + \mathrm{e}^{i\omega_k(s)\tau}\, b^{(2)}_{--}(s)\right) |-(s)\rangle_k \\ & + \left(\mathrm{e}^{i\omega_k(s)\tau}\, b^{(2)}_{+-}(s) + \mathrm{e}^{-i\omega_k(s)\tau}\, b^{(2)}_{++}(s)\right) |+(s)\rangle_k \,. \end{aligned} \tag{3.77}$$

The approximate expression of the k-mode evolved state up to second order is

$$|\Psi(s)\rangle_k = |\psi^{(0)}(s)\rangle_k + \tau^{-1} |\psi^{(1)}(s)\rangle_k + \tau^{-2} |\psi^{(2)}(s)\rangle_k + O\left(\tau^{-3}\right). \tag{3.78}$$

3.B.2 Perturbative Expansion

Using the approximate expression of the evolved state in Eq. (3.78) and noting that $\gamma_k^\tau \, |-(1)\rangle_k = 0$, which implies that at leading order $n_k(\tau) = 0$, the power series expansion of the occupation numbers up to fourth order in $1/\tau$ is

$$n_k(\tau) = \tau^{-2}\, n_k^{(2)}(\tau) + \tau^{-3}\, n_k^{(3)}(\tau) + \tau^{-4}\, n_k^{(4)}(\tau) + O\left(\tau^{-5}\right), \tag{3.79}$$

where

$$n_k^{(2)}(\tau) = \left|b_{++}^{(1)}(1)\right|^2 + \left|b_{+-}^{(1)}(1)\right|^2 - 2\cos\left(\varphi_k(\tau)\right)\left(b_{++}^{(1)}(1) b_{+-}^{(1)}(1)\right), \tag{3.80}$$

$$n_k^{(3)}(\tau) = 2\sin\left(\varphi_k(\tau)\right)\left(i\, b_{+-}^{(1)}(1) b_{++}^{(2)}(1) - i\, b_{++}^{(1)}(1) b_{+-}^{(2)}(1)\right), \tag{3.81}$$

$$n_k^{(4)}(\tau) \simeq \left(b_{++}^{(2)}(1)\right)^2 + \left(b_{+-}^{(2)}(1)\right)^2 + 2\cos\left(\varphi_k(\tau)\right)\left(b_{++}^{(2)}(1) b_{+-}^{(2)}(1)\right), \tag{3.82}$$

and

$$b_{++}^{(1)}(1) = (h_1 - h_0)\, \frac{i \sin(k)}{8\, \epsilon_{0k}^3}, \tag{3.83}$$

$$b_{+-}^{(1)}(1) = -(h_1 - h_0)\, \frac{i \sin(k)}{8\, \epsilon_{1k}^3}, \tag{3.84}$$

$$b_{++}^{(2)}(1) = (h_1 - h_0)^2\, \frac{\sin(k)}{32\, \epsilon_{0k}^3} \left[\frac{3\, \left(h_0 - \cos(k)\right)}{\epsilon_{0k}^3} + \frac{\sin^2(k)}{4} \int_{h_0}^{h_1} \mathrm{d}h\, \left(h^2 - 2h\cos(k) + 1\right)^{-5/2}\right], \tag{3.85}$$

$$b_{+-}^{(2)}(1) = -(h_1 - h_0)^2\, \frac{\sin(k)}{32\, \epsilon_{1k}^3} \left[\frac{3\, \left(h_1 - \cos(k)\right)}{\epsilon_{1k}^3} - \frac{\sin^2(k)}{4} \int_{h_0}^{h_1} \mathrm{d}h\, \left(h^2 - 2h\cos(k) + 1\right)^{-5/2}\right], \tag{3.86}$$

$$\varphi_k(\tau) = \frac{4\tau}{h_1 - h_0} \int_{h_0}^{h_1} \mathrm{d}h\, \left(h^2 - 2h\cos(k) + 1\right)^{1/2}. \tag{3.87}$$

We point out that in $n_k^{(4)}(\tau)$ we are neglecting the contribution of the term ${}_k\langle\psi^{(1)}(1)|{\gamma_k^\tau}^\dagger \gamma_k^\tau \, |\psi^{(3)}(1)\rangle_k + h.c.$,because it gives higher order corrections to the correlation length.

Inserting the expansion of Eq. (3.79) in Eq. (3.53) and keeping the terms up to fourth order, we obtain

$$\xi^{-1}(\tau) = \frac{1}{\pi}\left\{\tau^{-2} \int_{-\pi}^{\pi} \mathrm{d}k\; n_k^{(2)}(\tau) + \tau^{-3} \int_{-\pi}^{\pi} \mathrm{d}k\; n_k^{(3)}(\tau) + \tau^{-4} \int_{-\pi}^{\pi} \mathrm{d}k\, \left[n_k^{(4)}(\tau) + \left(n_k^{(2)}(\tau)\right)^2\right]\right\} + O\left(\tau^{-5}\right). \tag{3.88}$$

From Eq. (3.88), it is evident that oscillations in the correlation length appear as a consequence of oscillations in the occupation numbers.

Let us compute the integrals in the previous expression using Eqs. (3.80)–(3.87).

$$\begin{aligned}\mathcal{I}_1 &= \frac{1}{\pi}\int_{-\pi}^{\pi} \mathrm{d}k \;\left|b_{++}^{(1)}(1)\right|^2 + \left|b_{+-}^{(1)}(1)\right|^2 \\ &= \frac{(h_1-h_0)^2\left[\left(1-h_0^2\right)^3+\left(1-h_1^2\right)^3\right]}{64\left(1-h_0^2\right)^3\left(1-h_1^2\right)^3}.\end{aligned} \tag{3.89}$$

$$\begin{aligned}\mathcal{I}_2(\tau) &= -\frac{2}{\pi}\int_{-\pi}^{\pi} \mathrm{d}k \;\cos\left(\varphi_k(\tau)\right)\left(b_{++}^{(1)}(1)b_{+-}^{(1)}(1)\right) \\ &= -\frac{(h_1-h_0)^2}{16\pi}\,\Re\mathrm{e}\left[\int_{-\pi}^{\pi}\mathrm{d}k\;\frac{\sin^2(k)}{\epsilon_{0k}^3\,\epsilon_{1k}^3}\,\mathrm{e}^{i\varphi_k(\tau)}\right].\end{aligned} \tag{3.90}$$

The contribution of the integral (3.90) can be evaluated applying the stationary phase approximation. Since in the power series expansion (3.88) we are keeping only terms up to fourth order, we can neglect all the contributions of $\mathcal{I}_2(\tau)$ higher than the second order in $1/\tau$. We finally obtain

$$\begin{aligned}\mathcal{I}_2(\tau) &= -\,\tau^{-3/2}\,\frac{(h_1-h_0)^2}{64\sqrt{\pi}}\left[\frac{A_2}{{B_2}^{3/2}}\cos\left(B_0\,\tau+\frac{3\pi}{4}\right)\right. \\ &\qquad \left. +\,\frac{C_2}{|D_2|^{3/2}}\cos\left(D_0\,\tau+\frac{3\pi}{4}\right)\right]+O\left(\tau^{-5/2}\right) \\ &\equiv \tau^{-3/2}\,\Phi(\tau)+O\left(\tau^{-5/2}\right),\end{aligned} \tag{3.91}$$

where

$$A_2 = \frac{1}{(1-h_0)^3(1-h_1)^3}, \tag{3.92}$$

$$B_0 = 2\,(2-h_0-h_1), \tag{3.93}$$

$$B_2 = \frac{2}{h_1-h_0}\left[\ln\left(\frac{1-h_0}{1-h_1}\right)-h_1+h_0\right], \tag{3.94}$$

$$C_2 = \frac{1}{(1+h_0)^3(1+h_1)^3}, \tag{3.95}$$

$$D_0 = 2\,(2+h_0+h_1), \tag{3.96}$$

$$D_2 = -\frac{2}{h_1-h_0}\left[\ln\left(\frac{1+h_0}{1+h_1}\right)+h_1-h_0\right]. \tag{3.97}$$

All the other integrals containing an oscillatory part can be calculated using the stationary phase approximation. However, they give higher order corrections to the expansion (3.88), so their contribution is negligible.

So, the only integrals that we have to take into account are

$$\mathcal{I}_3 = \frac{1}{\pi}\int_{-\pi}^{\pi} \mathrm{d}k \, \left[\left(b_{++}^{(2)}(1)\right)^2 + \left(b_{+-}^{(2)}(1)\right)^2\right], \tag{3.98}$$

which has been evaluated numerically, and

$$\begin{aligned}\mathcal{I}_4 &= \frac{1}{\pi}\int_{-\pi}^{\pi} \mathrm{d}k \, \left(\left|b_{++}^{(1)}(1)\right|^2 + \left|b_{+-}^{(1)}(1)\right|^2\right)^2 \\ &= \frac{3(h_1-h_0)^4}{16384}\left[\frac{1+h_0^2}{(1-h_0^2)^7} + \frac{1+h_1^2}{(1-h_1^2)^7} + \frac{2(1+h_0h_1)}{(1-h_0^2)(1-h_1^2)(1-h_0h_1)^5}\right]. \end{aligned} \tag{3.99}$$

Replacing the contribution of integrals $\mathcal{I}_1$, $\mathcal{I}_2(\tau)$, $\mathcal{I}_3$, and $\mathcal{I}_4$ in Eq. (3.88), we get an expansion of $\xi^{-1}(\tau)$ in powers of $1/\tau$:

$$\xi^{-1}(\tau) = \mathcal{I}_1\,\tau^{-2} + \Phi(\tau)\,\tau^{-7/2} + (\mathcal{I}_3+\mathcal{I}_4)\,\tau^{-4} + O\left(\tau^{-9/2}\right), \tag{3.100}$$

Inverting this power series, we obtain the result of Eq. (3.55), i.e.,

$$\xi(\tau) = \frac{1}{\mathcal{I}_1}\,\tau^2 + \Xi(\tau)\,\sqrt{\tau} + \Lambda + O\left(\tau^{-1/2}\right), \tag{3.101}$$

with $\Xi(\tau) = -\Phi(\tau)/(\mathcal{I}_1)^2$ and $\Lambda = -(\mathcal{I}_3+\mathcal{I}_4)/(\mathcal{I}_1)^2$. Again, all the terms of the expansion are invariant if we exchange h_0 and h_1.

Chapter 4

Aging and coarsening in isolated quantum systems after a quench

Whether and how an isolated quantum system thermalizes after a quench of the parameters of its Hamiltonian is a subject of extensive investigation. Remarkably, the study of the approach to thermal equilibrium disclosed a number of novel features such as the existence of *prethermalized* quasistationary states. As discussed in Sec. 1.4, it was argued that prethermalization occurs due to the system retaining memory of the integrable part of the Hamiltonian, which, in the absence of nonintegrable terms, would lead the system towards a nonthermal state. We also mentioned (see Sec. 1.5) that a quantum system can undergo a *dynamical phase transition* (DPT) in the prethermalized regime, with some of the features of an equilibrium quantum phase transition, such as the appearance of diverging length and time scales. On this basis, one expects some degree of *universality* to emerge close to a DPT, with spatial and temporal correlations characterized by critical exponents which do not depend on the microscopic details of the system. In particular, the lack of time scales combined with the breaking of translational symmetry in time due to a sudden quench is expected to cause an algebraic relaxation of the system to its stationary state, a phenomenon which has been referred to as *quantum aging*, in analogy with the slow dynamics observed in glasses [149]. While aging is known to occur in classical critical systems [150, 151], only recently the same issue has been investigated after quenches in open [152–154] or isolated [119] quantum systems. However, while in the former case the critical point responsible for aging is the thermal one dictated by the presence of a thermal bath, in the latter the critical point has an intrinsic nonequilibrium nature.

The consequences of this difference was recently explored in Ref. [119], where a system with vector order parameter $\boldsymbol{\phi}$ with N components and a Hamiltonian with $O(N)$ symmetry was studied by means of a perturbative renormalization-group approach. Aging was shown to occur in an early stage of the evolution, when the system exhibits prethermalization, rather than in the eventual thermalized state. This prethermalized state was recognized to be similar to the nonequilibrium stationary state approached by the same model in the limit $N \to \infty$, in which it becomes integrable [116–118]. This fact suggests that the $O(N)$-symmetric Hamiltonian for $N \to \infty$ is the integrable Hamiltonian responsible for the prethermalization occurring for finite N.

In this Chapter, we report a complementary nonperturbative analysis of the problem analyzed perturbatively in Ref. [119], by considering the postquench dynamics in the limit $N \to \infty$, when the model is exactly solvable, starting from a ground state in the disordered phase. We characterize the dynamics in absence of time and length scales in the system, i.e., close to the dynamical critical point, by studying the universal exponents and scaling forms of the relevant two-time correlation functions, which can be calculated exactly. Our analytical predictions are confirmed by the numerical solution of the corresponding equations. Moreover, we find that the same scaling functions, yet with different exponents, also describe the coarsening dynamics for quenches below the dynamical critical point.

4.1 Model and quench protocol

We consider a system described by the following $O(N)$-symmetric Hamiltonian in d spatial dimensions

$$\mathcal{H}(r_0, u) = \int \mathrm{d}^d x \, \left[\frac{1}{2} \boldsymbol{\Pi}^2 + \frac{1}{2} \left(\nabla \boldsymbol{\phi} \right)^2 + \frac{r_0}{2} \boldsymbol{\phi}^2 + \frac{u}{4! N} \boldsymbol{\phi}^4 \right], \tag{4.1}$$

where $\boldsymbol{\phi} = (\phi_1, \ldots, \phi_N)$ is a bosonic field with N components, while $\boldsymbol{\Pi}$ is the canonically conjugated momentum with $[\phi_a(\mathbf{x}), \Pi_b(\mathbf{x}')] = i \, \delta^{(d)}(\mathbf{x} - \mathbf{x}') \, \delta_{a,b}$. The parameter r_0 corresponds to the bare (square) mass of the theory, while the coupling $u > 0$ controls the strength of the anharmonic interaction. In the following we will consider the limit $N \to \infty$ [155], where the model is exactly solvable.

At equilibrium [142], this system is described by a quadratic theory with an effective (square) mass r_{eff} and exhibits a phase transition between a paramagnetic phase and an ordered one, characterized by the spontaneous breaking of the $O(N)$ symmetry (Figure 4.1). This transition, identified by the condition $r_{\mathrm{eff}} = 0$, occurs

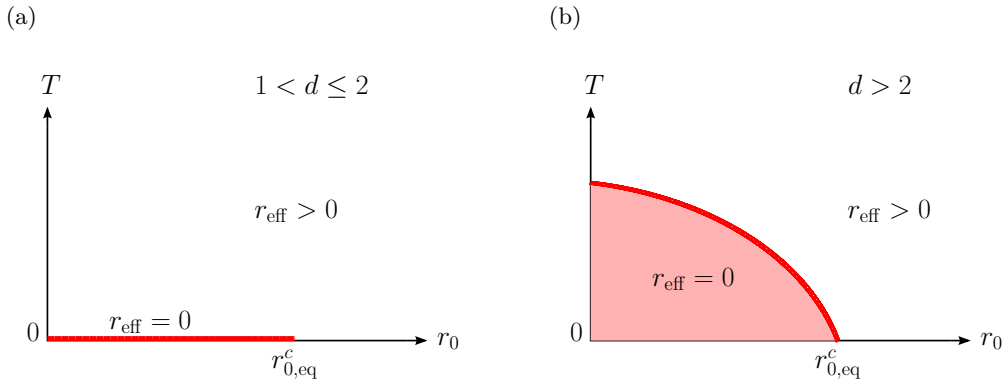

Figure 4.1: Schematic picture of the equilibrium phase diagram of the $O(N)$ model in the limit of large-N. (a) For $1 < d \leq 2$, the system undergoes a quantum phase transition at the equilibrium quantum critical point $r^c_{0,\mathrm{eq}}$. At $T = 0$ and for $r_0 < r^c_{0,\mathrm{eq}}$ the system is in an ordered state (red line). (b) For $d > 2$, a thermal transition exists. The red line indicates the locus of the finite temperature phase transition $r^c_{0,\mathrm{eq}}(T)$, below which the system is in an ordered state (colored area).

at the equilibrium critical value

$$r^c_{0,\mathrm{eq}}(T) = -\frac{u}{12}\int \frac{\mathrm{d}^d k}{(2\pi)^d}\,\frac{1}{k}\,\coth\left(\frac{k}{2T}\right) h\left(\frac{k}{\Lambda}\right), \tag{4.2}$$

where T is the temperature, and the function

$$h(x) = \begin{cases} 0 & \text{for } x \gg 1, \\ 1 & \text{for } x \ll 1, \end{cases} \tag{4.3}$$

implements a large-k cutoff at the scale Λ in order to make the theory well-defined at short distances, while it does not affect it for $k \ll \Lambda$. In particular, the quantum, zero-temperature phase transition occurs for $d > 1$, which is the lower critical dimension d_l, while the thermal transition appears for $d > 2$, having $d_l = 2$. The upper critical dimension, instead, is $d_c = 3$ for the quantum transition and $d_c = 4$ for the finite temperature one.

Our quench protocol consists in a sudden change of both the bare mass and the interaction strength: at time $t < 0$ the system is prepared in the disordered ground state $|\Psi_0\rangle$ of the prequench noninteracting Hamiltonian $\mathcal{H}(\Omega_0^2, 0)$, while the system is evolved with the postquench Hamiltonian $\mathcal{H}(r_0, u)$ for $t \geq 0$. This protocol was studied in Ref. [119], while in Refs. [113, 116–118] u had the same nonzero value in the pre- and postquench Hamiltonian. For the latter, it was

shown that the system undergoes a dynamical phase transition (DPT) at a certain dynamical critical value $r_0 = r_0^c$, which is always smaller than the equilibrium quantum critical point $r_{0,\mathrm{eq}}^c$. As argued in Ref. [119], a nonvanishing u in the present initial Hamiltonian would only renormalize the value of the initial bare mass Ω_0^2 and therefore we expect the model discussed here to undergo a DPT such as the one studied in Refs. [113,116–118]. The upper critical dimension of the DPT is $d_c = 4$, as in the corresponding equilibrium theory at finite temperature [118,119]. Accordingly, the critical, collective properties for $d > 4$ are completely described by the corresponding noninteracting theory (see Sec. 4.2). For d smaller than the lower critical dimensionality $d_l = 2$ [118], instead, this DPT is not expected to occur. However, since a counterpart of the Mermin-Wagner theorem is not known out of equilibrium, the occurrence of a different DPT cannot be ruled out for $d < d_l$.

In the following we exploit the fact that, if the $O(N)$ symmetry in the initial state is not broken, the average $\langle \phi_a \phi_b \rangle$ (where $\langle \ldots \rangle \equiv \langle \Psi_0 | \ldots | \Psi_0 \rangle$) vanishes unless $a = b$, with its nonvanishing value independent of a, and equal to the fluctuation $\langle \phi^2 \rangle$ of a generic component ϕ of the field. In the limit $N \to \infty$, the model can be solved by taking into account that, at the leading order, the quartic interaction in Eq. (4.1) decouples as [116–118,156]

$$\boldsymbol{\phi}^4 \to 2(N+2) \langle \phi^2 \rangle \boldsymbol{\phi}^2 - N(N+2) \langle \phi^2 \rangle^2 ; \tag{4.4}$$

as shown in Ref. [157], this decoupling corresponds to the Hartree-Fock approximation, which becomes exact for $N \to \infty$. Once inserted into Eq. (4.1), the dynamics of the various components of the fields decouples and each of them is ruled (up to an inconsequential additive constant) by the effective time-dependent quadratic Hamiltonian

$$\mathcal{H}_{\mathrm{eff}}(t) = \frac{1}{2} \int \mathrm{d}^d x \, \left[\Pi^2 + (\nabla \phi)^2 + r_{\mathrm{eff}}(t) \phi^2 \right] , \tag{4.5}$$

where $r_{\mathrm{eff}}(t)$ is determined by the condition

$$r_{\mathrm{eff}}(t) = r_0 + \frac{u}{6} \, \langle \phi^2(\mathbf{x}, t) \rangle \, . \tag{4.6}$$

In a field-theoretical language, $r_{\mathrm{eff}}(t)$ plays the role of a renormalized (square) effective mass of the field ϕ. Due to the quadratic nature of $\mathcal{H}_{\mathrm{eff}}$, it is convenient to decompose the field ϕ into its Fourier components $\phi_{\mathbf{k}}$, according to

$$\phi(\mathbf{x}, t) = \int \frac{\mathrm{d}^d k}{(2\pi)^d} \, \phi_{\mathbf{k}}(t) \, \mathrm{e}^{i \mathbf{k} \cdot \mathbf{x}} \tag{4.7}$$

with an analogous decomposition for Π. Each of these components can be written in terms of the annihilation and creation operators [116,118] $a_{\mathbf{k}}$ and $a_{\mathbf{k}}^\dagger$, respectively,

diagonalizing the initial Hamiltonian,

$$\phi_{\mathbf{k}}(t) = f_{\mathbf{k}}(t)\, a_{\mathbf{k}} + f^{\star}_{\mathbf{k}}(t)\, a^{\dagger}_{-\mathbf{k}}, \tag{4.8}$$

where $f_{\mathbf{k}}(t) = f_{-\mathbf{k}}(t)$ is a complex function depending on both time t and momentum $\mathbf{k}$. Note that the canonical commutation relations between ϕ and Π imply [116]

$$2\,\Im\mathrm{m}\left[f_{\mathbf{k}}(t)\dot{f}^{\star}_{\mathbf{k}}(t)\right] = 1. \tag{4.9}$$

The Heisenberg equation of motion for $\phi_{\mathbf{k}}(t)$ derived from the Hamiltonian (4.5) yields the following evolution equation for $f_{\mathbf{k}}(t)$,

$$\ddot{f}_{\mathbf{k}} + \left(k^2 + r_{\mathrm{eff}}(t)\right) f_{\mathbf{k}} = 0, \tag{4.10}$$

with $k = |\mathbf{k}|$. This equation is supplemented by the initial conditions

$$f_{\mathbf{k}}(0) = \frac{1}{\sqrt{2\omega_{0k}}} \quad \text{and} \quad \dot{f}_{\mathbf{k}}(0) = -\,i\sqrt{\frac{\omega_{0k}}{2}}, \tag{4.11}$$

where $\omega_{0k}^2 = k^2 + \Omega_0^2$, which can be obtained by diagonalizing the quadratic prequench Hamiltonian and by imposing the continuity [4, 158] of $\phi_{\mathbf{k}}(t)$ at $t = 0$.

Since the Hamiltonian is quadratic, all the information on the dynamics is encoded in its two-time functions, such as the Keldysh (G_K) and retarded (G_R) Green's functions, which are defined by [159]

$$\delta_{\mathbf{k},-\mathbf{k}'}\, i\, G_K(k,t,t') = \langle\{\phi_{\mathbf{k}}(t), \phi_{\mathbf{k}'}(t')\}\rangle\,, \tag{4.12}$$

$$\delta_{\mathbf{k},-\mathbf{k}'}\, i\, G_R(k,t,t') = \theta(t-t')\,\langle[\phi_{\mathbf{k}}(t), \phi_{\mathbf{k}'}(t')]\rangle\,, \tag{4.13}$$

where $\delta_{\mathbf{k},\mathbf{k}'} \equiv (2\pi)^d\,\delta^{(d)}(\mathbf{k}-\mathbf{k}')$, while $\theta(t<0) = 0$ and $\theta(t\geq 0) = 1$. Accordingly, $r_{\mathrm{eff}}(t)$ in Eq. (4.6) can be expressed in terms of G_K as

$$r_{\mathrm{eff}}(t) = r_0 + \frac{u}{12}\int \frac{\mathrm{d}^d k}{(2\pi)^d}\; i\, G_K(k,t,t)\, h\!\left(\frac{k}{\Lambda}\right). \tag{4.14}$$

By using Eq. (4.8) in Eqs. (4.12) and (4.13), we find that $G_{K,R}$ can be written in terms of the function $f_{\mathbf{k}}$ as:

$$i\, G_K(k,t,t') = 2\,\Re\mathrm{e}\left[f_{\mathbf{k}}(t) f^{\star}_{\mathbf{k}}(t')\right], \tag{4.15}$$

$$G_R(k,t,t') = 2\,\theta(t-t')\,\Im\mathrm{m}\left[f_{\mathbf{k}}(t) f^{\star}_{\mathbf{k}}(t')\right]. \tag{4.16}$$

The dynamics of the system can be determined by solving the set of self-consistent equations given by Eqs. (4.10), (4.14), and (4.15). Generically, these equations do not admit an analytic solution and therefore one has to resort to numerical integration. Nevertheless, in the following section, we show that some quantities can be analytically calculated when the postquench Hamiltonian is close to the dynamical critical point.

4.2 Dynamical phase transition and scaling equations

In Refs. [116–118] it was shown that, after the quench, the system approaches a stationary state, in which the effective Hamiltonian becomes time-independent. Such a stationary state was then argued to be nonthermal as a consequence of the integrability of the model. In particular, in Ref. [118], it was demonstrated that when the bare mass r_0 in Eq. (4.1) is tuned to a critical value r_0^c, the long-time limit r_* of the corresponding effective mass $r_{\rm eff}(t)$ in Eq. (4.5) vanishes and therefore the fluctuations of the order parameter become critical, signaling the occurrence of a DPT. More precisely, as a consequence of the divergence of the spatial correlation length $\xi \equiv (r_*)^{-1/2}$, the correlation functions at long times acquire scaling forms characterized by universal critical exponents.

Similarly to the case of classical systems after a quench of the temperature [151], the correlation functions exhibit dynamical scaling forms not only in the steady state, but also while approaching it [119]: in particular, relying on dimensional analysis and on the lack of additional time and length scales at $r_0 = r_0^c$, one expects the effective value $r_{\rm eff}(t)$ to scale as

$$r_{\rm eff}(t) = \frac{a}{t^2}\,\sigma(\Lambda t), \tag{4.17}$$

where the function $\sigma(x)$ is normalized by requiring $\sigma(\infty) = 1$, such that $r_{\rm eff}(t)$ vanishes at long times as

$$r_{\rm eff}(t) = \frac{a}{t^2} \quad \text{for } \Lambda t \gg 1, \tag{4.18}$$

while a is a dimensionless quantity. The nonuniversal corrections introduced by $\sigma(\Lambda t) - 1$ to this long-time limit are negligible for $\Lambda t \gg 1$. On the contrary, for $\Lambda t \lesssim 1$, they become dominant and nonuniversal behavior is displayed. Accordingly, one can identify a *microscopic time* [119] $t_\Lambda \simeq \Lambda^{-1}$ which separates these two regimes: for $0 \leq t \lesssim t_\Lambda$ the dynamics is dominated by nonuniversal microscopic details; for $t \gtrsim t_\Lambda$, instead, the dynamics becomes universal. This discussion assumes that the function $\sigma(x)$ has a well-defined limit as $x \to \infty$, which might not be the case in the presence of oscillatory terms. In fact, as shown in the numerical analysis presented in Sec. 4.3, the nonuniversal function $\sigma(x)$ depends on how the cutoff Λ is implemented in the model, i.e., on the choice of the function $h(x)$ in Eq. (4.14). In particular, the choice of a sharp cutoff turns out to make $\sigma(x)$ oscillate, masking the universal long-time behavior $r_{\rm eff}(t) \sim t^{-2}$.

As a consequence of the universal form of Eq. (4.18) for $t \gtrsim t_\Lambda$, the correlation functions are expected to exhibit scaling properties. In order to show this, it

is convenient to rescale time and write the function $f_{\mathbf{k}}(t)$ as $f_{\mathbf{k}}(t) = g_{\mathbf{k}}(kt)$. Inserting Eq. (4.18) into Eq. (4.10), one finds the equation for $g_{\mathbf{k}}(x)$,

$$g''_{\mathbf{k}}(x) + \left(1 + \frac{a}{x^2}\right) g_{\mathbf{k}}(x) = 0, \tag{4.19}$$

valid for $x \equiv kt \gtrsim kt_\Lambda$, whose solution is

$$g_{\mathbf{k}}(x) = \sqrt{x}\,(A_{\mathbf{k}} J_\alpha(x) + B_{\mathbf{k}} J_{-\alpha}(x))\,, \tag{4.20}$$

where $J_\alpha(x)$ is the Bessel function of the first kind and

$$\alpha = \sqrt{\frac{1}{4} - a}. \tag{4.21}$$

Below we show that it is consistent to assume $a < 1/4$ and therefore α to be real. The constants $A_{\mathbf{k}}$ and $B_{\mathbf{k}}$ in Eq. (4.20) are fixed by the initial condition of the evolution, as discussed below. For later reference, we recall that

$$J_\alpha(x) \simeq \begin{cases} (x/2)^\alpha/\Gamma(1+\alpha), & \text{for } x \ll 1, \\ \cos(x - \alpha\pi/2 - \pi/4)\sqrt{2/(\pi x)}, & \text{for } x \gg 1, \end{cases} \tag{4.22}$$

where $\Gamma(x)$ is the Euler Γ function [160]. Note that Eq. (4.20) encodes the complete dependence of $f_{\mathbf{k}}(t)$ on time t for $t \gtrsim t_\Lambda$, whereas its dependence on the wave vector $\mathbf{k}$ is encoded in the yet unknown functions $A_{\mathbf{k}}$ and $B_{\mathbf{k}}$. By using the following identity for the Wronskian of Bessel functions [160]

$$J_\alpha(x) J'_{-\alpha}(x) - J_{-\alpha}(x) J'_\alpha(x) = -\frac{2\sin(\alpha\pi)}{\pi x}, \tag{4.23}$$

one can show that Eq. (4.9) requires the coefficients $A_{\mathbf{k}}$, $B_{\mathbf{k}}$ to satisfy the relation

$$\Im\mathrm{m}\,[A_{\mathbf{k}} B^\star_{\mathbf{k}}] = -\frac{\pi}{4\sin(\alpha\pi)}\,\frac{1}{k}. \tag{4.24}$$

This relation is not sufficient in order to determine completely $A_{\mathbf{k}}$ and $B_{\mathbf{k}}$ unless the full functional form of $r_{\mathrm{eff}}(t)$ is taken into account, including its nonuniversal behavior for $t \lesssim t_\Lambda$; this would allow us to fix $A_{\mathbf{k}}$ and $B_{\mathbf{k}}$ on the basis of the initial conditions for the evolution, which at present cannot be reached from Eq. (4.20), being it valid only for $t \gtrsim t_\Lambda$. However, for a deep quench —such as that one investigated in Ref. [119]— with $\Omega_0 \gg \Lambda$, the initial conditions (4.11) for the evolution of $f_{\mathbf{k}}(t)$ become essentially independent of $\mathbf{k}$ and read

$$f_{\mathbf{k}}(0) \simeq \frac{1}{\sqrt{2\Omega_0}}, \quad \dot{f}_{\mathbf{k}}(0) \simeq -\,i\,\sqrt{\frac{\Omega_0}{2}}. \tag{4.25}$$

At time $t \simeq t_\Lambda \simeq \Lambda^{-1}$, $f_{\mathbf{k}}(t_\Lambda)$ can be calculated from a series expansion $f_{\mathbf{k}}(t_\Lambda) = f_{\mathbf{k}}(0) + t_\Lambda \dot{f}_{\mathbf{k}}(0) + t_\Lambda^2 \ddot{f}_{\mathbf{k}}(0) + O(t_\Lambda^3)$ and by using Eqs. (4.10) and (4.25) one may readily conclude that its dependence on k comes about via $(k/\Lambda)^2$ and $k/(\Omega_0 \Lambda)$; accordingly, at the leading order, it can be neglected for $k \ll \Lambda$. On the other hand, $f_{\mathbf{k}}$ at t_Λ can be evaluated from Eq. (4.20) and, since $k t_\Lambda \simeq k/\Lambda \ll 1$, we can use the asymptotic form of the Bessel functions for small arguments, finding

$$f_{\mathbf{k}}(t_\Lambda) \propto A_{\mathbf{k}} \left(\frac{k}{\Lambda}\right)^{1/2+\alpha} + B_{\mathbf{k}} \left(\frac{k}{\Lambda}\right)^{1/2-\alpha} . \tag{4.26}$$

In order to have $f_{\mathbf{k}}(t_\Lambda)$ independent of $\mathbf{k}$ at the leading order, it is then necessary that

$$A_{\mathbf{k}} \simeq A \left(\frac{k}{\Lambda}\right)^{-1/2-\alpha} , \quad B_{\mathbf{k}} \simeq B \left(\frac{k}{\Lambda}\right)^{-1/2+\alpha} , \tag{4.27}$$

where A and B are yet unknown complex numbers. While this scaling is expected to be true for $k \ll \Lambda$, nonuniversal corrections may appear for $k \simeq \Lambda$. Note that Eq. (4.27) is consistent with (4.24), provided that

$$\Im\mathrm{m}\left[A B^\star\right] = -\frac{\pi}{4 \sin(\alpha\pi)} \frac{1}{\Lambda}. \tag{4.28}$$

The numerical analysis discussed in Sec. 4.3 actually shows that $A_{\mathbf{k}}$ turns out to be purely imaginary, while $B_{\mathbf{k}}$ is real. Combining Eqs. (4.27) with (4.20), (4.15), and (4.16), one finds a simple form for the retarded Green's function

$$G_R(k,t,t') = -\theta(t-t') \frac{\pi}{2 \sin \alpha\pi} \sqrt{t t'} \left[J_\alpha(kt) J_{-\alpha}(kt') - J_{-\alpha}(kt) J_\alpha(kt')\right] , \tag{4.29}$$

while the one for $i\,G_K(k,t,t')$ is somewhat lengthy and thus we do not report it here explicitly. In order to determine a and therefore α from the self-consistent condition in Eq. (4.14), it is actually sufficient to know $i\,G_K(k,t,t')$ for $t = t'$, which is given by

$$\begin{aligned} i\,G_K(k,t,t) = 2\Lambda t \Bigg[& |A|^2 \left(\frac{k}{\Lambda}\right)^{-2\alpha} J_\alpha^2(kt) + |B|^2 \left(\frac{k}{\Lambda}\right)^{2\alpha} J_{-\alpha}^2(kt) \\ & + 2\,\Re\mathrm{e}\left[A B^\star\right] J_\alpha(kt) J_{-\alpha}(kt) \Bigg] . \end{aligned} \tag{4.30}$$

Accordingly, while Eq. (4.24) is sufficient in order to determine the complete form of G_R, the one of G_K still contains unknown coefficients A and B which are eventually determined by the initial conditions; nevertheless, the scaling properties of both of these functions are already apparent. In fact, their dynamics is characterized

by two temporal regimes, which we refer to as *short* ($kt \ll 1$) and *long* ($kt \gg 1$) *times*. Stated differently, the temporal evolution of each mode $\mathbf{k}$ has a typical time scale $\sim k^{-1}$ determined by the value of the momentum itself and the corresponding short-time regime extends to macroscopically long times for vanishing momenta.

Let us focus on G_R in Eq. (4.29): at short times $t' < t \ll k^{-1}$ it becomes independent of k

$$G_R(k,t,t') \simeq -\frac{t}{2\alpha}\left(\frac{t'}{t}\right)^{1/2-\alpha}\left[1-\left(\frac{t'}{t}\right)^{2\alpha}\right], \tag{4.31}$$

where we used the asymptotic expansion in Eq. (4.22). For well-separated times $t \gg t'$, the second term in brackets is negligible and $G_R(k, t \gg t', t')$ displays an algebraic dependence on the ratio t'/t. At long times $k^{-1} \ll t', t$, instead, G_R becomes time-translational invariant and, by keeping the leading order of the asymptotic expansion of the Bessel functions in Eq. (4.22), it reads

$$G_R(k,t,t') \simeq -\theta(t-t')\,\frac{\sin\left(k(t-t')\right)}{k}, \tag{4.32}$$

which is nothing but the G_R of a critical Gaussian Hamiltonian ($u = 0$) after a deep quench [119].

Similarly, at short times $t \ll k^{-1}$ and to leading order in Λt, $G_K(k,t,t)$ reads (see Eqs. (4.30) and (4.22))

$$i\,G_K(k,t,t) \simeq \frac{2^{1-2\alpha}\,|A|^2}{\Gamma^2(1+\alpha)}\,(\Lambda t)^{1+2\alpha}\,, \tag{4.33}$$

which is independent of the momentum k, as it is the case for G_R within the same temporal regime. At long times $t \gg k^{-1}$, instead, one finds

$$i\,G_K(k,t,t) \simeq \frac{2|A|^2}{\pi}\left(\frac{\Lambda}{k}\right)^{1+2\alpha}, \tag{4.34}$$

to leading order in k/Λ, where the possible oscillating terms have been neglected, as they are supposed to average to zero when an integration over momenta is performed. The resulting expression turns out to be time-independent and, contrary to what happens with G_R, it *does not* correspond to the G_K of a critical Gaussian theory after a deep quench [119], reported further below in Eq. (4.35). This fact should be regarded as a consequence of the nonthermal nature of the stationary state which is eventually reached by the system and which retains memory of the initial state. Since the effective Hamiltonian (4.5) is Gaussian, it is tempting to interpret the anomalous momentum dependence $\sim k^{-1-2\alpha}$ in Eq. (4.34) in terms of a quench in

a truly Gaussian theory. In the latter case, it was shown [4, 158, 161] that, for deep quenches,

$$i\,G_K(k,t,t) \simeq \frac{\Omega_0}{2k^2}, \tag{4.35}$$

which is similar to an equilibrium distribution with an effective temperature $T_{\rm eff} \simeq \Omega_0$. Accordingly, Eq. (4.34) can be regarded as resulting from a quench of a Gaussian theory with a momentum-dependent initial "temperature" $\Omega_0(k) \sim k^{1-2\alpha}$.

Eqs. (4.33) and (4.34) show that the term proportional to $|A|^2$ in the expression (4.30) of $G_K(k,t,t)$ is dominant at both long and short times: accordingly, we can neglect the remaining ones and the Keldysh Green's function with two different times t, t' acquires the scaling form

$$i\,G_K(k,t,t') = 2|A|^2 \left(\frac{\Lambda}{k}\right)^{1+2\alpha} \sqrt{k^2tt'}J_\alpha(kt)J_\alpha(kt'), \tag{4.36}$$

which can be derived from Eqs. (4.20), (4.27), and (4.15). This expression can now be used in order to derive from Eq. (4.14) the value of the constant a and therefore of the exponent α (see Eq. (4.21)) which characterizes the scaling forms (4.29) and (4.36). For $\Lambda t \gg 1$ one can approximate $r_{\rm eff}(t)$ with Eq. (4.18) and, by assuming a sharp cutoff $h(x) = \theta(1-x)$, Eq. (4.14) becomes

$$\frac{a}{t^2} = r_0^c + \frac{a_d}{6}\,|A|^2\,u\,\Lambda^d\,\mathcal{I}_{d,\alpha}(\Lambda t) \tag{4.37}$$

at the critical value $r_0 = r_0^c$. In this expression we introduced the function

$$\mathcal{I}_{d,\alpha}(x) = x\int_0^1 {\rm d}y\; y^{d-1-2\alpha}\,J_\alpha^2(xy), \tag{4.38}$$

while $a_d = \Omega_d/(2\pi)^d$ with $\Omega_d = 2\pi^{d/2}/\Gamma(d/2)$ the d-dimensional solid angle. Expanding $\mathcal{I}_{d,\alpha}(x)$ for large arguments $x \gg 1$, one finds that

$$\mathcal{I}_{d,\alpha}(x) = W_{d,\alpha}(x) + c_{d,\alpha}^{(0)} + \frac{c_{d,\alpha}^{(1)}}{x^{d-1-2\alpha}} + \frac{c_{d,\alpha}^{(2)}}{x^2} + O\left(\frac{1}{x^4}\right), \tag{4.39}$$

where $W_{d,\alpha}(x)$ is a fast oscillating function which is a consequence of the sharp cutoff considered in the integral over momenta and $c_{d,\alpha}^{(i)}$ are certain coefficients, the relevant values of which are provided further below. Once the expansion of $\mathcal{I}_{d,\alpha}(x)$ is plugged into Eq. (4.37), the r.h.s. of this equation can be expanded in decreasing powers of Λt which have to match the term on its l.h.s., resulting in a set of conditions fixing the values of r_0^c, α, and u. Notice that the oscillations contained in $W_{d,\alpha}(x)$ would be compensated by subleading terms in the l.h.s. of Eq. (4.37) (which are not

reported), thus confirming the nonuniversal nature of $W_{d,\alpha}(x)$. The value of r_0^c is determined such as to cancel the constant contribution $\propto c_{d,\alpha}^{(0)}$ on the r.h.s., while α has to be fixed such that $c_{d,\alpha}^{(1)} = 0$ in order to cancel the term $\propto (\Lambda t)^{1+2\alpha-d}$ which cannot be matched by the l.h.s. of Eq. (4.37) [1]. This procedure —typically used for solving this kind of self-consistent equations [150, 162, 163]— can be regarded as a systematic way of canceling terms which result from corrections to scaling and, therefore, it allows a comparison with the results obtained within a renormalization group approach (with some exceptions, see Ref. [163]). For our purposes, it is sufficient to focus on the condition

$$c_{d,\alpha}^{(1)} = \frac{1}{2\sqrt{\pi}} \frac{\Gamma\left(\frac{1}{2} - \frac{d}{2} + \alpha\right) \Gamma\left(\frac{d}{2}\right)}{\Gamma\left(1 - \frac{d}{2} + \alpha\right) \Gamma\left(1 - \frac{d}{2} + 2\alpha\right)} = 0, \tag{4.40}$$

which is solved by requiring the argument of one of the two Γ functions in the denominator to equal a nonpositive integer. The two corresponding infinite sets of solutions $\mathcal{S}'$ and $\mathcal{S}$ for α are given by

$$\mathcal{S}' = \left\{ \frac{d-2}{2} - n \right\}_{n \geq 0}, \quad \mathcal{S} = \left\{ \frac{d-2}{4} - \frac{n}{2} \right\}_{n \geq 0}, \tag{4.41}$$

with integer n. The physically relevant one can be selected by requiring a to match its Gaussian value $a = 0$ (or, equivalently, $\alpha = 1/2$, see Eq. (4.21)) at the upper critical dimensionality $d_c = 4$ of the model [118, 119]. Note that this Gaussian value of a can be easily inferred by inspecting the scaling behavior of $G_{K,R}$ for the quench towards a noninteracting theory (compare, e.g., Eqs. (4.34) and (4.35)). Accordingly, one finds a single possible solution from $\mathcal{S}$, i.e.,

$$\alpha = \frac{d-2}{4} \quad \text{and} \quad a = \frac{d}{4}\left(1 - \frac{d}{4}\right), \tag{4.42}$$

with $a > 0$ for all values of d between $d_l = 2$ and $d_c = 4$, while for $d > 4$ the Gaussian theory applies and therefore

$$\alpha = \frac{1}{2} \quad \text{and} \quad a = 0. \tag{4.43}$$

[1] In passing we mention that, alternatively, one might require the exponent of this term to equal the one on the l.h.s. of Eq. (4.37), i.e., $1 + 2\alpha - d = -2$. Correspondingly, the divergence of $c_{d,\alpha}^{(2)} \propto a/[2\pi(3 + 2\alpha - d)]$ cancels the one of $c_{d,\alpha}^{(1)}$ reported in Eq. (4.40): the eventual contribution $\propto t^{-2}$ on the r.h.s. of Eq. (4.37) is finite but negative and it would therefore require an unphysical negative value of the coupling constant u in order to match the term on the l.h.s. of the same equation.

For $d \geq d_c$, $c^{(2)}_{d,\alpha} \propto a$ vanishes and the leading temporal dependence of the r.h.s. of Eq. (4.37) at long times is $\propto c^{(1)}_{d,\alpha=1/2}(\Lambda t)^{-(d-2)}$ and therefore

$$r_{\rm eff}(t) \propto (\Lambda t)^{-(d-2)}\,, \tag{4.44}$$

up to oscillating terms, instead of the behavior $\propto t^{-2}$ in Eq. (4.18). Eqs. (4.42) and (4.43) together with Eqs. (4.29) and (4.36) completely characterize the scaling behavior of $G_{K,R}$ after a deep quench to the critical point. These results can be compared with the predictions of Ref. [119], formulated with a dimensional expansion around the upper critical dimensionality d_c of the $O(N)$ model, which is expected to reduce to the present one for $N \to \infty$. There, the time dependence of $G_{K,R}$ for $kt, kt' \ll 1$ and $t' \ll t$ was parametrized in terms of the exponent θ as

$$G_K(k,t,t') \propto \left(tt'\right)^{1-\theta} \quad \text{and} \quad G_R(k,t,t') \propto -t\left(\frac{t'}{t}\right)^{\theta}, \tag{4.45}$$

from which it follows that θ is related to the exponent α introduced in Eqs. (4.29) and (4.36) by $\theta = 1/2 - \alpha$. Moreover, it was found in Ref. [119] that $\theta = \epsilon/4 + O(\epsilon^2)$ with $\epsilon \equiv 4 - d$, in agreement with Eq. (4.42), which yields $\theta = 1 - d/4$ for $d < 4$.

We note here that among the remaining solutions of Eq. (4.40) in $\mathcal{S}$ and $\mathcal{S}'$ which do not match the Gaussian value at $d = d_c$, only one turns out to be compatible with having a positive value of the coupling constant u in Eq. (4.37). This solution belongs to $\mathcal{S}'$, and is given by

$$\alpha_{\rm co} = \frac{d-2}{2} \qquad \text{with} \qquad a_{\rm co} = \frac{(3-d)(d-1)}{4}; \tag{4.46}$$

remarkably, it turns out to be related to the coarsening occurring after a quench to $r_0 < r_0^c$, as we argue and demonstrate further below.

4.3 Numerical results

In order to test the quality of the analytical predictions of the previous section, we studied in detail the numerical solution of the evolution equation (4.10) for $f_{\mathbf{k}}(t)$, under the constraint provided by Eq. (4.14), with $G_K(k,t,t)$ given by Eq. (4.15).

In Sec. 4.3.1 we consider the case of a quench to the critical point, comparing the numerical results for the relevant correlation functions with the analytical predictions derived in Sec. 4.2. In Sec. 4.3.2 we present, instead, results for a quench below the critical point, and show some numerical evidence of the emergence of scaling properties during coarsening.

4.3.1 Quench to the critical point

In order to determine the critical value r_0^c of the bare mass r_0 in Eq. (4.1) one can conveniently use the ansatz proposed in Ref. [118], i.e.,

$$r_0^c = -\frac{u}{4!}\int \frac{\mathrm{d}^d k}{(2\pi)^d}\,\frac{2k^2+\Omega_0^2}{k^2\sqrt{k^2+\Omega_0^2}}\,h\!\left(\frac{k}{\Lambda}\right), \tag{4.47}$$

which turns out to correctly predict r_0^c also beyond the case of a deep quench. The rationale behind this ansatz relies on the assumption that $G_K(k,t,t)$ at $t\to\infty$ has approximately the same form as for the case of a quench to $r_0 = 0$ in the noninteracting case $u = 0$ [156]. Although the validity of this assumption for a quench to the critical point is questionable because, as shown in Sec. 4.2, G_K differs significantly from the noninteracting case $u = 0$ (see, e.g., Ref. [119]), Eq. (4.47) anyhow provides accurate predictions for the value of r_0^c.

The accuracy of the ansatz (4.18) for the long-time behavior of $r_{\mathrm{eff}}(t)$ can be tested by calculating $r_{\mathrm{eff}}(t)$ according to Eqs. (4.14) and (4.15), based on the numerical solution of the evolution equation (4.10) for $f_{\mathbf{k}}(t)$.

In Fig. 4.2 we show the time dependence of $r_{\mathrm{eff}}(t)$ after a deep quench. In particular, Figure 4.2(a) demonstrates, in spatial dimension $d = 3.4$, that while $r_{\mathrm{eff}}(t)$ at long times approaches a finite value for $r_0 > r_0^c$, it generically vanishes for both $r_0 = r_0^c$ and $r_0 < r_0^c$. In particular, the corresponding decay turns out to be $\sim t^{-2}$ in both cases, as indicated by the dashed lines, in agreement with the ansatz (4.18) at criticality. Such an algebraic behavior actually sets in after some time $t_\Lambda \sim O(\Lambda^{-1})$, where Λ is the cutoff employed in the algorithm. As expected, the actual possibility of detecting this algebraic decay depends on the way the model is regularized, i.e., on the specific function $h(x)$ used in Eq. (4.14) in order to introduce the cutoff Λ. This is illustrated by Figure 4.2(b) for a quench at criticality $r_0 = r_0^c$ in $d = 3$, in which the momentum integral in Eq. (4.14) is regularized with a sharp cutoff $h(x) = \theta(1-x)$ or with a smooth exponential $h(x) = \mathrm{e}^{-x}$ or Gaussian $h(x) = \mathrm{e}^{-x^2/2}$ function, with characteristic scale Λ. Note that the value of r_0^c is also affected by this choice, according to Eq. (4.47). While the sharp cutoff causes persistent oscillations in $r_{\mathrm{eff}}(t)$, which mask the expected behavior $\sim t^{-2}$, the smooth ones are qualitatively similar and they reveal this algebraic decay after some time t_Λ. The persistent oscillations displayed for a sharp cutoff function are expected to be subleading compared to the Λ-independent decay $\sim t^{-2}$ in a formal expansion in decreasing powers of Λ: accordingly, their amplitude is expected to decrease as Λ increases. This is clearly demonstrated by the curves in Figure 4.2(c), which slowly approach the expected algebraic behavior (dashed

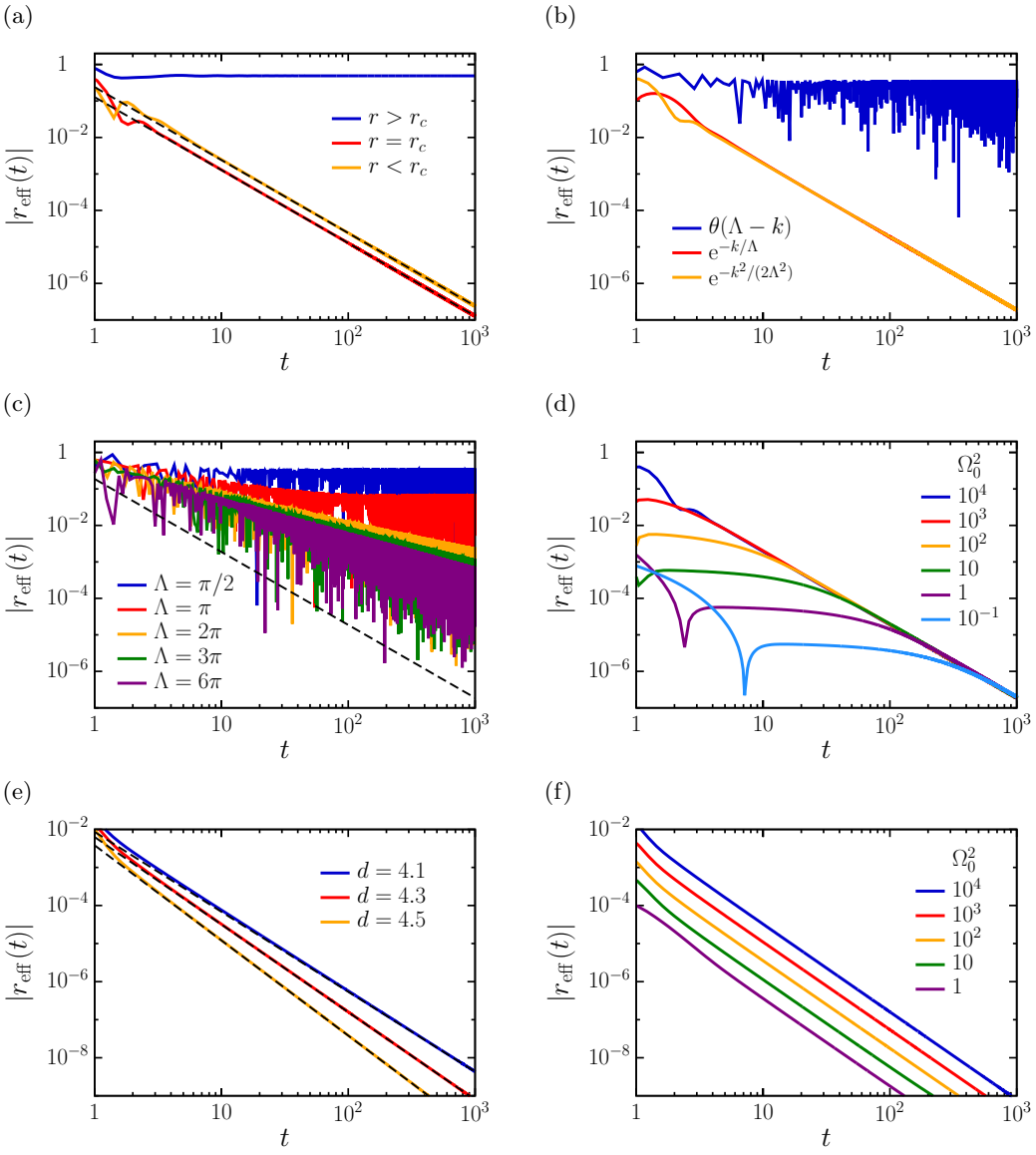

Figure 4.2: Effective mass $r_{\rm eff}$ as a function of time t. (a) $r_{\rm eff}$ for a quench above, at, and below the critical point r_0^c in $d = 3.4$. The black dashed lines indicate an algebraic decay $\sim t^{-2}$. (b) $r_{\rm eff}$ at $r_0 = r_0^c$ for the various cutoff functions with $\Lambda = \pi/2$ in $d = 3$. (c) $r_{\rm eff}$ at $r_0 = r_0^c$ for a sharp cutoff function with various values of Λ in $d = 3$. The black dashed line indicates the expected algebraic decay $\sim t^{-2}$. (d) $r_{\rm eff}$ at $r_0 = r_0^c$ for various values of the initial mass Ω_0^2, in $d = 3$. (e) $r_{\rm eff}$ at $r_0 = r_0^c$ for various values of $d > d_c = 4$. The black dashed lines indicate an algebraic decay $\sim t^{-(d-2)}$. (f) $r_{\rm eff}$ at $r_0 = r_0^c$ for various values of Ω_0 in $d = 4.3$.

line) upon increasing the value of Λ. Accordingly, in order to detect the universal behavior $\sim t^{-2}$ in the presence of a sharp cutoff, very large values of Λ have to be used, resulting in a longer computational time with respect to that required by an exponential or Gaussian cutoff function $h(x)$. The onset of a scaling regime for $r_{\rm eff}(t)$ for a quench at criticality is also expected to be influenced by the value of the prequench mass Ω_0^2, as discussed in Sec. 4.2 and in Ref. [119]. In particular, while the analytic investigation in Sec. 4.2 assumes a deep quench, i.e., $\Omega_0 \gg \Lambda$, it is instructive to check numerically how the actual value of Ω_0 influences the time t_Λ after which the expected universal algebraic behavior $\sim t^{-2}$ sets in. The curves in Figure 4.2(d) show that t_Λ increases significantly upon decreasing the value of Ω_0^2, until the eventual algebraic behavior is completely masked by the initial nonuniversal transient occurring at $t < t_\Lambda$ when $\Omega_0 \ll \Lambda$. If the spatial dimensionality d of the model is larger than the upper critical dimensionality $d_c = 4$, the leading-order temporal decay of $r_{\rm eff}(t)$ is no longer proportional to t^{-2}, because the corresponding proportionality constant a vanishes (see Eq. (4.18)). In this case, $r_{\rm eff}(t)$ still vanishes at long times with the algebraic law $\sim t^{-(d-2)}$ given in Eq. (4.44). This dependence is shown in Figure 4.2(e) for $d = 4.1$, 4.3, and 4.5. The theoretical prediction for the exponent of this decay is indicated by the corresponding dashed lines, while its prefactor is a nonuniversal constant which depends —in contrast to the case $d < 4$— on the actual values of the parameters of the system, e.g., Ω_0, as shown in Figure 4.2(f) for $d = 4.3$.

As discussed in Sec. 4.2, the scaling behavior of $r_{\rm eff}(t)$ implies the emergence of an algebraic dependence on time in $G_{K,R}$, numerical evidences for which are presented in Figure 4.3 for a deep quench occurring in $d = 3$. In particular, $G_K(k,t,t)$ at criticality is expected to display the short-time scaling in Eq. (4.33) for $t \ll k^{-1}$ (which actually extends to long times for $k = 0$), while in the long-time limit $t \gg k^{-1}$, G_K displays (up to oscillating terms) the scaling in Eq. (4.34) as a function of k. In order to corroborate these predictions, Figure 4.3(a) and 4.3(b) show the dependence on time t and momentum k, respectively, of G_K within these two regimes, for quenches occurring at $r_0 > r_0^c$, $r_0 = r_0^c$, and $r_0 < r_0^c$. Figure 4.3(a) demonstrates that $G_K(k = 0, t, t)$, after a quench to criticality, grows in time as $\sim t^{3/2}$ in agreement with Eqs. (4.33) and (4.42) for $d = 3$. If the quench occurs above criticality, instead, G_K displays oscillations with an asymptotic period $\propto \xi = (r_*)^{-1/2}$, where $r_* = r_{\rm eff}(t \to \infty)$ as expected on general grounds [119]. Remarkably, an algebraic behavior $\sim t^2$ emerges for quenches occurring below the critical point (i.e., with $r_0 < r_0^c$), which signals that the corresponding coarsening

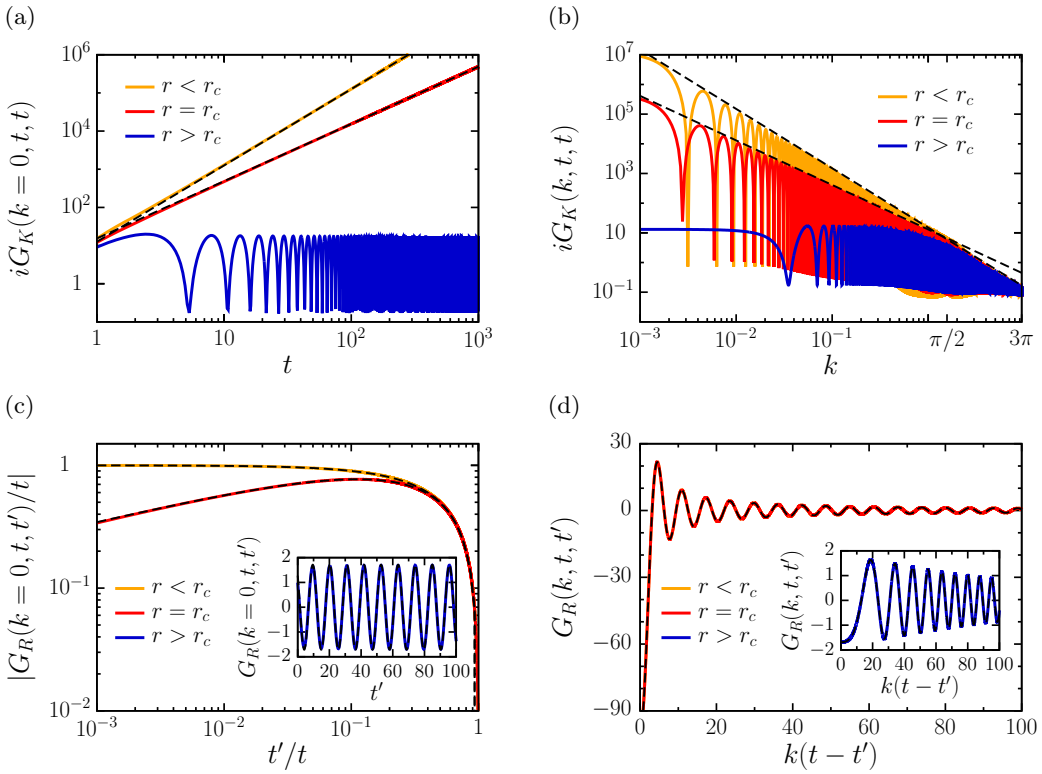

Figure 4.3: Keldysh (G_K) and retarded (G_R) Green's functions. (a) $G_K(k,t,t)$ at $k = 0$ and equal times as a function of time t for a quench above, at, and below the critical point r_0^c in $d = 3$. The black dashed lines superimposed on the curves for $r_0 = r_0^c$ and $r_0 < r_0^c$ are proportional to $t^{3/2}$ and t^2, respectively. (b) $G_K(k,t,t)$ at equal times $t = 10^3$ as a function of momentum k (cutoff $\Lambda = \pi/2$) for a quench above, at, and below the critical point r_0^c in $d = 3$. The black dashed lines superimposed on the curves for $r_0 = r_0^c$ and $r_0 < r_0^c$ are proportional to $k^{-3/2}$ and k^{-2}, respectively. (c) Main plot: $|G_R(k,t,t')/t|$ for $k = 0$ and $t = 2 \times 10^3$ as a function of t'/t for a quench at and below the critical point r_0^c in $d = 3$. The black dashed lines superimposed on the curves for $r_0 = r_0^c$ and $r_0 < r_0^c$ indicate the analytical predictions $2\,\Xi_{1/4}(t'/t)$ and $\Xi_{1/2}(t'/t)$, respectively. Inset: $G_R(k,t,t')$ for $k = 0$ and $t = 2 \times 10^3$ as a function of t' for a quench above the critical point r_0^c in $d = 3$. The black dashed line indicates the analytical prediction in Eq. (4.32) with $k \to \sqrt{r_*}$ and $r_* \simeq 0.34$. (d) $G_R(k,t,t')$ for $t = 2 \times 10^3$ and $t' = 1.9 \times 10^3$ as a function of $k\,(t-t')$ (cutoff $\Lambda = \pi/2$) for a quench above (inset), at, and below the critical point r_0^c in $d = 3$. Main plot: the superimposed black dashed line indicates the analytical prediction in Eq. (4.32). Inset: the superimposed black dashed line indicates the analytical prediction in Eq. (4.32) with $k \to \sqrt{k^2 + r_*}$ and $r_* \simeq 0.34$.

occurs on a dynamical length scale which grows in time [164]. Further below (see Figure 4.5), we discuss the dependence of the power of this algebraic decay on the spatial dimensionality d. We anticipate here that the present law $\sim t^2$ agrees with what one would obtain by extending the scaling prediction in Eq. (4.33) to quenches below r_0^c and by using the value $\alpha_{\rm co} = 1/2$ from Eq. (4.46) instead of α. Figure 4.3(b), instead, reports the dependence on k of the value eventually reached by $G_K(k,t,t)$ at a fixed but long time $t \gg k^{-1}$. In particular, at criticality, $r_0 = r_0^c$, G_K approaches, up to oscillatory terms, the algebraic behavior $\sim k^{-3/2}$, in agreement with Eqs. (4.34) and (4.42) in $d = 3$. For $r_0 < r_0^c$, G_K still displays, up to oscillatory terms, an algebraic dependence on k, but with a different power $\sim k^{-2}$, which again agrees with the extension of the critical scaling form (4.34) below r_0^c, with α replaced with $\alpha_{\rm co}$. When the quench occurs, instead, above the critical point, G_K tends to a constant, up to oscillations. In all the cases illustrated in Figure 4.3, nonuniversal contributions affect the various curves for $k \gtrsim \Lambda = \pi/2$, due to the effects of the regularizing function $h(x)$. As far as $G_R(k,t,t')$ is concerned, Eq. (4.29) provides its complete expression within the scaling regime at criticality $r_0 = r_0^c$. In particular, $G_R(k = 0,t,t')$ acquires the scaling form (4.31), while $G_R(k,t,t')$ becomes time-translational invariant at long times $k^{-1} \ll t' < t$ as in Eq. (4.32). Figure 4.3(c) shows that $G_R(k = 0,t,t')/t$ with $t' < t$ becomes indeed a function of the ratio t'/t only. At criticality this agrees with what is expected on the basis of Eqs. (4.31) and (4.42) in $d = 3$ (which renders $\alpha = 1/4$), with $|G_R(k = 0,t,t')/t| \propto \Xi_{1/4}(t'/t)$, where we define

$$\Xi_\alpha(x) \equiv x^{1/2-\alpha} - x^{1/2+\alpha}. \tag{4.48}$$

For a quench below r_0^c, instead, the same quantity becomes $|G_R(k = 0,t,t')/t| \propto 1 - (t'/t)$; this agrees with $\Xi_{1/2}(t'/t)$, i.e., with what one would infer by extending the critical scaling function (4.31) below r_0^c and by using the value $\alpha_{\rm co} = 1/2$ in Eq. (4.46) for the exponent α. The inset shows, instead, the numerical data for $G_R(k = 0,t,t')$ after a quench to $r_0 > r_0^c$, as a function of t' and fixed $t > t'$, which is characterized by persistent oscillations. As mentioned above, for this kind of quench, $r_{\rm eff}(t)$ approaches a finite asymptotic value r_* at large times and, up to the leading order, the system behaves as a Gaussian model quenched at r_*, for which the response function is given by [119] Eq. (4.32) with $k \to \sqrt{k^2 + r_*}$. The dashed line reported in the inset of the figure corresponds to this theoretical prediction with $k = 0$ (see also Figure 4.3(d)), confirming its accuracy. Figure 4.3(d) shows $G_R(k,t,t')$ as a function of $k\,(t - t')$ for two fixed long times t and $t' < t$ and upon varying k. The main plot shows the corresponding numerical curves

both for $r_0 = r_0^c$ and $r_0 < r_0^c$, which are however perfectly superimposed on the theoretical prediction in Eq. (4.32), the latter being independent of the actual value of α. The inset, instead, shows G_R for $r_0 > r_0^c$: also in this case, the numerical data are indistinguishable from the corresponding theoretical prediction obtained on the basis of Eqs. (4.32) with $k \to \sqrt{k^2 + r_*}$, as explained above while illustrating Figure 4.3(c).

The numerical results presented in Figure 4.2 and 4.3 refer to a quench of the model in a certain spatial dimensionality d. In order to test both the predictions in Eq. (4.42) and some of the features of the scaling functions at criticality we repeated the analysis of the previous Figures for a variety of values of d, the results of which are reported in Figure 4.4. In particular, the long-time behavior of $r_{\rm eff}(t)$ after a quench at $r_0 = r_0^c$ (such as the one displayed for $d = 3.4$ in Figure 4.2(a)) can be fitted with the expected algebraic law $a\, t^{-2}$ in order to extract the value of a as a function of d. The resulting numerical estimates are indicated by the dots in Figure 4.4(a), where they are compared with the theoretical prediction in Eq. (4.42). While the agreement between the latter and the numerical data is very good for $d \lesssim 3.6$, slight deviations appear upon approaching the upper critical dimensionality $d_c = 4$ of the model, due to the expected corrections to scaling which are known to become increasingly relevant as $d \to d_c$ [163]. Analogously, by fitting the time dependence of the critical $i\, G_K(k = 0, t, t)$ with the algebraic law $\sim t^\gamma$, one can estimate the numerical value of γ as a function of d. These estimates, reported in Figure 4.4(b), can then be compared with the analytical prediction $\gamma \equiv 1+2\alpha = d/2$ for $d < 4$ and $\gamma = 2$ for $d \geq 4$ which follows from Eqs. (4.33), (4.42), and (4.43). Also in this case the agreement between the data and the analytical prediction is very good apart from a region around $d_c = 4$, where corrections to scaling make the extraction of the exponent from the data more difficult. While both of the previous evidences in favor of the theoretical predictions of Sec. 4.2 are based on the scaling properties of G_K and of $r_{\rm eff}(t)$, an independent and more stringent test is provided by the analysis of the response function G_R, whose analytical form in Eqs. (4.29) and (4.31) does not involve unknown parameters (such as those which fix, instead, the amplitude of $G_K(k = 0, t, t)$ in Eq. (4.33)). In particular, another estimate of α can be obtained by fitting $|G_R(k = 0, t, t')/t|$ with $C\, \Xi_\alpha(t'/t)$ as predicted by Eq. (4.31). The resulting values of α are reported in Figure 4.4(c) together with the analytical prediction of Eqs. (4.42) and (4.43). Alternatively, one can estimate the value of the proportionality constant C by fitting $|G_R(k = 0, t, t')/t|$ with $C\, \Xi_\alpha(t'/t)$ where α is now fixed to the theoretically expected value reported in

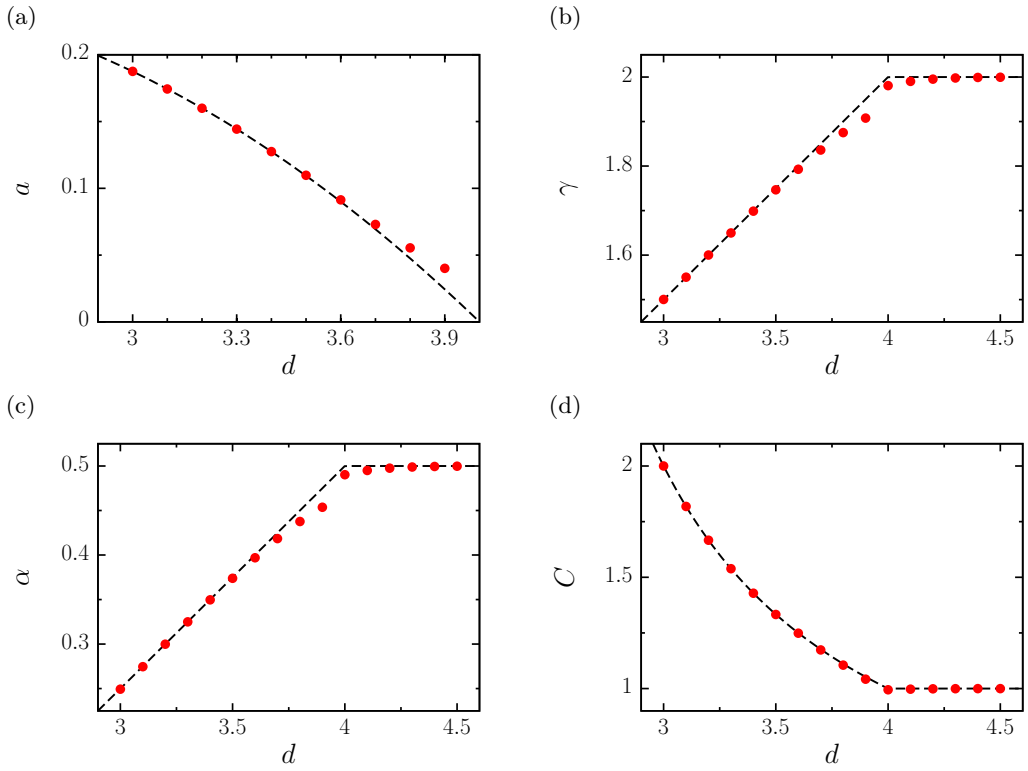

Figure 4.4: Numerical values (red dots) of exponents γ and α, and prefactors a and C as functions of the spatial dimensionality d for a quench at the critical point r_0^c. (a) Prefactor a obtained by fitting $r_{\rm eff}(t)$ as a/t^2. The black dashed line indicates the analytical value $a = d(1-d/4)/4$. (b) Exponent γ obtained by fitting $i\,G_K(k=0,t,t)$ with an algebraic law $\propto t^\gamma$. The black dashed line indicates the analytical value $\gamma = d/2$ for $d < 4$ and $\gamma = 2$ for $d \geq 4$. (c) Exponent α obtained by fitting $|G_R(k=0,t=2\times 10^3,t')/t|$ as $C\,\Xi_\alpha(t'/t)$. The black dashed line indicates the analytical value $\alpha = (d-2)/4$ for $d < 4$ and $\alpha = 1/2$ for $d \geq 4$. (d) Prefactor C obtained by fitting $|G_R(k=0,t=2\times 10^3,t')/t|$ as $C\,\Xi_\alpha(t'/t)$, with α given by the analytical value reported above. The black dashed line indicates the analytical value $C = 2/(d-2)$ for $d < 4$ and $C = 1$ for $d \geq 4$. The error bars on numerical data are smaller than the symbol size.

Eqs. (4.42) and (4.43). The resulting numerical estimates are indicated by the dots in Figure 4.4(d) together with the analytical prediction $C = 1/(2\alpha)$ which follows from Eq. (4.31) and from the theoretical values of α of Eqs. (4.42) and (4.43). Also for Figure 4.4(c), the agreement with theoretical predictions is good, except for values close to $d_c = 4$, while it is remarkably good for Figure 4.4(d).

Further below we argue that the exponent $\gamma = 1 + 2\alpha$ which describes the algebraic behavior of $G_K(k,t,t)$ at both short and long times (see Eqs. (4.33) and (4.34)) is the same as the one introduced in Ref. [118] in order to characterize the small-momentum behavior $\sim k^{-\gamma}$ of $\rho_{\mathbf{k}}(t)$ up to a cutoff $k^* \sim t^{-1}$. The quantity $\rho_{\mathbf{k}}(t)$ corresponds to the average number of excitations with momentum k of the prequench Hamiltonian which are produced after a so-called double quench, i.e., when the parameters of the postquench Hamiltonian are restored suddenly to their initial values after a time t has elapsed from the first quench occurring at $t = 0$ (more details on $\rho_{\mathbf{k}}(t)$ in Sec. 5.3). The values of γ which were numerically determined in Ref. [118] for a quench to the critical point in $d = 3$ and 4, i.e., $\gamma = 3/2$ and 2 are in perfect agreement with our numerical estimates and analytical predictions reported in Figure 4.4(b).

4.3.2 Quench below the critical point

The Keldysh (Figure 4.3(a) and 4.3(b)) and the retarded (Figure 4.3(c) and 4.3(d)) Green's functions G_K and G_R, respectively, for $r_0 > r_0^c$ are characterized by an oscillatory behavior, which denotes the presence of a finite length scale ξ in the model, set by the asymptotic value r_* of $r_{\rm eff}(t)$. On the contrary, for $r_0 < r_0^c$, the effective mass $r_{\rm eff}(t)$ turns out to decay to zero as $\simeq a_{\rm co}\, t^{-2}$ (see Figure 4.2(a)), i.e., with the same power law as at criticality: correspondingly, $G_{K,R}$ exhibit algebraic behaviors, which, however, differ from the critical ones. In fact, it is rather related to the phenomenon of *coarsening* which we discuss further below in Sec. 4.3.3. As we discussed in Sec. 4.2, the value of $a_{\rm co}$ —as well as of a for $r_0 = r_0^c$— can, in principle, be determined in such a way as to satisfy the self-consistent equations (4.37) and (4.40), which indeed admit two different solutions, reported in Eqs. (4.42) and (4.46). While the former correctly describes the observed behavior at criticality (see Figure 4.4), it is quite natural to expect the latter to describe the other possible scaling behavior, i.e., the one associated with coarsening. Numerical evidence of this fact is presented in Figure 4.5. In particular, Figure 4.5(a) shows the value of $a_{\rm co}$ for various values of d, as inferred by fitting the corresponding numerical data of $r_{\rm eff}(t)$ for $r_0 < r_0^c$ with $a_{\rm co}\, t^{-2}$. The dashed line corresponds to the theoretical prediction reported in Eq. (4.46). Although the numerical data reported in Figure 4.5 refer to a quench with $r_0 = -3 < r_0^c$, we have verified that these numerical estimates are not affected by the choice of $r_0 < r_0^c$. Note that while a at $r_0 = r_0^c$ as a function of the dimensionality d shows a marked change in behavior upon crossing the upper critical dimensionality $d_c = 4$ (see Figure 4.4(a)),

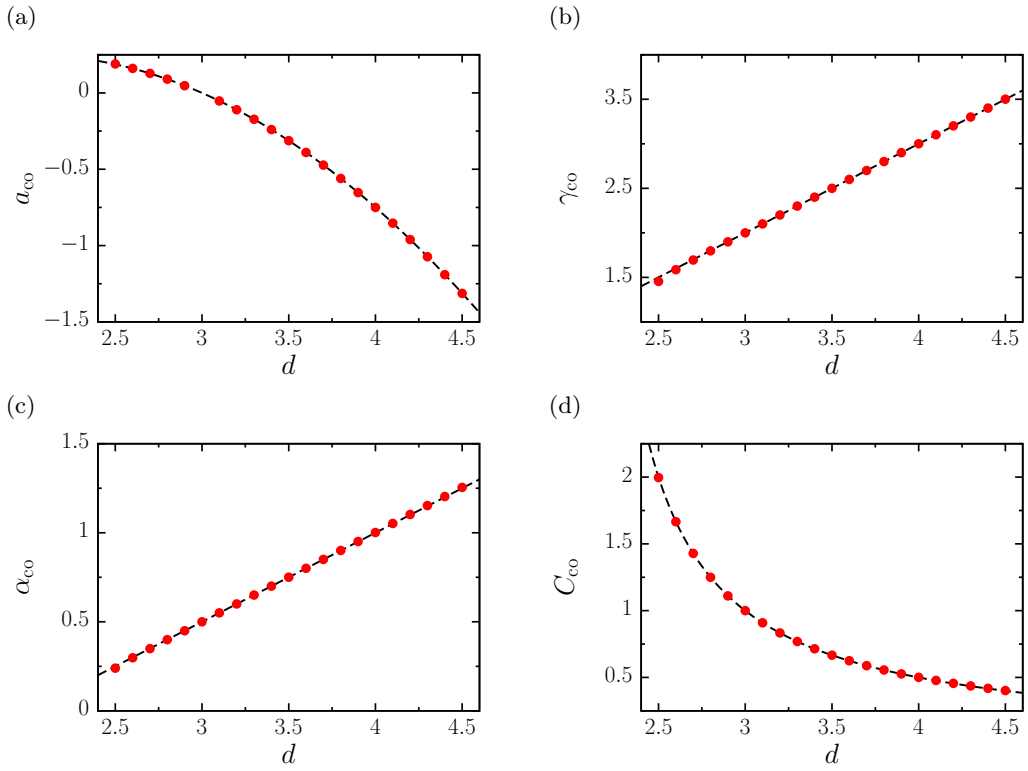

Figure 4.5: Numerical values (red dots) of exponents $\gamma_{\rm co}$ and $\alpha_{\rm co}$, and prefactors $a_{\rm co}$ and $C_{\rm co}$ as functions of the spatial dimensionality d for a quench below the critical point r_0^c. (a) Prefactor $a_{\rm co}$ obtained by fitting $r_{\rm eff}(t)$ as $a_{\rm co}/t^2$. The black dashed line indicates the analytical value $a_{\rm co} = (3-d)(d-1)/4$. (b) Exponent $\gamma_{\rm co}$ obtained by fitting $i\,G_K(k=0,t,t)$ with an algebraic law $\propto t^{\gamma_{\rm co}}$. The black dashed line indicates the analytical value $\gamma_{\rm co} = d-1$. (c) Exponent $\alpha_{\rm co}$ obtained by fitting $|G_R(k=0,t=2\times10^3,t')/t|$ as $C_{\rm co}\,\Xi_{\alpha_{\rm co}}(t'/t)$. The black dashed line indicates the analytical value $\alpha_{\rm co} = (d-2)/2$. (d) Prefactor $C_{\rm co}$ obtained by fitting $|G_R(k=0,t=2\times10^3,t')/t|$ as $C_{\rm co}\,\Xi_{\alpha_{\rm co}}(t'/t)$, with $\alpha_{\rm co}$ given by the analytical value reported above. The black dashed line indicates the analytical value $C_{\rm co} = 1/(d-2)$. The error bars on numerical data are smaller than the symbol size.

being zero above it, this is not the case for $a_{\rm co}$. Analogous consideration holds for the other quantities discussed further below, when compared with the corresponding ones at criticality. Heuristically this might be expected based on the fact that —as in the case of classical systems [164, 165]— coarsening for $r_0 < r_0^c$ is generally driven by a different mechanism compared to the one controlling the behavior

at $r_0 = r_0^c$, which is related to critical fluctuations and which is therefore affected upon crossing d_c (see Sec. 4.3.3). As a peculiar feature of $a_{\rm co}$, we note that it vanishes for $d = 3$. As argued above and demonstrated by the curves in Figure 4.3(a) and 4.3(b), $G_K(k = 0, t, t)$ grows algebraically both at $r_0 = r_0^c$ and for $r_0 < r_0^c$, in the latter case as $\sim t^{\gamma_{\rm co}}$. Figure 4.5(b) shows the estimates of $\gamma_{\rm co}$ obtained by fitting the numerical data for $G_K(k = 0, t, t)$, as a function of the dimensionality d. The dashed line corresponds to the theoretical prediction $\gamma_{\rm co} = 1 + 2\alpha_{\rm co}$ with $\alpha_{\rm co}$ given by Eq. (4.46). As it was done in Figure 4.4 for $r_0 = r_0^c$, Figure 4.5(c) and 4.5(d) consider $G_R(k, t, t')$ at $k = 0$. By assuming that the scaling behavior in Eq. (4.31) carries over to $r_0 < r_0^c$, $|G_R(k, t, t')/t|$ is fitted by $C_{\rm co}\, \Xi_{\alpha_{\rm co}}(t'/t)$ in order to extract $\alpha_{\rm co}$ (Figure 4.5(c)) or to estimate $C_{\rm co}$ once $\alpha_{\rm co}$ has been fixed to its theoretical value in Eq. (4.46) (Figure 4.5(d)). In both Figures, the corresponding theoretical predictions are reported as dashed lines and, as in the case of the upper panels, the agreement with the numerical data is excellent, with a hint of slight deviations upon approaching the lower critical dimensionality $d_l = 2$ of this model.

As we mentioned at the end of Sec. 4.3.1, the exponent $\gamma_{\rm co} = 1 + 2\alpha_{\rm co}$ discussed here in connection to the scaling of $G_K(k, t, t)$ (see Eqs. (4.33) and (4.34)) is the same as the exponent γ introduced in Ref. [118] in order to characterize the scaling behavior of $\rho_{\mathbf{k}}(t)$. The values of γ which were numerically determined in Ref. [118] for a quench below the critical point in $d = 3$ and 4, i.e., $\gamma = 2$ and 3 are in perfect agreement with our numerical estimates and analytical predictions reported in Figure 4.5(b).

4.3.3 Coarsening

The numerical data presented in Sec. 4.3.2 clearly show that the nonequilibrium dynamics of the system after a quench to $r_0 < r_0^c$ features an emerging scaling behavior which we partly rationalized in Sec. 4.2 and which is characterized by scaling exponents depending on the spatial dimensionality d. As anticipated, these scaling forms are expected to be related to the coarsening dynamics [116, 117], analogously to what happens in classical systems after a quench below the critical temperature [164–166] (see Appendix 4.A for the discussion of a specific example). In fact, when a classical system prepared in a disordered state is quenched below the critical temperature, the global symmetry cannot be dynamically broken and, consequently, the order parameter remains zero on average. Nevertheless, symmetry is broken locally by the creation of domains within which the order parameter φ takes the value characterizing one of the possible different and competing phases.

The average linear extension $L(t)$ of the ordered domains increases with time t, until a specific domain possibly prevails over the others, establishing the equilibrium state. However, because of such competition, $L(t)$ grows algebraically as $L(t) \propto t^{1/z_c}$, where $z_c > 0$ is an exponent depending on the universal properties of the model, and equilibrium is reached only in an infinite time. Consequently, this lack of an intrinsic length scale in the system affects the equal-time two-point correlation function

$$C(\mathbf{r}, t) = \langle \varphi(\mathbf{x} + \mathbf{r}, t)\varphi(\mathbf{x}, t)\rangle \,, \tag{4.49}$$

and its spatial Fourier transform $C(k, t)$, which, according to the scaling hypothesis [164], are expected to display the scaling forms

$$C(\mathbf{r}, t) = f\left(\frac{r}{L(t)}\right) \quad \text{and} \quad C(k, t) = [L(t)]^d \, \widetilde{f}\,(kL(t)) \,, \tag{4.50}$$

where d is the spatial dimensionality and $\widetilde{f}(x)$ the Fourier transform of $f(x)$.

The scaling forms for a quench below r_0^c highlighted in Sec. 4.3.2 *do not* satisfy the scaling hypothesis (4.50), as it was noticed for $d = 3$ in Refs. [116, 117]. In fact, the Keldysh Green's function at equal times $G_K(k, t, t)$ —which corresponds to the correlation function $C(k, t)$ mentioned above— can be written as a scaling form by using Eqs. (4.36) and (4.46), which reads

$$G_K(k, t, t) = [L(t)]^{\gamma_{\rm co}} \, \mathcal{G}_d(kL(t)), \tag{4.51}$$

where $\mathcal{G}_d(x)$ is the scaling function, $L(t) \propto t$ (i.e., the coarsening exponent takes the value $z_c = 1$) and $\gamma_{\rm co} = d - 1$. As this $\gamma_{\rm co}$ differs from d, Eq. (4.51) violates the scaling form (4.50) in all spatial dimensions.

4.4 Concluding remarks

In this Chapter we provided a complete characterization of the dynamical scaling which emerges after a deep quench of an isolated quantum vector model with $O(N)$ symmetry at or below the point of its DPT. The lack of intrinsic time and length scales is responsible for the occurrence of aging phenomena similar to the ones observed in nonequilibrium classical systems [150, 151] or, more recently, in isolated [119] quantum many body systems. While previous investigations of this phenomenon were based on a perturbative, dimensional expansion around the upper critical dimensionality $d_c = 4$ of the model [119], here we carry out our analysis within the exactly solvable (nonperturbative) limit $N \to \infty$, which allows us to

obtain exact results for scaling exponents and scaling functions of the relevant dynamical correlations, depending on the dimensionality d of the model. We find that the value of the prequench spatial correlation length (assumed to be small) controls the microscopic time t_Λ after which the aging behavior emerges: in addition, it acts as an effective temperature for the dynamics after the quench, which, *inter alia*, determines a shift of the upper critical dimensionality d_c of the model, as it occurs in equilibrium quantum systems at finite temperature [142, 167]. Moreover, we provide evidence of the emergence of a dynamical scaling behavior for quenches below r_0^c, associated with coarsening, which we characterized numerically and analytically by studying the dependence of the relevant exponents on the spatial dimensionality d of the system.

The exactly solvable model considered here provides a prototypical example of a DPT and of the associated aging occurring in a nonthermal stationary state. This state is expected to become unstable in systems with finite N, when the nonintegrable terms of the Hamiltonian become relevant, causing thermalization. Nonetheless, this DPT might be still realized in the prethermalized stage of the relaxation of actual quantum systems evolving in isolation from the surrounding environment [19, 85, 88–90, 93, 95, 96, 98, 102, 168, 169]. The latter are nowadays rather easily realized in trapped ultracold atoms, the behavior of which can be analyzed with remarkable spatial and temporal resolution [12, 13, 15–17, 170–172]. In general, physical systems which can be described by some effective Hamiltonian with $O(N)$ symmetry include experimental realizations with ultracold atoms of the Bose-Hubbard model [5, 171, 172] (corresponding to $N = 2$) and one-dimensional tunnel-coupled condensates [169, 173] ($N = 1$). In passing, we mention that an alternative and promising experimental realization of these models currently under investigation [174] is based on fluids of light propagating in nonlinear optical media, which is expected to be ready for testing in the near future.

At least in principle, the universal dynamical scaling behavior emerging after a sudden quench which is highlighted in the present work can be experimentally studied by determining directly the two-time linear response and correlation functions of the system. Alternatively, one can exploit the statistics of excitations produced after a (double) quench, as proposed in Ref. [118] (more details on the statistics of excitations in Sec. 5.3). In fact, the n-th cumulant $C_n(t)$ of the corresponding distribution was shown to grow as a function of the time t elapsed since the quench, with a behavior which may saturate, grow logarithmically or algebraically, depending on n, d, and on whether the quench occurs above, at, or below criticality. In

particular, it was shown [118] that the increase in time of $C_n(t)$ is proportional to the integral over $\mathbf{k}$ of the n-th power of the quantity $\rho_{\mathbf{k}}(t)$ related to the number of excitations (see Sec. 4.3.1). In turn, at long times, the leading growth of $\rho_{\mathbf{k}}(t)$ is the same as the one of $|f_{\mathbf{k}}(t)|^2$, i.e., of $i\,G_K(k,t,t)$ (see Eq. (4.15)). As a result, a simple comparison with Eqs. (4.33) and (4.34) yields

$$C_n(t) \propto \int \mathrm{d}^d k\ [i\,G_K(k,t,t)]^n \propto t^{n(1+2\alpha)-d}, \tag{4.52}$$

for a quench to the critical point; for a quench below it, instead, one finds the same expression with α replaced with α_{co}, i.e.,

$$C_n(t) \propto \int \mathrm{d}^d k\ [i\,G_K(k,t,t)]^n \propto t^{n(1+2\alpha_{\mathrm{co}})-d}, \tag{4.53}$$

where the values of the exponents α and α_{co} are given in Eqs. (4.42), (4.43), and (4.46). As a result, a measure of the statistics of the number of excitations for a quench would provide direct information on the aging and coarsening properties of the system.

The quantum aging and coarsening discussed here enrich the list of mechanisms underlying the scale-invariant nonthermal fixed points (NTFP) [175–177], which have been so far interpreted in terms of quantum turbulence [178–180] and dynamics of topological defects [181, 182]. The extent to which these mechanisms are interconnected and combined in the dynamics of physical systems represents an intriguing yet challenging question for future investigations.

Appendix

4.A Comparison with aging after a classical quench

In this section, we briefly review the phenomena of aging and coarsening in classical systems evolving in contact with a thermal bath after quenching its temperature either at or below a critical point of the system [149]. In both cases, the lack of intrinsic time and length scales causes the emergence of algebraic behaviors in the temporal dependence of, e.g., two-time correlation and response functions which can be characterized in terms of scaling exponents and scaling functions with a certain degree of universality. The stochastic dynamics of these classical statistical systems can be simply described by effective models [183], which take the form of Langevin equations for the (coarse-grained) relevant degrees of freedom of the system. For example, a N-component real field $\boldsymbol{\varphi} = (\varphi_1, \ldots, \varphi_N)$ obeying purely dissipative dynamics evolves according to the so-called model A

$$\partial_t \varphi_a(\mathbf{x}, t) = -D \, \frac{\delta H[\boldsymbol{\varphi}]}{\delta \varphi_a(\mathbf{x}, t)} + \zeta_a(\mathbf{x}, t), \tag{4.54}$$

where D is a diffusion coefficient, H a $O(N)$-symmetric effective Hamiltonian in d spatial dimensions

$$H[\boldsymbol{\varphi}] = \int \mathrm{d}^d x \, \left[\frac{1}{2} \, (\nabla \boldsymbol{\varphi})^2 + \frac{r}{2} \boldsymbol{\varphi}^2 + \frac{u}{4! N} \boldsymbol{\varphi}^4 \right] \tag{4.55}$$

and ζ_a is a zero-mean Gaussian white noise describing the thermal fluctuations of the reservoir, with correlations

$$\langle \zeta_a(\mathbf{x}, t) \zeta_b(\mathbf{x}', t') \rangle = 2 \, D \, T \, \delta_{a,b} \, \delta^{(d)}(\mathbf{x} - \mathbf{x}') \, \delta(t - t'). \tag{4.56}$$

The evolution prescribed by Eq. (4.54) is such that the distribution of the fluctuating field $\boldsymbol{\varphi}$ at long times relaxes to the equilibrium distribution $P_{\mathrm{eq}}[\boldsymbol{\varphi}] \propto \mathrm{e}^{-H[\boldsymbol{\varphi}]/T}$,

independently of the initial condition. In this stationary state, and upon varying r, the system undergoes a second-order phase transition at the critical point $r = r_c$ of H. Generically, r in the effective Hamiltonian (4.55) is actually a function of the temperature T, with $r - r_c \propto T - T_c$, where T_c is the critical temperature of the classical system.

A classical quench protocol [150, 151] consists of preparing the system in, e.g., a disordered state at high temperature (i.e., with vanishing correlation length) at $t = 0$ and in letting it evolve with fixed $r = r_c$ or $r < r_c$ for $t > 0$. As a result, in both cases, the system relaxes to the equilibrium distribution with an algebraic behavior characterized by universal exponents which control, e.g., the scaling of the Fourier transform in space of the two-time and two-point correlation and response function $C(k, t, t')$ and $R(k, t, t')$, respectively. In particular, for a quench to the critical point, $C(k, t, t')$ and $R(k, t, t')$ can be calculated exactly in the limit $N \to \infty$ [150, 184] and they read (by rescaling time one can set $D = 1$) for $2 < d < 4$:

$$R(k, t, t') = \theta(t - t') \left(\frac{t}{t'}\right)^{(4-d)/4} \mathrm{e}^{-k^2(t-t')}, \tag{4.57}$$

and

$$C(k, t, t') = \frac{1}{k^2} F(k^2 t, k^2 t'), \tag{4.58}$$

with $F(x, y)$ a scaling function defined as

$$F(x, y) = (4xy)^{(4-d)/4} \int_0^{2\min[x,y]} \mathrm{d}t \; t^{(d-4)/2} \, \mathrm{e}^{t-x-y}. \tag{4.59}$$

Assuming for simplicity $t > t'$, the asymptotic expression of $C(k, t, t')$ at short times t, $t' \ll k^{-2}$ is

$$C(k, t, t') \simeq \frac{4}{d-2} \, t' \left(\frac{t}{t'}\right)^{(4-d)/4}, \tag{4.60}$$

while, at long times t, $t' \gg k^{-2}$, it reads

$$C(k, t, t') \simeq \left(\frac{t}{t'}\right)^{(4-d)/4} \frac{\mathrm{e}^{-k^2(t-t')}}{k^2}. \tag{4.61}$$

The effective classical dynamics prescribed by Eq. (4.54) is actually relevant also for the quantum system with Hamiltonian (4.1) investigated in this Chapter, when the field $\boldsymbol{\phi}$ is linearly coupled to a bath of harmonic oscillators with Ohmic spectral density and at equilibrium with temperature T. This *open* quantum system is then characterized by an *equilibrium* critical point at $r = r_c^{\mathrm{eq}}(T)$ at which the microscopically large-distance, long-time properties are effectively described by the

critical classical model described above [159]. In fact, a critical quench in this open quantum system was recently studied in Refs. [153, 154] starting from a disordered prequench state and the scaling functions of G_R and G_K —which correspond, respectively, to the classical R and C— turn out to agree with Eqs. (4.57), (4.60), and (4.61).

The effect of having an isolated instead of an open quantum system is not only revealed by the different value of the dynamical exponent z (1 and 2, respectively) but also by the scaling form of the corresponding correlation and response functions at short times, where the actual value of z does not appear explicitly. In fact, from Eqs. (4.36), (4.42), and (4.22) one finds that $i\,G_K(k=0,t,t') \sim (tt')^{d/4}$, which can be compared with $C(k=0,t,t')$ in Eq. (4.60). While the dependence of the earliest time t' is characterized by the same exponent $d/4$ this does not apply to the dependence on t and in fact the overall scaling form is significantly different, as expected on the basis of the different scaling dimensions of the relevant fields [119, 150]. Comparing, instead, the corresponding short-time response functions in Eqs. (4.31) (see also Eq. (4.42)) and (4.57), one finds that the dependence on the time t' is characterized by opposite powers, whereas the ones on t are seemingly unrelated.

The classical model can be exactly solved in the limit $N \to \infty$ also if the quench occurs from the disordered state to below the critical point $r < r_c$ [184]; for $d > 2$, the corresponding response function reads

$$R(k,t,t') = \theta(t-t') \left(\frac{t}{t'}\right)^{d/4} \mathrm{e}^{-k^2(t-t')}, \tag{4.62}$$

while the correlation function is (with $t > t'$)

$$C(k,t,t') = M_{\mathrm{eq}}^2 \left(8\pi t'\right)^{d/2} \left(\frac{t}{t'}\right)^{d/4} \mathrm{e}^{-k^2(t+t')}, \tag{4.63}$$

with M_{eq} being the value that the order parameter would have in equilibrium in the system described by the postquench classical Hamiltonian. Accordingly, this system exhibits coarsening in the strict sense [164], as Eq. (4.63) satisfies the dynamical scaling in the form indicated by Eq. (4.50) with the proper value $z_c = 2$ of the coarsening exponent.

Chapter 5

Dynamical transitions and statistics of excitations

Among all the possible ways of taking an isolated quantum system out of equilibrium, the most natural one is to vary in time some of the parameters of the Hamiltonian. The following nonequilibrium dynamics is expected to depend on the choice of the way that parameters are changed from their initial to their final values, i.e., in the choice of the specific protocol. The two extreme cases of an instantaneous variation (sudden quench) and an adiabatic one (slow quench) are the most studied in literature. On the other hand, considering more generic procedures, such as a linear ramp, is important to understand which dynamical features are unaffected by the changes of the protocol and which ones depend on its details (for example, the dependence on its duration). Moreover, the study of generic protocols can be useful in experiments to prepare a system in particular excited states, or when an instantaneous change of the parameters is difficult to perform.

One of the most interesting features of the dynamics induced by nonequilibrium protocols is the emergence of nonthermal quasistationary state which may display dynamical critical behaviors, usually studied in the context of sudden quenches. However, how to characterize such nonequilibrium phase transitions and their critical behavior and how to distinguish them from a thermal transitions is not so clear. In this context, a simple protocol based on the statistics of excitations produced in a sudden quench was recently proposed [118].

In this Chapter, we discuss the characterization of the dynamical phase transition of the $O(N)$ vector model in the large-N limit, introduced in Chapter 4. We focus on the case in which the system is driven out of equilibrium by a linear variation

in time of the bare mass, starting in the disordered phase, rather than by a sudden quench. We show that the presence of a dynamical phase transition and its critical properties are robust against the change of the protocol and that a characterization based on the critical dimensions and exponents does not allow to distinguish the dynamical transition to the equilibrium thermal one. However, its nonequilibrium nature becomes evident analyzing the statistics of excitations produced in the ramp process. In particular, the critical properties are encoded in the fluctuations in the number of excitations, which display *qualitatively* different behaviors depending on the ramp being performed above, at, or below the dynamical critical point. These behaviors bear no dependence on the duration of the protocol.

5.1 Model and quench protocol

Let us start our study by recalling the Hamiltonian of the model of interest, slightly changing the notation with respect to Chapter 4, and briefly reviewing some properties of the system in two known cases, at equilibrium and for a sudden quench. We consider an interacting N component bosonic scalar field $\boldsymbol{\phi}$ in d spatial dimensions, described by the Hamiltonian

$$\mathcal{H}(r_0) = \int \mathrm{d}^d x \, \left[\frac{1}{2}\boldsymbol{\Pi}^2 + \frac{1}{2}\left(\nabla\boldsymbol{\phi}\right)^2 + \frac{r_0}{2}\boldsymbol{\phi}^2 + \frac{u}{4!N}\boldsymbol{\phi}^4 \right], \tag{5.1}$$

where $\boldsymbol{\Pi}$ is the canonically conjugated momentum field, with $[\phi_a(\mathbf{x}), \Pi_b(\mathbf{x}')] = i\,\delta^{(d)}(\mathbf{x}-\mathbf{x}')\,\delta_{a,b}$. In the following we will focus on the $N \to \infty$ limit [155], where the $O(N)$ vector model is exactly solvable and can be effectively described by a quadratic Hamiltonian parametrized by an effective mass r_{eff}.

In this limit and in equilibrium this system undergoes a phase transition between a paramagnetic phase and an ordered one, schematically shown in Figure 4.1. At the equilibrium critical point, identified by the vanishing of the effective mass r_{eff}, the bare mass is given by

$$r^c_{0,\mathrm{eq}}(T) = -\frac{u}{12}\int^{\Lambda} \frac{\mathrm{d}^d k}{(2\pi)^d}\,\frac{1}{k}\,\coth\!\left(\frac{k}{2T}\right), \tag{5.2}$$

where T is the temperature, while Λ implements the ultraviolet sharp cutoff. From Eq. (5.2), one may easily see that the lower critical dimension for the quantum transition is $d_l = 1$, while the thermal one has $d_l = 2$. Moreover, one can compute the critical exponent ν describing the divergent behavior of the correlation length ξ close to the critical point, i.e., $\xi \sim (\delta r_0)^{-\nu}$, with $\delta r_0 = r_0 - r^c_{0,\mathrm{eq}}(T)$. At $T = 0$,

one finds

$$\begin{aligned} \nu &= \frac{1}{d-1} \quad \text{for} \quad 1 < d < 3, \\ \nu &= \frac{1}{2} \quad \text{for} \quad d \geq 3, \end{aligned} \tag{5.3}$$

being $d_c = 3$ the upper critical dimension of the quantum phase transition. In the finite temperature case, one gets instead

$$\begin{aligned} \nu &= \frac{1}{d-2} \quad \text{for} \quad 2 < d < 4, \\ \nu &= \frac{1}{2} \quad \text{for} \quad d \geq 4, \end{aligned} \tag{5.4}$$

which implies that $d_c = 4$ is the upper critical dimension for the thermal transition.

Focusing now on the dynamics, it was numerically shown [116–118] that this model can undergo a dynamical phase transition (DPT) due to a sudden quench in the bare mass, i.e., suddenly changing its value from $r_{0\mathrm{i}}$ to $r_{0\mathrm{f}}$. Considering the case of a quench starting in the paramagnetic ground state, the dynamical critical point is reached if the final bare mass satisfy the ansatz [118]

$$r_{0\mathrm{f}}^c = -\frac{u}{4!} \int^{\Lambda} \frac{\mathrm{d}^d k}{(2\pi)^d} \frac{2k^2 + r_{\mathrm{i}}^2}{k^2 \sqrt{k^2 + r_{\mathrm{i}}^2}}, \tag{5.5}$$

where r_{i} denotes the effective mass before the quench. From this equation one obtains that the lower critical dimension for the dynamical transition is $d_l = 2$, and that the dynamical critical value is always smaller than the equilibrium quantum critical one, $r_{0,\mathrm{eq}}^c$. Similarly to the equilibrium case, we denote with ξ_* the correlation length in the stationary state and with ν_* the exponent describing its divergence close to the dynamical critical point. We find

$$\begin{aligned} \nu_* &= \frac{1}{d-2} \quad \text{for} \quad 2 < d < 4, \\ \nu_* &= \frac{1}{2} \quad \text{for} \quad d \geq 4, \end{aligned} \tag{5.6}$$

and therefore $d_c = 4$ is the upper critical dimension of the DPT. Even if these critical exponents are similar to those of a finite temperature transition at equilibrium and could suggest that the two might be analogous [116, 118], in contrast to the thermal case the dynamical transition can be characterized by the statistics of the excitations produced in the quench [118]. In particular, it can be detected by studying how the fluctuations in the number of excitations scale as a function of time.

We are now interested in studying the dynamics of the system resulting from a different protocol: a linear ramp of the bare mass. The system is prepared in the

ground state of the disordered phase ($r_{0\mathrm{i}} > r^c_{0,\mathrm{eq}}$). Then, the bare mass is linearly decreased to a final value $r_{0\mathrm{f}}$ in a total time τ, according to the following protocol:

$$r_0(t) = \begin{cases} r_{0\mathrm{i}} & \text{if } t \leq 0, \\ r_{0\mathrm{i}} + \dfrac{r_{0\mathrm{f}} - r_{0\mathrm{i}}}{\tau}\, t & \text{if } 0 \leq t \leq \tau, \\ r_{0\mathrm{f}} & \text{if } t \geq \tau. \end{cases} \tag{5.7}$$

In extending the exact solution of the dynamics of the system to this case, we will be interested in particular in two main issues: is the presence of a dynamical phase transition, as well as its critical properties, robust against change of the protocol ? Is a characterization in terms of the statistics of excitations still expected to give useful information on the system ?

5.2 Dynamical critical properties

Let us start addressing quantitatively the first question. Similarly to the case of a sudden quench, the dynamics of the system is described by an effective quadratic Hamiltonian with a time dependent effective mass $r_{\mathrm{eff}}(t)$, as that of Eq (4.5). Expanding the Fourier components $\phi_{\mathbf{k}}$ of the field in terms of the annihilation and creation operators $a_{\mathbf{k}}$ and $a^\dagger_{\mathbf{k}}$ diagonalizing the initial Hamiltonian at $t = 0$ (see Eq. (4.8)) and imposing the Heisenberg equations of motion, we derive the equation for the evolution of the mode function $f_{\mathbf{k}}(t)$,

$$\ddot{f}_{\mathbf{k}} + \left(k^2 + r_{\mathrm{eff}}(t)\right) f_{\mathbf{k}} = 0, \tag{5.8}$$

where

$$r_{\mathrm{eff}}(t) = r_0(t) + \frac{u}{6} \int^{\Lambda} \frac{\mathrm{d}^d k}{(2\pi)^d}\, |f_{\mathbf{k}}(t)|^2. \tag{5.9}$$

The initial conditions are

$$f_{\mathbf{k}}(0) = \frac{1}{\sqrt{2\omega_{k\mathrm{i}}}} \quad \text{and} \quad \dot{f}_{\mathbf{k}}(0) = -\,i \sqrt{\frac{\omega_{k\mathrm{i}}}{2}}, \tag{5.10}$$

with $\omega_{k\mathrm{i}} = \sqrt{k^2 + r_{\mathrm{i}}}$,

We solved the self-consistent equations (5.8) and (5.9) analytically for the case of a linear ramp in the special case of $u = 0$ (see Appendix 5.A). For any finite u we resorted instead to numerical integration. Varying the duration of the ramp and the value of the final bare mass, the system is found to display a DPT: as shown in Figure 5.1, for long times after the end of the ramp the effective mass $r_{\mathrm{eff}}(t)$ relaxes

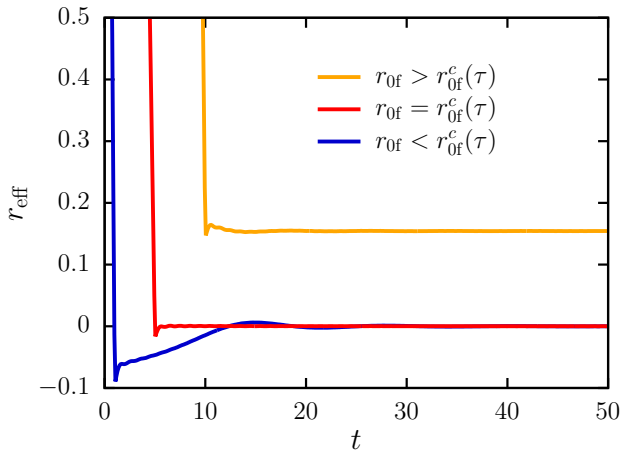

Figure 5.1: Time evolution of the effective mass $r_{\rm eff}(t)$ for different ramp durations τ and initial bare masses $r_{0\rm i}$ in $d = 3$. Final values of the bare mass below, at, and above the dynamical critical point are shown.

to a stationary value, which is positive up to a certain τ-dependent dynamical critical point $r^c_{0\rm f}(\tau)$, and vanishes for $r_{0\rm f} \leq r^c_{0\rm f}(\tau)$.

In order to make some progress in characterizing the dynamical phase transition in this case, it is very important to be able, as in the case of a sudden quench, to predict analytically the stationary value of the effective mass r_*. In order to achieve this goal, we introduce an ansatz for the stationary effective mass inspired by the one used before for a sudden quench [118,156]: we assume the stationary part of the equal-time two-point correlation function $\langle \phi_{\mathbf{k}}(t)\phi_{-\mathbf{k}}(t)\rangle = |f_{\mathbf{k}}(t)|^2 = i\,G_K(k,t,t)/2$ to be equal to the noninteracting ($u = 0$) one, but with the bare masses replaced by the renormalized ones, namely $r_{0\rm i} \to r_{\rm i}$ and $r_{0\rm f} \to r_*$ (see Appendix 5.A). We therefore obtain the following self-consistent equation for r_*

$$r_* = r_{0\rm f} + \frac{u}{12}\int^{\Lambda} \frac{{\rm d}^d k}{(2\pi)^d} \left(|f^0_{\mathbf{k}}(r_*,\tau)|^2 + \frac{|\dot{f}^0_{\mathbf{k}}(r_*,\tau)|^2}{k^2 + r_*} \right), \tag{5.11}$$

where $f^0_{\mathbf{k}}$ denotes the mode function for $u = 0$ and we explicitly write down its dependence on r_*. According to this ansatz, we can identify the dynamical critical point, i.e., the point at which r_* vanishes, as

$$r^c_{0\rm f}(\tau) = -\frac{u}{12}\int^{\Lambda} \frac{{\rm d}^d k}{(2\pi)^d} \left(|f^0_{\mathbf{k}}(0,\tau)|^2 + \frac{|\dot{f}^0_{\mathbf{k}}(0,\tau)|^2}{k^2} \right). \tag{5.12}$$

The mere fact that the stationary state can be described by an ansatz such as Eq. (5.11) allows to deduce many of the properties of the dynamical phase

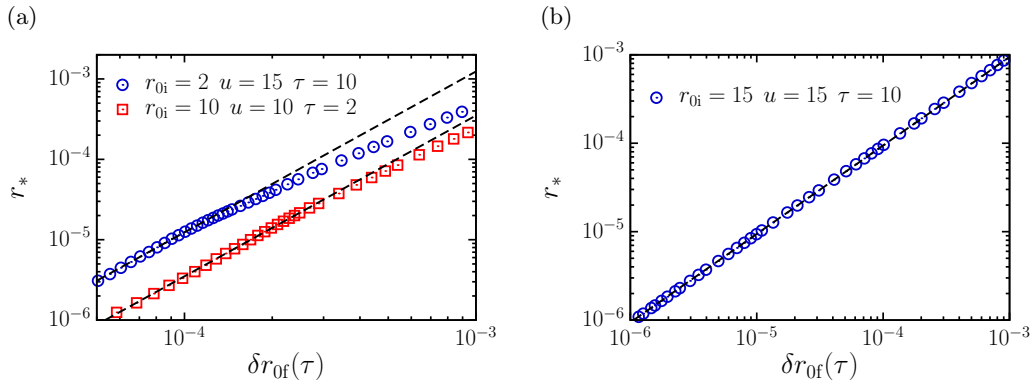

Figure 5.2: Stationary value of the effective mass r_* as a function of the distance from the dynamical critical point in $d = 3$ (a) and $d = 4$ (b). Black dashed lines are quadratic (a) and linear (b) fits.

transition. Note however that Eq. (5.11) provides the correct stationary value for $r_{0\mathrm{f}} \geq r^c_{0\mathrm{f}}(\tau)$ only provided the ramp duration τ on the r.h.s. is also renormalized to an effective ramp duration $\tilde{\tau}$.

One may nevertheless establish the lower critical dimension of the dynamical transition by analyzing the behavior for low momenta of the integrand of Eq. (5.12) (see Appendix 5.B). Indeed, for every finite τ, the most relevant modes are those with $k \ll (r_{\mathrm{i}}/\tilde{\tau})^{1/3}$ and $k \ll \sqrt{r_{\mathrm{i}}}$, where both $|f^0_{\mathbf{k}}(0,\tilde{\tau})|^2$ and $|\dot{f}^0_{\mathbf{k}}(0,\tilde{\tau})|^2$ go to a constant. At small momenta the integrand behaves thus as $1/k^2$, implying that the dynamical critical point $r^c_{0\mathrm{f}}(\tau)$ is finite for $d > 2$, $d_l = 2$ being the lower critical dimension for every finite τ. We observe that when τ increases, the region considered above shrinks and when τ is strictly infinite the lower critical dimension is $d_l = 1$, recovering the result of the quantum transition. This can be seen noticing that as τ gets larger and larger the intermediate asymptotics in the region $(r_{\mathrm{i}}/\tilde{\tau})^{1/3} \ll k \ll \sqrt{r_{\mathrm{i}}}$, where $|f^0_{\mathbf{k}}(0,\tilde{\tau})|^2 \sim 1/k$ and $|\dot{f}^0_{\mathbf{k}}(0,\tilde{\tau})|^2 \sim k$, become more and more important.

Combining Eqs. (5.11) and (5.12), we can compute the critical exponent ν_*, describing the divergence of the correlation length ξ_* in the stationary state close to the dynamical critical point, i.e., $\xi_* \sim (\delta r_{0\mathrm{f}}(\tau))^{-\nu_*}$, with $\delta r_{0\mathrm{f}}(\tau) = r_{0\mathrm{f}} - r^c_{0\mathrm{f}}(\tau)$. As shown in detail in Appendix 5.B, for $2 < d < 4$ the stationary value of effective mass at the leading order scales as $r_* \sim (\delta r_{0\mathrm{f}}(\tau))^{2/(d-2)}$, while for $d \geq 4$ the scaling becomes linear, i.e., $r_* \sim \delta r_{0\mathrm{f}}(\tau)$. Since the effective theory is Gaussian, $\xi_* \sim$

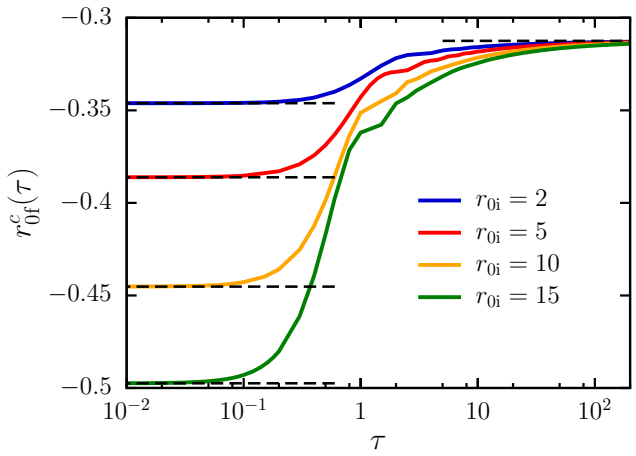

Figure 5.3: Dynamical critical point $r^c_{0\mathrm{f}}(\tau)$ as a function the ramp duration τ in $d = 3$. Different values of the initial bare mass $r_{0\mathrm{i}}$ are shown, while the interaction is $u = 15$. Horizontal black dashed lines indicate the dynamical critical point for a sudden quench ($\tau \to 0$) and the equilibrium quantum critical point ($\tau \to \infty$).

$(r_*)^{-1/2}$. We conclude that

$$\begin{aligned} \nu_* &= \frac{1}{d-2} \quad \text{for} \quad 2 < d < 4, \\ \nu_* &= \frac{1}{2} \quad \text{for} \quad d \geq 4, \end{aligned} \tag{5.13}$$

$d_c = 4$ being the upper critical dimension. Figure 5.2 shows that numerical results for $d = 3$ and $d = 4$ agree with this prediction. We note that for $d = 3$ (Figure 5.2(a)) numerical data follow the relation $r_* \sim (\delta r_{0\mathrm{f}}(\tau))^2$ for sufficiently small values of r_* and then depart from this scaling, eventually approaching a linear relation for larger r_*.

The critical dimensions and the critical exponent of the dynamical transition are the same as the thermal one, even though the former occurs in a pure state, generated by the unitary dynamics of the model, while the latter occurs in a mixed state. Moreover, for every finite τ the dynamical transition displays the same critical properties which occur when a sudden quench of the bare mass is performed, while only when τ is strictly infinite we recover the behavior of a quantum transition.

A crucial observation to check the above result is that, since the parameter $\tilde{\tau}$ is unknown *a priori*, we can not predict the value of the dynamical critical point analytically and we have to detect it numerically. As shown in Figure 5.3, the values of $r^c_{0\mathrm{f}}(\tau)$ interpolate between the dynamical critical point for a sudden quench, corresponding to $\tau \to 0$, and the quantum critical point at equilibrium, in the limit

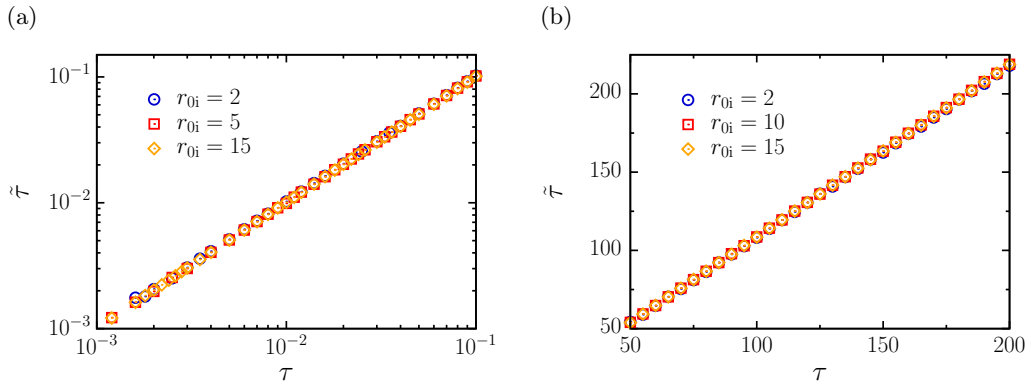

Figure 5.4: Effective ramp duration $\tilde{\tau}$ as a function of the true ramp duration τ at the dynamical critical point in $d = 3$ for small (a) and large (b) τ. Different values of the initial bare mass r_{0i} are shown, while the interaction is $u = 15$.

of large τ.

Once the dynamical critical point has been identified, we can compute *a posteriori* the effective ramp duration $\tilde{\tau}$ using Eq. (5.12). Analyzing the behavior of $\tilde{\tau}$ as a function of the true ramp duration τ at the critical point and for r_{0i} and u fixed, it emerges that in the limits of small and large τ these two quantities have a linear relation, as can be seen in Figure 5.4. Moreover, varying the value of the initial bare mass r_{0i} (but keeping u fixed) the different $\tilde{\tau}(\tau)$ collapse on the same line, for large and small ramp durations. We may therefore use the ansatz (5.12) to analytically study how the dynamical critical value depends on τ in two limiting cases, for $\tau \to \infty$ (adiabatic switching) and $\tau \to 0$ (sudden quench).

5.2.1 Dynamical critical point for large τ

In order to use Eq. (5.12) to study the approach of $r_{0f}^c(\tau)$ to the equilibrium quantum critical point as τ increases, we consider the exact expression of the noninteracting mode functions $f_{\mathbf{k}}^0(t)$ in terms of Airy functions (see Appendix 5.A). By means of the asymptotic expansion of the Airy functions for large and negative arguments (see Appendix 5.B), for $\tilde{\tau} \gg 1/\sqrt{r_i}$ Eq. (5.12) reads

$$r_{0f}^c(\tau) \simeq -\frac{u}{12}\frac{\Omega_d}{(2\pi)^d}\left(\mathcal{I}_1(d) + \mathcal{I}_2(d)\right), \tag{5.14}$$

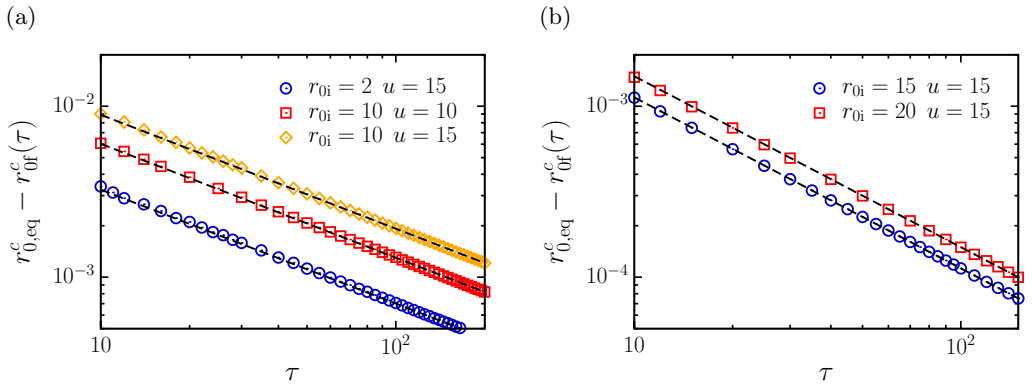

Figure 5.5: Difference between the equilibrium quantum critical point $r^c_{0,\mathrm{eq}}$ and the dynamical critical point $r^c_{0\mathrm{f}}(\tau)$ for large ramp duration τ in $d = 3$ (a) and $d = 4$ (b). Different values of the interaction u and of the initial bare mass $r_{0\mathrm{i}}$ are shown. Black dashed lines are proportional to $\tau^{-2/3}$ (a) and to τ^{-1} (b).

being Ω_d the solid angle in d dimensions and

$$\mathcal{I}_1(d) = \frac{\pi}{4}\,\Lambda^d \left(\frac{\tilde{\tau}}{r_{\mathrm{i}}}\right)^{1/3} \int_0^1 \mathrm{d}z\, z^{\frac{d-2}{2}} \left[\mathrm{Ai}^2\left(-\frac{\Lambda^2 \tilde{\tau}^{2/3}\, z}{r_{\mathrm{i}}^{2/3}}\right) + \mathrm{Bi}^2\left(-\frac{\Lambda^2 \tilde{\tau}^{2/3}\, z}{r_{\mathrm{i}}^{2/3}}\right)\right], \tag{5.15}$$

$$\mathcal{I}_2(d) = \frac{\pi}{4}\,\Lambda^{d-2} \left(\frac{r_{\mathrm{i}}}{\tilde{\tau}}\right)^{1/3} \int_0^1 \mathrm{d}z\, z^{\frac{d-4}{2}} \left[\mathrm{Ai}'^2\left(-\frac{\Lambda^2 \tilde{\tau}^{2/3}\, z}{r_{\mathrm{i}}^{2/3}}\right) + \mathrm{Bi}'^2\left(-\frac{\Lambda^2 \tilde{\tau}^{2/3}\, z}{r_{\mathrm{i}}^{2/3}}\right)\right], \tag{5.16}$$

where we introduced the dimensionless variable $z = k^2/\Lambda^2$.

Integrals (5.15) and (5.16) can be computed exactly both in $d = 3$ and $d = 4$ (see Appendix 5.C). The asymptotic value of the dynamical critical point for large τ and $d = 3$ is

$$r^c_{0\mathrm{f}}(\tau) = r^c_{0,\mathrm{eq}} + \frac{u\,\Gamma(-1/3)}{288 \cdot 2^{2/3} \cdot 3^{1/3}\,\pi^2} \left(\frac{r_{\mathrm{i}}}{\tilde{\tau}}\right)^{2/3} + O\left(\left(\frac{r_{\mathrm{i}}}{\Lambda^3\,\tilde{\tau}}\right)^{4/3}\right), \tag{5.17}$$

while for $d = 4$ is

$$r^c_{0\mathrm{f}}(\tau) = r^c_{0,\mathrm{eq}} - \frac{u}{1152\sqrt{3}\,\pi^2} \left(\frac{r_{\mathrm{i}}}{\tilde{\tau}}\right) + O\left(\left(\frac{r_{\mathrm{i}}}{\Lambda^3\,\tilde{\tau}}\right)^2\right), \tag{5.18}$$

where $r^c_{0,\mathrm{eq}}$ is the quantum critical point at equilibrium.

Since for large τ the relation between $\tilde{\tau}$ and τ is linear at the critical point, we conclude that the dynamical critical point approaches the equilibrium quantum critical value as $\tau^{-2/3}$ for $d = 3$ and as τ^{-1} for $d = 4$. These scalings can be verified numerically by linearly fitting the relation between $\tilde{\tau}$ and τ for large τ and replacing the result in Eqs. (5.17) and (5.18). We get an excellent agreement with numerical data, as shown in Figure 5.5.

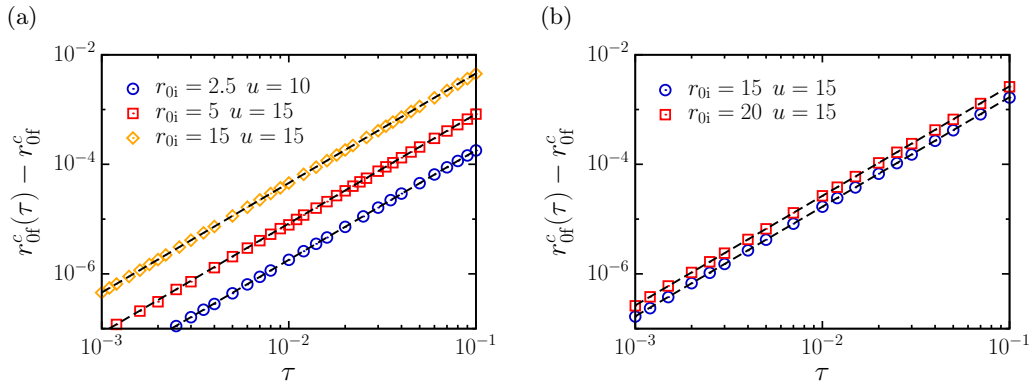

Figure 5.6: Difference between the dynamical critical point for a ramp, $r^c_{0f}(\tau)$, and for a sudden quench, r^c_{0f}, for small ramp duration τ in $d = 3$ (a) and $d = 4$ (b). Different values of the interaction u and of the initial bare mass r_{0i} are shown. Black dashed lines are proportional to τ^2.

5.2.2 Dynamical critical point for small τ

We now consider the fate of dynamical critical point in the limit of small τ. By means of the asymptotic expansion of the Airy functions for small arguments (see Appendix 5.B), we find

$$|f^0_{\mathbf{k}}(0,\tilde{\tau})|^2 \simeq \frac{1}{2\sqrt{k^2+r_i}} + \frac{r_i}{6\sqrt{k^2+r_i}}\,\tilde{\tau}^2, \tag{5.19}$$

$$|\dot{f}^0_{\mathbf{k}}(0,\tilde{\tau})|^2 \simeq \frac{\sqrt{k^2+r_i}}{2} - \frac{4k^2 r_i + r_i^2}{24\sqrt{k^2+r_i}}\,\tilde{\tau}^2. \tag{5.20}$$

Replacing these expressions in Eq. (5.12), we obtain

$$r^c_{0f}(\tau) \simeq r^c_{0f} + \frac{u}{12}\,\tilde{\tau}^2 \int^{\Lambda} \frac{\mathrm{d}^d k}{(2\pi)^d}\, \frac{r_i^2}{24\,k^2\,\sqrt{k^2+r_i}}, \tag{5.21}$$

where r^c_{0f} is the dynamical critical point for a sudden quench.

Since at criticality $\tilde{\tau} \sim \tau$ for small τ, we conclude that the dynamical critical point departs from the sudden quench value as τ^2, both in $d = 3$ and $d = 4$. This behavior is confirmed by numerical data (Figure 5.6).

5.3 Statistics of excitations

Let us now discuss the characterization of the dynamical transition through the statistics of excitations produced by the ramp of the bare mass, generalizing the

approach proposed in Ref. [118]. As we will show, the growth in time of the fluctuations in the number of excitations bears strong signatures of the dynamical transition.

After the end of the ramp, we let the system evolve for a certain waiting time and then we suddenly quench the bare mass back to its initial value $r_{0\mathrm{i}}$. The number of excitations generated in this process is a fluctuating quantity characterized by a certain probability distribution and it is related to the operator

$$\hat{\mathcal{N}} = \int^{\Lambda} \frac{d^d k}{(2\pi)^d}\, a^{\dagger}_{\mathbf{k}} a_{\mathbf{k}}. \tag{5.22}$$

An equivalent and more convenient description can be given in terms of the moment generating function

$$G(s,t) = \langle \Psi(t) | \mathrm{e}^{-s\hat{\mathcal{N}}} | \Psi(t) \rangle\,, \tag{5.23}$$

where $|\Psi(t)\rangle = U(t)\,|0\rangle$ is the evolved state at time t and $|0\rangle$ denotes the initial ground state.

For the $O(N)$ model in the large-N limit this quantity can be computed exactly. Indeed, since the effective theory is quadratic and different k-modes are coupled only via $r_{\mathrm{eff}}(t)$, the moment generating function can be factorized as

$$G(s,t) = \prod_{\mathbf{k}} G_{\mathbf{k}}(s,t), \tag{5.24}$$

where $G_{\mathbf{k}}(s,t)$ is the moment generating function for a single k-mode. In order to calculate $G_{\mathbf{k}}(s,t)$, we have to write the evolved state $|\Psi(t)\rangle$ in terms of the operators $a_{\mathbf{k}}$ and $a^{\dagger}_{\mathbf{k}}$ diagonalizing the initial Hamiltonian. To this purpose, we expand the fields $\phi_{\mathbf{k}}(t)$ and $\Pi_{\mathbf{k}}(t)$ in the same basis and, translating form Heisenberg to Schrœdinger picture, we find

$$\phi_{\mathbf{k}}(0) = f_{\mathbf{k}}(t)\tilde{a}_{\mathbf{k}}(t) + f^{\star}_{\mathbf{k}}(t)\tilde{a}^{\dagger}_{-\mathbf{k}}(t), \tag{5.25}$$

$$\Pi_{\mathbf{k}}(0) = \dot{f}_{\mathbf{k}}(t)\tilde{a}_{\mathbf{k}}(t) + \dot{f}^{\star}_{\mathbf{k}}(t)\tilde{a}^{\dagger}_{-\mathbf{k}}(t), \tag{5.26}$$

where we introduced a time-dependent operator $\tilde{a}_{\mathbf{k}}(t)$ such that it annihilates the time-evolved state, i.e., $\tilde{a}_{\mathbf{k}}(t)\,|\Psi(t)\rangle = 0$. Furthermore, we know that at $t = 0$

$$\phi_{\mathbf{k}}(0) = \frac{1}{\sqrt{2\omega_{k\mathrm{i}}}}(a_{\mathbf{k}} + a^{\dagger}_{-\mathbf{k}}), \tag{5.27}$$

$$\Pi_{\mathbf{k}}(0) = i\sqrt{\frac{\omega_{k\mathrm{i}}}{2}}(a^{\dagger}_{-\mathbf{k}} - a_{\mathbf{k}}). \tag{5.28}$$

Combining Eqs. (5.25) and (5.26) with Eqs. (5.27) and (5.28), and taking into account that $f_{\mathbf{k}}(t)\dot{f}^{\star}_{\mathbf{k}}(t) - f^{\star}_{\mathbf{k}}(t)\dot{f}_{\mathbf{k}}(t) = i$, we get

$$\tilde{a}_{\mathbf{k}}(t) = \alpha^{\star}_{\mathbf{k}}(t)a_{\mathbf{k}} - \beta^{\star}_{\mathbf{k}}(t)a^{\dagger}_{-\mathbf{k}}, \tag{5.29}$$

with

$$\alpha_{\mathbf{k}}(t) = \sqrt{\frac{\omega_{k\mathrm{i}}}{2}} f_{\mathbf{k}}(t) + \frac{i}{\sqrt{2\omega_{k\mathrm{i}}}}\dot{f}_{\mathbf{k}}(t), \tag{5.30}$$

$$\beta_{\mathbf{k}}(t) = \sqrt{\frac{\omega_{k\mathrm{i}}}{2}} f_{\mathbf{k}}(t) - \frac{i}{\sqrt{2\omega_{k\mathrm{i}}}}\dot{f}_{\mathbf{k}}(t). \tag{5.31}$$

Since the evolved state must be annihilated by the operator $\tilde{a}_{\mathbf{k}}(t)$ of Eq. (5.29), we finally obtain

$$|\Psi(t)\rangle_{\mathbf{k}} = \frac{1}{\sqrt{|\alpha_{\mathbf{k}}(t)|}} \exp\left(\frac{\beta^{\star}_{\mathbf{k}}(t)}{2\alpha^{\star}_{\mathbf{k}}(t)} a^{\dagger}_{\mathbf{k}} a^{\dagger}_{-\mathbf{k}}\right)|0\rangle\,, \tag{5.32}$$

with $a_{\mathbf{k}}\,|0\rangle = 0$.

Using coherent states, we can readily compute the moment generating function for a single k-mode, which reads

$$G_{\mathbf{k}}(s,t) = \frac{1}{\sqrt{1 + \rho_{\mathbf{k}}(t)\,(1 - \mathrm{e}^{-2s})}}, \tag{5.33}$$

where

$$\rho_{\mathbf{k}}(t) = |\beta_{\mathbf{k}}(t)|^2 = \frac{1}{2}\left(\omega_{k\mathrm{i}}|f_{\mathbf{k}}(t)|^2 + \frac{|\dot{f}_{\mathbf{k}}(t)|^2}{\omega_{k\mathrm{i}}} - 1\right). \tag{5.34}$$

For our purpose, it is more convenient to deal with the logarithm of $G(s,t)$,

$$\ln G(s,t) = -\frac{V}{2}\int^{\Lambda} \frac{\mathrm{d}^d k}{(2\pi)^d}\ \ln\left[1 + \rho_{\mathbf{k}}(t)\left(1 - \mathrm{e}^{-2s}\right)\right], \tag{5.35}$$

where $V = L^d$, L being the linear size of the system.

The dynamical critical properties of the model can be studied by analyzing the cumulants of the distribution of excitations, defined as

$$C_n(t) = (-1)^n\ \frac{\partial^n}{\partial s^n} \ln G(s,t)\bigg|_{s=0}. \tag{5.36}$$

In the following, we will focus on the first two cumulants, i.e., the average $\overline{\mathcal{N}}(t)$ and the variance $\sigma^2(t)$, in $d = 3$ and $d = 4$ and numerically study their time dependence,

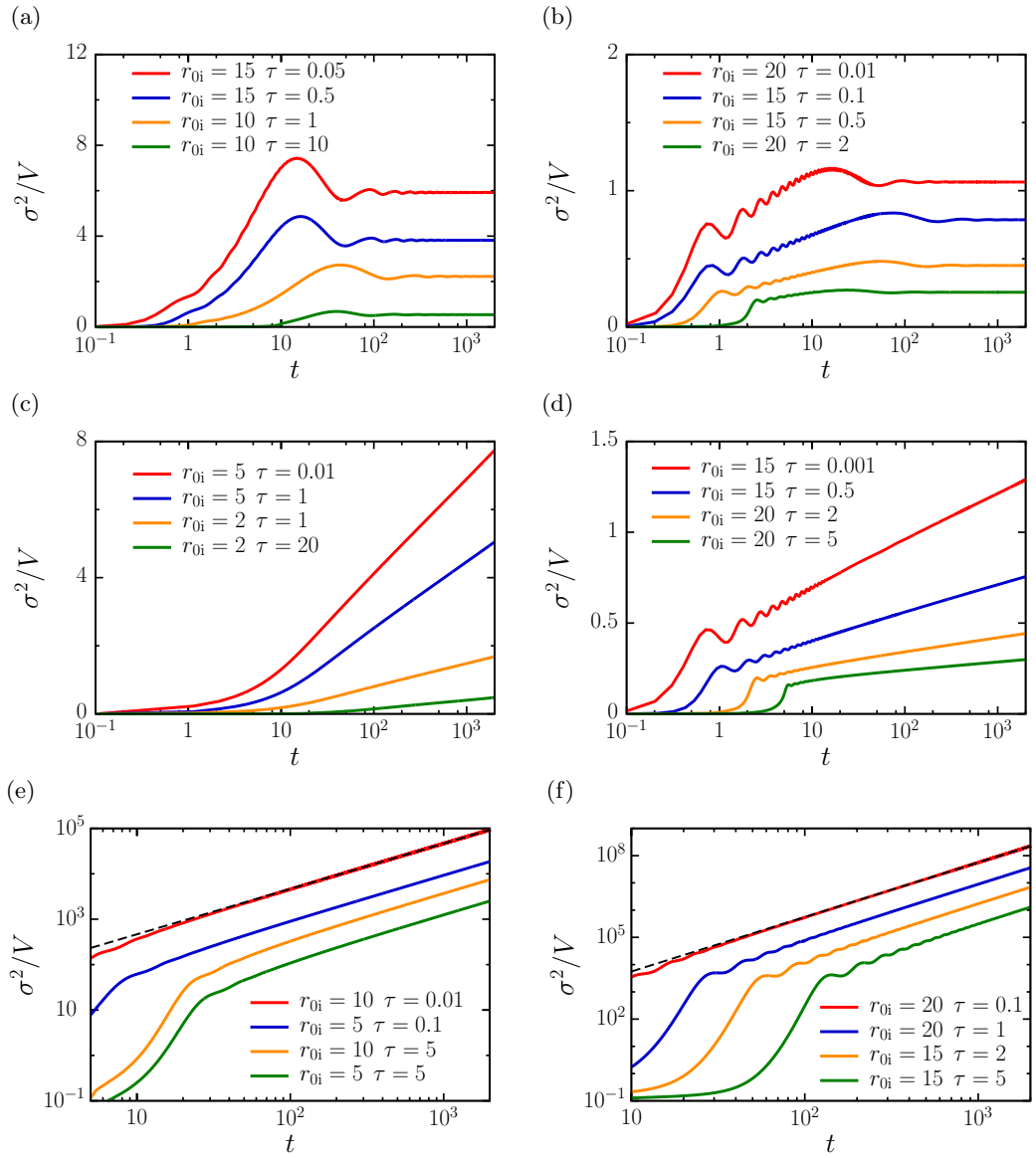

Figure 5.7: Variance per unit volume for ramps above (a, b), at (c, d), and below (e, f) the dynamical critical point in $d = 3$ (left column) and $d = 4$ (right column). Different values of the initial bare mass r_{0i} and of the ramp duration τ are shown, while the interaction is $u = 15$. Black dashed lines in (e) and (f) are proportional respectively to t and t^2.

trying to distinguish qualitatively different behaviors for different values of the bare mass at the end of the ramp. Their explicit expressions in terms of $\rho_{\mathbf{k}}(t)$ are

$$\frac{\overline{\mathcal{N}}(t)}{V} = \int^{\Lambda} \frac{\mathrm{d}^d k}{(2\pi)^d}\, \rho_{\mathbf{k}}(t), \tag{5.37}$$

$$\frac{\sigma^2(t)}{V} = \int^{\Lambda} \frac{\mathrm{d}^d k}{(2\pi)^d}\, 2\rho_{\mathbf{k}}(t)\left(1+\rho_{\mathbf{k}}(t)\right). \tag{5.38}$$

For large times, the average number of excitations relaxes to a finite value for every value of $r_{0\mathrm{f}}$, both in $d = 3$ and $d = 4$. Remarkably, the variance per unit volume displays a non-trivial behavior at large times, depending on the final value of the bare mass $r_{0\mathrm{f}}$. For ramps ending above the dynamical critical point, i.e., $r_{0\mathrm{f}} > r^c_{0\mathrm{f}}(\tau)$, the variance saturates to a finite value, both in $d = 3$ and in $d = 4$ (Figures 5.7(a) and 5.7(b)). For $r_{0\mathrm{f}} < r^c_{0\mathrm{f}}(\tau)$, the variance increases algebraically: for $d = 3$ it scales as $\sim t$ (Figure 5.7(e)), while for $d = 4$ it scales as $\sim t^2$ (Figure 5.7(f)). Finally, for ramps at the critical point, i.e., $r_{0\mathrm{f}} = r^c_{0\mathrm{f}}(\tau)$, the variance grows logarithmically in time, both in $d = 3$ and in $d = 4$ (Figures 5.7(c) and 5.7(d)).

We note that these behaviors are the same observed in the case of a sudden quench [118], showing that the critical scaling of the variance is unaffected by the change of the protocol.

5.4 Linear ramp below the dynamical critical point

Let us finally focus on the case of a ramp below the dynamical critical point. As we discuss in Sec. 4.3.3, performing a sudden quench below the dynamical critical point induces the emergence of scaling forms in the correlation functions, associated with coarsening dynamics. However, the exponent characterizing these functions differs from the one expected in usual classical coarsening. We now investigate how this behavior is affected by a linear ramp in the bare mass. To this end, we consider the equal-time two-point correlation function $\langle \phi_{\mathbf{k}}(t)\phi_{-\mathbf{k}}(t)\rangle = i\, G_K(k,t,t)/2$ and its Fourier transform $\langle \phi(\mathbf{x},t)\phi(\mathbf{y},t)\rangle$ in $d = 3$ and $d = 4$.

As a consequence of the ramp protocol, the dependence of $\langle \phi_{\mathbf{k}}(t)\phi_{-\mathbf{k}}(t)\rangle$ on momentum k displays two different regimes. In particular, studying the correlation function right at the end of the ramp (Figures 5.8(a) and 5.8(b)), we note that it exhibits the following scaling form:

$$\langle \phi_{\mathbf{k}}(\tau)\phi_{-\mathbf{k}}(\tau)\rangle = \tau^d \mathcal{F}_d(k\tau), \tag{5.39}$$

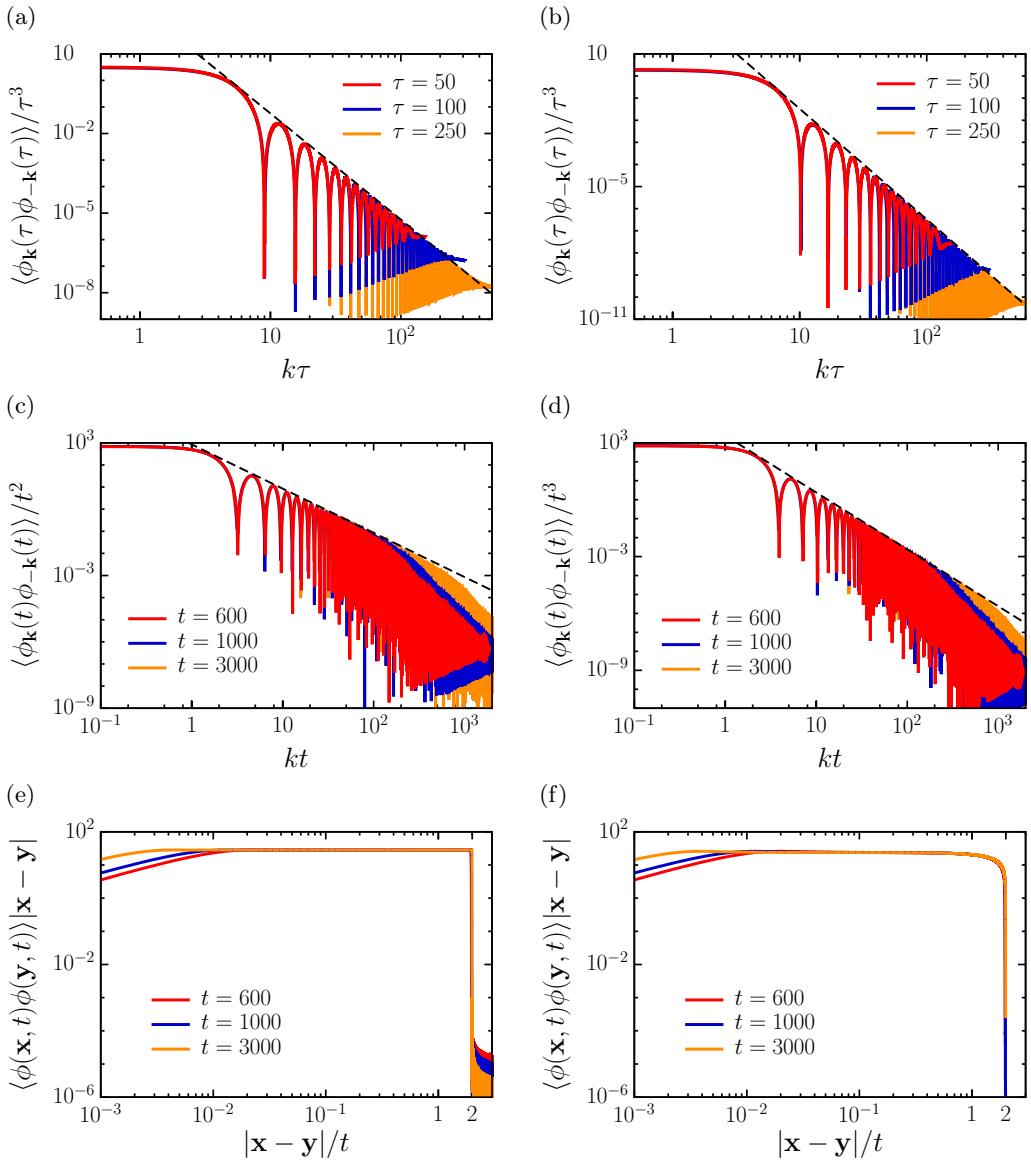

Figure 5.8: Equal-time two-point correlation functions for ramps below the dynamical critical point in $d = 3$ (left column) and $d = 4$ (right column). In all the figures the initial bare mass is $r_{0,i} = 15$, the final bare mass is $r_{0,f} = -15$ and the interaction is $u = 15$. In (a) and (b) different values of the ramp duration τ are shown and the black dashed lines are proportional respectively to $(k\tau)^{-4}$ and $(k\tau)^{-5}$. In (c) and (d) different values of the evolution time t are shown, for a ramp of duration $\tau = 20$, and the black dashed lines are proportional respectively to $(kt)^{-2}$ and $(kt)^{-3}$. In (e) and (f) different values of the evolution time t are shown, for a ramp of duration $\tau = 20$.

where $\mathcal{F}_d(k\tau)$ is an oscillating function decaying as $\sim (k\tau)^{-(d+1)}$ for $k\tau \gtrsim 1$.

In the subsequent evolution for $t > \tau$, reported in Figures5.8(c) and 5.8(d), the correlation function acquires a different dependence on momentum for $1/t \lesssim k \lesssim 1/\tau$ and, for long times after the end of the ramp, the scaling form found in the case of a sudden quench is recovered, namely,

$$\langle \phi_{\mathbf{k}}(t)\phi_{-\mathbf{k}}(t)\rangle = t^{d-1}\mathcal{G}_d(kt), \tag{5.40}$$

where $\mathcal{G}_d(kt)$ is an oscillating function decaying as $\sim (kt)^{-(d-1)}$ for $1 \lesssim kt \lesssim t/\tau$. For $k \gtrsim 1/\tau$, instead, the correlation function still decays as $\sim k^{-(d+1)}$. We note that in the limit $\tau \to 0$ the latter regime, which is due to the finite duration of the ramp, is suppressed.

The corresponding Fourier transform in real space, $\langle \phi(\mathbf{x},t)\phi(\mathbf{y},t)\rangle$, shown in Figures 5.8(e) and 5.8(f), exhibits a light-cone structure [16, 117, 158], vanishing for $|\mathbf{x}-\mathbf{y}| > 2t$ as a consequence of the finite speed of propagation of excitations, and it decays as $|\mathbf{x}-\mathbf{y}|^{-1}$ for $\tau \lesssim |\mathbf{x}-\mathbf{y}| < 2t$, both in $d = 3$ and in $d = 4$.

While in the limit $\tau \to 0$ the results of a sudden quench is fully recovered, for $\tau \to \infty$ we do not find the corresponding equilibrium correlation function, since the $O(N)$ symmetry can not be globally broken by the dynamics. Moreover, adiabaticity is not expected to hold, since the system crosses the dynamical critical point and enters a gapless phase.

5.5 Concluding remarks

In this Chapter we have investigated the dynamical phase transition of the $O(N)$ vector model in the large-N limit induced by linearly varying in time the bare mass of the system.

We analytically identified the critical dimensions of the transition and computed the critical exponent ν_*, related to the divergence of the correlation length in the stationary state close to the dynamical critical point, finding that for any finite duration of the switching protocol they are analogous to those of a finite temperature transition, despite the fact that the system is in a pure state throughout the dynamics. Only when the duration of the ramp is strictly infinite, such critical properties are those of an equilibrium system at zero temperature, i.e. the dynamical phase transition resembles a quantum phase transition. We detected numerically the dynamical critical point $r^c_{0\mathrm{f}}(\tau)$, characterizing its algebraic approach as a function of τ to both the sudden quench value (for $\tau \to 0$) and the equilibrium zero-temperature one (for $\tau \to \infty$).

The nonequilibrium nature of the dynamical transition, however, leaves strong signatures on the statistics of the excitations. We observed three qualitatively different behaviors of the fluctuations in the number of excitations as a function of time, depending on the ramp being performed above, at, or below the dynamical critical point of the system in $d = 3$ and $d = 4$. In particular, above the critical point the variance saturates at large times, below it behaves as a power law, and at the critical point it grows logarithmically. These qualitative behaviors are the same observed in the case of a sudden quench: modifying the protocol from an instantaneous change of the bare mass to a linear ramp does not affect the critical scaling of the variance.

Finally, we analyzed the equal-time two-point correlation function for ramps below the dynamical critical point and found the emergence of two different scaling behaviors, one related to the finite duration of the ramp and the other to the subsequent time evolution.

While so far the investigation of dynamical phase transitions and related universal behaviors has been mainly theoretical, the characterization of these phenomena through the statistics of excitations could be a suitable tool for experimental studies with ultracold atoms, even in realistic systems such as the Bose-Hubbard model.

Appendix

5.A Noninteracting theory and stationary values

In this section we explicitly solve Eqs. (5.8) and (5.9) in the case of a free theory, i.e., $u = 0$, and give additional details on the ansatz of Eq. (5.11).

Obviously, when $u = 0$ the effective mass is equal to the bare one, so we have to solve the equation

$$\ddot{f}^0_{\mathbf{k}}(t) + \left(k^2 + r_0(t)\right) f^0_{\mathbf{k}}(t) = 0 \tag{5.41}$$

with initial conditions

$$f^0_{\mathbf{k}}(0) = \frac{1}{\sqrt{2}\,(k^2 + r_{0\mathrm{i}})^{1/4}} \quad \text{and} \quad \dot{f}^0_{\mathbf{k}}(0) = -\,i\,\frac{(k^2 + r_{0\mathrm{i}})^{1/4}}{\sqrt{2}}. \tag{5.42}$$

For $0 < t < \tau$, the solution is given by

$$\begin{aligned} f^0_{\mathbf{k}}(t) = \frac{\pi}{\sqrt{2}\,(k^2 + r_{0\mathrm{i}})^{1/4}} \Bigg[& \mathrm{Ai}\left(\gamma t - \frac{k^2 + r_{0\mathrm{i}}}{\gamma^2}\right) \mathrm{Bi}'\left(-\frac{k^2 + r_{0\mathrm{i}}}{\gamma^2}\right) \\ & - \mathrm{Ai}'\left(-\frac{k^2 + r_{0\mathrm{i}}}{\gamma^2}\right) \mathrm{Bi}\left(\gamma t - \frac{k^2 + r_{0\mathrm{i}}}{\gamma^2}\right) \Bigg] \\ + \frac{i\pi\,(k^2 + r_{0\mathrm{i}})^{1/4}}{\sqrt{2}\,\gamma} \Bigg[& \mathrm{Ai}\left(\gamma t - \frac{k^2 + r_{0\mathrm{i}}}{\gamma^2}\right) \mathrm{Bi}\left(-\frac{k^2 + r_{0\mathrm{i}}}{\gamma^2}\right) \\ & - \mathrm{Ai}\left(-\frac{k^2 + r_{0\mathrm{i}}}{\gamma^2}\right) \mathrm{Bi}\left(\gamma t - \frac{k^2 + r_{0\mathrm{i}}}{\gamma^2}\right) \Bigg], \end{aligned} \tag{5.43}$$

where $\gamma = ((r_{0\mathrm{i}} - r_{0\mathrm{f}})/\tau)^{1/3}$, and $\mathrm{Ai}(x)$ and $\mathrm{Bi}(x)$ denote the Airy functions. For $t > \tau$, instead,

$$f^0_{\mathbf{k}}(t) = f^0_{\mathbf{k}}(\tau) \cos\Big(\sqrt{k^2 + r_{0\mathrm{f}}}\,(t - \tau)\Big) + \frac{\dot{f}^0_{\mathbf{k}}(\tau)}{\sqrt{k^2 + r_{0\mathrm{f}}}} \sin\Big(\sqrt{k^2 + r_{0\mathrm{f}}}\,(t - \tau)\Big), \tag{5.44}$$

where $f^0_{\mathbf{k}}(\tau)$ and $\dot{f}^0_{\mathbf{k}}(\tau)$ have to be read from Eq. (5.43).

By means Eqs. (5.43) and (5.44), we can explicitly compute the equal-time two-point correlation function $\langle \phi_{\mathbf{k}}(t)\phi_{-\mathbf{k}}(t)\rangle = |f^0_{\mathbf{k}}(t)|^2$, which, for $t > \tau$, reads

$$|f^0_{\mathbf{k}}(t)|^2 = \frac{1}{2}\left[|f^0_{\mathbf{k}}(\tau)|^2 + \frac{|\dot{f}^0_{\mathbf{k}}(\tau)|^2}{k^2+r_{0\mathrm{f}}} + \left(|f^0_{\mathbf{k}}(\tau)|^2 - \frac{|\dot{f}^0_{\mathbf{k}}(\tau)|^2}{k^2+r_{0\mathrm{f}}}\right)\cos\Big(\sqrt{k^2+r_{0\mathrm{f}}}\,(t-\tau)\Big) + \frac{2\,\Re\mathrm{e}[f^0_{\mathbf{k}}(\tau)\dot{f}^{0\star}_{\mathbf{k}}(\tau)]}{\sqrt{k^2+r_{0\mathrm{f}}}}\sin\Big(\sqrt{k^2+r_{0\mathrm{f}}}\,(t-\tau)\Big)\right]. \tag{5.45}$$

When $u \neq 0$, we have to resort to numerical integration of Eqs. (5.8) and (5.9), which shows that for long times after the end of the ramp the effective mass $r_{\mathrm{eff}}(t)$ relaxes to a stationary value r_*. In order to predict r_*, we adopt the following ansatz: after the end of the ramp, we assume the stationary part of the equal-time two-point correlation function to be equal to the noninteracting one, but with the bare masses and the ramp duration replaced by the renormalized ones. Namely, we take Eq. (5.45), disregard all the oscillatory terms, and replace $r_{0\mathrm{i}} \to r_{\mathrm{i}}$, $r_{0\mathrm{f}} \to r_*$, and $\tau \to \tilde{\tau}$. Thus, we obtain the following self-consistent equation for r_*

$$r_* = r_{0\mathrm{f}} + \frac{u}{12}\int^{\Lambda}\frac{\mathrm{d}^d k}{(2\pi)^d}\left(|f^0_{\mathbf{k}}(r_*,\tilde{\tau})|^2 + \frac{|\dot{f}^0_{\mathbf{k}}(r_*,\tilde{\tau})|^2}{k^2+r_*}\right), \tag{5.46}$$

where

$$\begin{aligned} f^0_{\mathbf{k}}(r_*,\tilde{\tau}) = {} & \frac{\pi}{\sqrt{2}\,(k^2+r_{\mathrm{i}})^{1/4}}\left[\mathrm{Ai}\left(-\frac{k^2+r_*}{\tilde{\gamma}^2}\right)\mathrm{Bi}'\left(-\frac{k^2+r_{\mathrm{i}}}{\tilde{\gamma}^2}\right) - \mathrm{Ai}'\left(-\frac{k^2+r_{\mathrm{i}}}{\tilde{\gamma}^2}\right)\mathrm{Bi}\left(-\frac{k^2+r_*}{\tilde{\gamma}^2}\right)\right] \\ & + \frac{i\pi\,(k^2+r_{\mathrm{i}})^{1/4}}{\sqrt{2}\,\tilde{\gamma}}\left[\mathrm{Ai}\left(-\frac{k^2+r_*}{\tilde{\gamma}^2}\right)\mathrm{Bi}\left(-\frac{k^2+r_{\mathrm{i}}}{\tilde{\gamma}^2}\right) - \mathrm{Ai}\left(-\frac{k^2+r_{\mathrm{i}}}{\tilde{\gamma}^2}\right)\mathrm{Bi}\left(-\frac{k^2+r_*}{\tilde{\gamma}^2}\right)\right], \end{aligned} \tag{5.47}$$

$$\begin{aligned} \dot{f}^0_{\mathbf{k}}(r_*,\tilde{\tau}) = {} & \frac{\pi\,\tilde{\gamma}}{\sqrt{2}\,(k^2+r_{\mathrm{i}})^{1/4}}\left[\mathrm{Ai}'\left(-\frac{k^2+r_*}{\tilde{\gamma}^2}\right)\mathrm{Bi}'\left(-\frac{k^2+r_{\mathrm{i}}}{\tilde{\gamma}^2}\right) - \mathrm{Ai}'\left(-\frac{k^2+r_{\mathrm{i}}}{\tilde{\gamma}^2}\right)\mathrm{Bi}'\left(-\frac{k^2+r_*}{\tilde{\gamma}^2}\right)\right] \\ & + \frac{i\pi\,(k^2+r_{\mathrm{i}})^{1/4}}{\sqrt{2}}\left[\mathrm{Ai}'\left(-\frac{k^2+r_*}{\tilde{\gamma}^2}\right)\mathrm{Bi}\left(-\frac{k^2+r_{\mathrm{i}}}{\tilde{\gamma}^2}\right) - \mathrm{Ai}\left(-\frac{k^2+r_{\mathrm{i}}}{\tilde{\gamma}^2}\right)\mathrm{Bi}'\left(-\frac{k^2+r_*}{\tilde{\gamma}^2}\right)\right], \end{aligned} \tag{5.48}$$

with $\tilde{\gamma} = ((r_{\mathrm{i}} - r_*)/\tilde{\tau})^{1/3}$.

5.B Dynamical critical properties

In this section we provide the detailed computation of the critical dimensions and critical exponent ν_*.

For studying the lower critical dimension, it is useful to remind the expansions of the Airy functions both for small and large arguments [160]. For small x we have

$$\begin{aligned}
\mathrm{Ai}(-x) &= \frac{1}{3^{2/3}\,\Gamma(2/3)} + \frac{x}{3^{1/3}\,\Gamma(1/3)} + O\left(x^3\right), \\
\mathrm{Ai}'(-x) &= -\frac{1}{3^{1/3}\,\Gamma(1/3)} + \frac{x^2}{2\cdot 3^{2/3}\,\Gamma(2/3)} + O\left(x^3\right), \\
\mathrm{Bi}(-x) &= \frac{1}{3^{1/6}\,\Gamma(2/3)} - \frac{3^{1/6}\,x}{\Gamma(1/3)} + O\left(x^3\right), \\
\mathrm{Bi}'(-x) &= \frac{3^{1/6}}{\Gamma(1/3)} + \frac{x^2}{2\cdot 3^{1/6}\,\Gamma(2/3)} + O\left(x^3\right),
\end{aligned} \tag{5.49}$$

while for large and positive x we have

$$\begin{aligned}
\mathrm{Ai}(-x) &= \frac{1}{\sqrt{\pi}\,x^{1/4}}\,\sin\left(\frac{\pi}{4} + \frac{2}{3}\,x^{3/2}\right) + O\left(x^{-7/4}\right), \\
\mathrm{Ai}'(-x) &= -\frac{x^{1/4}}{\sqrt{\pi}}\,\cos\left(\frac{\pi}{4} + \frac{2}{3}\,x^{3/2}\right) + O\left(x^{-5/4}\right), \\
\mathrm{Bi}(-x) &= \frac{1}{\sqrt{\pi}\,x^{1/4}}\,\cos\left(\frac{\pi}{4} + \frac{2}{3}\,x^{3/2}\right) + O\left(x^{-7/4}\right), \\
\mathrm{Bi}'(-x) &= \frac{x^{1/4}}{\sqrt{\pi}}\,\sin\left(\frac{\pi}{4} + \frac{2}{3}\,x^{3/2}\right) + O\left(x^{-5/4}\right),
\end{aligned} \tag{5.50}$$

We analyze the behavior for low momenta of the integrand of Eq. (5.46) with $r_* = 0$. For every finite τ, the most relevant modes are those with $k \ll (r_\mathrm{i}/\tilde{\tau})^{1/3}$ and $k \ll \sqrt{r_\mathrm{i}}$. In this region and for $r_* = 0$, we can replace all the Airy functions with argument $-(k^2 + r_*)/\tilde{\gamma}^2$ with their value in zero (see Eq. (5.49)), while the leading order of all the other terms is obtained setting $k = 0$. Thus, we conclude that both $f^0_{\mathbf{k}}(0,\tilde{\tau})$ and $\dot{f}^0_{\mathbf{k}}(0,\tilde{\tau})$ are constant in k. As a consequence, the lower critical dimension for every finite τ is $d = 2$.

To understand, instead, what happens in the limit $\tau \to \infty$, we have to take into account the region $(r_\mathrm{i}/\tilde{\tau})^{1/3} \ll k \ll \sqrt{r_\mathrm{i}}$. Here, and for $r_* = 0$, we have to replace the Airy functions with argument $-(k^2 + r_*)/\tilde{\gamma}^2$ with their asymptotic expansions of Eq. (5.50), and set $k = 0$ in all the other terms. Thus, we see that $f^0_{\mathbf{k}}(0,\tilde{\tau}) \sim 1/\sqrt{k}$ and $\dot{f}^0_{\mathbf{k}}(0,\tilde{\tau}) \sim \sqrt{k}$. Therefore, when τ is strictly infinite the lower critical dimension is $d = 1$.

In order to compute the critical exponent ν_*, we analyze the behavior of the asymptotic mass r_* when $r_{0\mathrm{f}}$ is close to the dynamical critical point. Defining $\delta r_{0\mathrm{f}}(\tau) = r_{0\mathrm{f}} - r_{0\mathrm{f}}^c(\tau)$ and the dimensionless variable $\mathbf{y} = \mathbf{k}/\sqrt{r_*}$, and combining Eqs. (5.11) and (5.12), one obtains

$$r_* = \delta r_{0\mathrm{f}}(\tau) + \frac{u}{12}\,(r_*)^{\frac{d-2}{2}} \int^{\Lambda/\sqrt{r_*}} \frac{\mathrm{d}^d y}{(2\pi)^d}\, \frac{y^2\, g(y\sqrt{r_*}, r_*) - (y^2+1)\, g(y\sqrt{r_*}, 0)}{y^2\,(y^2+1)}, \tag{5.51}$$

with

$$g(k, r_*) = |f_{\mathbf{k}}^0(r_*, \tilde{\tau})|^2\,(k^2 + r_*) + |\dot{f}_{\mathbf{k}}^0(r_*, \tilde{\tau})|^2. \tag{5.52}$$

The asymptotic behavior of the integral in Eq. (5.51) for small r_* is determined by the behavior of the integrand in the region $1 \ll y \ll \sqrt{r_{\mathrm{i}}/r_*}$, where it scales as $g(0,0)/y^4$. Thus, for $2 < d < 4$ the dominant contribution to the integral in powers of r_* is obtained by replacing the upper limit of integration with infinity and the integrand with its leading order in r_*, namely

$$\begin{aligned} r_* &\simeq \delta r_{0\mathrm{f}}(\tau) - \frac{u}{12}\,\frac{\Omega_d}{(2\pi)^d}\,(r_*)^{\frac{d-2}{2}} \int_0^\infty \mathrm{d}y\; y^{d-1}\, \frac{g(0,0)}{y^2\,(y^2+1)} \\ &= \delta r_{0\mathrm{f}}(\tau) + \frac{u}{12}\,\frac{\Omega_d}{(2\pi)^d}\,(r_*)^{\frac{d-2}{2}}\, \frac{\pi\, g(0,0)}{2\sin\left(d\pi/2\right)}, \end{aligned} \tag{5.53}$$

where Ω_d is the solid angle in d dimensions. We conclude that at the leading order $r_* \sim (\delta r_{0\mathrm{f}}(\tau))^{2/(d-2)}$. For $d = 4$ we have logarithmic corrections to this scaling, while for $d > 4$ the divergence of the integral can be deduced by considering the scaling of the integrand mentioned above. We have that the integral diverges as $(r_*)^{-(d-4)/2}$, giving a linear dependence $r_* \sim \delta r_{0\mathrm{f}}(\tau)$ at the leading order. Therefore, we can recover the values of Eq. (5.13) for the critical exponent ν_*.

5.C Asymptotic expansions for large τ

In this section we provide additional details on the derivation of Eqs. (5.17) and (5.18).

Let us start by considering the case of $d = 3$. Computing the integrals (5.15)

and (5.16), we obtain

$$\begin{aligned}\mathcal{I}_1(3) = \Lambda^2 \Bigg[& \frac{2\pi}{3^{1/3}\,\Gamma^2(-1/3)}\ {}_2F_3\left(\frac{1}{6},\frac{1}{2};\frac{1}{3},\frac{2}{3},\frac{3}{2};-\frac{4}{9}\,y^2\right) y^{1/3} \\ & - \frac{1}{5\sqrt{3}}\ {}_2F_3\left(\frac{1}{2},\frac{5}{6};\frac{2}{3},\frac{4}{3},\frac{11}{6};-\frac{4}{9}\,y^2\right) y \\ & + \frac{\Gamma(5/6)}{2^{1/3}\cdot 3^{1/6}\cdot 7\,\sqrt{\pi}}\ {}_2F_3\left(\frac{5}{6},\frac{7}{6};\frac{4}{3},\frac{5}{3},\frac{13}{6};-\frac{4}{9}\,y^2\right) y^{5/3}\Bigg], \end{aligned} \tag{5.54}$$

$$\begin{aligned}\mathcal{I}_2(3) = \Lambda^2 \Bigg[& -\frac{3^{1/3}\,\Gamma(-1/3)\,\Gamma(5/3)}{4\,\pi}\ {}_2F_3\left(-\frac{1}{6},\frac{1}{6};-\frac{1}{3},\frac{1}{3},\frac{7}{6};-\frac{4}{9}\,y^2\right) y^{-1/3} \\ & + \frac{1}{10\sqrt{3}}\ {}_2F_3\left(\frac{1}{2},\frac{5}{6};\frac{1}{3},\frac{5}{3},\frac{11}{6};-\frac{4}{9}\,y^2\right) y \\ & + \frac{\Gamma(1/6)}{2^{2/3}\cdot 3^{5/6}\cdot 36\,\sqrt{\pi}}\ {}_2F_3\left(\frac{7}{6},\frac{3}{2};\frac{5}{3},\frac{7}{3},\frac{5}{2};-\frac{4}{9}\,y^2\right) y^{7/3}\Bigg], \end{aligned} \tag{5.55}$$

where ${}_2F_3(a,b;c,d,e;x)$ denotes the hypergeometric function and $y = \Lambda^3\tilde{\tau}/r_\mathrm{i}$. Asymptotically expanding the hypergeometric functions for large y, namely

$$\begin{aligned}
{}_2F_3\left(\frac{1}{6},\frac{1}{2};\frac{1}{3},\frac{2}{3},\frac{3}{2};-\frac{4}{9}\,y^2\right) &= \frac{3^{5/6}\,\sqrt{\pi}}{2^{1/3}\,\Gamma(1/6)}\,y^{-1/3} - \frac{\sqrt{3\pi}\,\Gamma(-1/3)}{24\,\Gamma(1/6)}\,y^{-1} + O\Big(y^{-5/3}\Big), \\
{}_2F_3\left(\frac{1}{2},\frac{5}{6};\frac{2}{3},\frac{4}{3},\frac{11}{6};-\frac{4}{9}\,y^2\right) &= \frac{5}{4\sqrt{3}}\,y^{-1} - \frac{5\,\Gamma(-1/3)}{2^{8/3}\cdot 3^{11/6}}\,y^{-5/3} + O\Big(y^{-7/3}\Big), \\
{}_2F_3\left(\frac{5}{6},\frac{7}{6};\frac{4}{3},\frac{5}{3},\frac{13}{6};-\frac{4}{9}\,y^2\right) &= \frac{7\,\sqrt{\pi}}{2^{2/3}\cdot 3^{5/6}\,\Gamma(5/6)}\,y^{-5/3} + \frac{7\,\sqrt{\pi}\,\Gamma(-1/3)}{2^{7/3}\cdot 3^{13/6}\,\Gamma(5/6)}\,y^{-7/3} \\
&\quad + O\big(y^{-3}\big), \\
{}_2F_3\left(-\frac{1}{6},\frac{1}{6};-\frac{1}{3},\frac{1}{3},\frac{7}{6};-\frac{4}{9}\,y^2\right) &= \frac{\Gamma(4/3)}{3^{5/6}\,\Gamma(5/3)}\,y^{1/3} + \frac{\pi}{2^{2/3}\cdot 3^{5/3}\,\Gamma(5/3)}\,y^{-1/3} \\
&\quad + O\big(y^{-1}\big), \\
{}_2F_3\left(\frac{1}{2},\frac{5}{6};\frac{1}{3},\frac{5}{3},\frac{11}{6};-\frac{4}{9}\,y^2\right) &= -\frac{5}{2\sqrt{3}}\,y^{-1} - \frac{5\,\Gamma(-1/3)}{2^{5/3}\cdot 3^{5/6}}\,y^{-5/3} + O\Big(y^{-7/3}\Big), \\
{}_2F_3\left(\frac{7}{6},\frac{3}{2};\frac{5}{3},\frac{7}{3},\frac{5}{2};-\frac{4}{9}\,y^2\right) &= \frac{2^{2/3}\cdot 3^{5/6}\cdot 6\,\sqrt{\pi}}{\Gamma(1/6)}\,y^{-7/3} - \frac{27\,\sqrt{3\pi}\,\Gamma(5/3)}{4\,\Gamma(1/6)}\,y^{-3} \\
&\quad + O\Big(y^{-11/3}\Big),
\end{aligned} \tag{5.56}$$

we find

$$\mathcal{I}_1(3) = \frac{\Lambda^2}{4} + \frac{\Gamma(-1/3)}{2^{11/3}\cdot 3^{4/3}}\left(\frac{r_\mathrm{i}}{\tilde{\tau}}\right)^{2/3} + O\left(\left(\frac{r_\mathrm{i}}{\Lambda^3\,\tilde{\tau}}\right)^{4/3}\right), \tag{5.57}$$

$$\mathcal{I}_2(3) = \frac{\Lambda^2}{4} - \frac{\Gamma(-1/3)}{2^{11/3}\cdot 3^{1/3}}\left(\frac{r_\mathrm{i}}{\tilde{\tau}}\right)^{2/3} + O\left(\left(\frac{r_\mathrm{i}}{\Lambda^3\,\tilde{\tau}}\right)^{4/3}\right). \tag{5.58}$$

Using these results, we can recover Eq. (5.17).

For $d = 4$, we have

$$\begin{aligned}\mathcal{I}_1(4) + \mathcal{I}_2(4) = \Lambda^3 \Bigg\{ & \frac{1}{12\sqrt{3}}\, y^{-1} + \frac{\pi}{12} \Big[2\, y^{1/3} \left(\mathrm{Ai}^2(-y^{2/3}) + \mathrm{Bi}^2(-y^{2/3}) \right) \\ & + 2 y^{-1/3} \left(\mathrm{Ai}'^{\,2}(-y^{2/3}) + \mathrm{Bi}'^{\,2}(-y^{2/3}) \right) \\ & - y^{-1} \left(\mathrm{Ai}(-y^{2/3}) \mathrm{Ai}'(-y^{2/3}) + \mathrm{Bi}(-y^{2/3}) \mathrm{Bi}'(-y^{2/3}) \right) \Big] \Bigg\}, \end{aligned} \tag{5.59}$$

where we introduced $y = \Lambda^3 \tilde{\tau}/r_\mathrm{i}$. Expanding the Airy functions for large and negative arguments, we finally get

$$\mathcal{I}_1(4) + \mathcal{I}_2(4) = -\frac{\Lambda^3}{3} + \frac{1}{12\sqrt{3}} \left(\frac{r_\mathrm{i}}{\tilde{\tau}} \right) + O\left(\left(\frac{r_\mathrm{i}}{\Lambda^3\, \tilde{\tau}} \right)^2 \right), \tag{5.60}$$

from which Eq. (5.18) follows.

Conclusions

In this Thesis we discussed several issues related to the dynamics of isolated quantum many-body systems. The brief overview of Chapter 1 highlighted a series of open fundamental theoretical questions which are crucial for the investigation of nonequilibrium phenomena. Among them, we mainly focused on the emergence of thermal behaviors and on the characterization of dynamical phase transitions and of the associated universal dynamics. To this end, we analyzed some paradigmatic models, such as the Fermi-Hubbard model, the quantum Ising chain, and the $O(N)$ model.

As reported in Sec. 1.4, the issue of thermalization of a Landau-Fermi liquid after an interaction quench is controversial and not settled yet [88, 91, 97]. On the one hand, indeed, if such a system is supplied with an excess energy, the common expectation is that it thermalizes because of the continuum of gapless excitations that can redistribute that energy. On the other hand, however slowly the interaction is turned on, if thermalization occurs, the extensive amount of energy supplied in the switching process would translate into a finite temperature. However, in a Landau-Fermi liquid all equal-time correlation functions decay as a power-law in the distance at zero temperature and exponentially at any finite temperature. This would imply that, no matter how slow the switching protocol is, if thermalization holds the initial noninteracting Fermi sea can never evolve into the interacting ground state, in stark contrast with Landau's adiabatic assumption which is at the ground of the Fermi-liquid theory [122, 123]. We contributed to this puzzle in Chapter 2 with two perturbative calculations. First we focused on the structure factor $S(\mathbf{q})$, which is nonanalytic at zero temperature for $|\mathbf{q}| \to 0$, but turns analytic at finite temperature. Thus, if thermalization indeed holds, the analytic properties of the long-wavelength structure factor should totally change during the time evolution. Perturbatively and under some general assumptions, such an analyticity switch must show up as a singularity at the second-order in the perturbative expansion in the interaction strength of the steady-state structure

factor. Remarkably, we found that second-order corrections are not singular as required by thermalization. In particular, the long-wavelength structure factor has an analytical component compatible with thermalization, but it retains also a nonanalytic term characteristic of a Fermi liquid at zero-temperature. We next considered the case of a dilute Fermi gas, where one can obtain results valid at any order in the interaction strength but at leading in the density. We found that in the steady state the momentum distribution jump at the Fermi surface is strictly finite, though smaller than at equilibrium, up to second order in $k_F f_0$, where f_0 is the scattering length of two particles in the vacuum. These two calculations question the expectation of thermalization of a Landau-Fermi liquid. Even though the main criticism to our results is that they are not valid because time-dependent perturbation theory is unjustified as $t \to \infty$ and at some higher order a singularity arises invalidating also the second order calculation, there are some other arguments which leave open this issue hence worth to be further investigated. For example, it was suggested [131] that a nonintegrable model whose low-energy properties can be described by an integrable effective Hamiltonian, which is the case of a Landau-Fermi liquid, will posses Poisson's level statistics of the low-energy many-body spectrum. If that conjecture were true, it would imply no equipartition of the low-energy density that is injected during the switching process, which might explain our results. We also pointed out that, rigorously speaking, thermalization can be justified only when the Hamiltonian density is local and in reference to local observables in real space. This restriction of the notion of thermalization would have no contradiction with our findings, since the long-wavelength limit of the static structure factor or the momentum distribution close to k_F are not local observable.

The study of the universal dynamics resulting from the variation of a control parameter through the quantum critical point of a system received a lot of attention in the recent literature. An example in this context is the generalization of the classical Kibble-Zurek mechanism describing the scaling of the excitation density with the rate at which the critical point is crossed. However, the dynamics of interacting quantum systems has interesting features even when the system is fully gapped for the entire duration of the protocol [1]. In the latter case, it was shown that corrections with respect to the equilibrium value of the excitation density and of the excess energy vanish quadratically in the switching rate for linear ramps, and it was suggested that other thermodynamic quantities could share the same property [136]. However, a different scenario arises when considering the dynamics

of the order parameter in a phase with spontaneous symmetry breaking for low-dimensional systems. In Chapter 3 we studied in details the case of a quantum Ising chain subject to the linear variation in time of the transverse field within the ferromagnetic phase. We found that, however small the switching rate is, the stationary value of the spontaneous magnetization does not behave in an adiabatic way, even though performing a ramp within a gapped phase seems to be the most favorable situation for adiabaticity. In particular, focusing on the value of the order parameter at the end of the ramp, we showed that the smaller the switching rate is the closer it gets to its ground state value. Nonetheless, this apparently small correction eventually leads to the disruption of the order exponentially fast in the subsequent time evolution. Such a behavior of the order parameter has to be expected whenever the system has a phase transition only at zero temperature and it is driven within the ordered phase. Indeed, a finite density of excitations will always be generated and in this situation will be always sufficient to destroy order. A natural question that emerges is what happens instead in an analogous system where the transition survives at finite temperature. One possibility is the existence of a transition in the value of the order parameter as a function of the switching rate, namely, for sufficiently slow ramps its asymptotic value is finite, while it goes to zero for fast ramps.

In Chapter 4 and 5 we considered the nonequilibrium dynamics of a bosonic interacting scalar field theory with $O(N)$ symmetry. In the limit of large N, the model is exactly solvable and can be effectively described by a quadratic Hamiltonian. Integrability prevents the thermalization of the system, which approaches a stable nonthermal steady state. This simple model reveals some interesting features, such as the occurrence of a dynamical phase transition [113, 116–119].

In the case of a sudden quench (Chapter 4) to the dynamical critical point, the lack of time and length scales leads to aging behavior, which we characterized by computing scaling forms and critical exponents acquired by the Keldysh (G_K) and retarded (G_R) Green's functions. In particular, we found that at long times the G_K exhibits an anomalous momentum dependence if compared to the corresponding G_K of a critical truly Gaussian (noninteracting) theory after a deep quench. This anomalous dependence reveals the nonthermal nature of the stationary state eventually attained by the system, which retains memory of the initial state, and can be interpreted in terms of a momentum-dependent effective temperature. Moreover, quenching below the dynamical critical point revealed that the two-time correlation functions still display scaling behaviors, but with different exponents

with respect to the critical case. The scaling forms are related to the coarsening dynamics, analogously to what happens in classical systems quenched below the critical temperature. However, the exponent characterizing these functions differs from the one expected in usual classical coarsening. The reason for this discrepancy between quantum and classical systems is till now unclear and subject of active research. It could be a consequence of the nonthermal nature of the steady state and thus could disappear taking into account $1/N^2$-terms.

The presence of a dynamical phase transition, as well as its critical properties, are robust against the change of the protocol, as we showed performing a linear ramp of one of the parameters in the Hamiltonian (Chapter 5). We detected the dynamical critical point, whose value interpolates between the limiting cases of the sudden quench and the adiabatic switching, and found that for any finite duration of the protocol the critical dimensions and exponents are the same as those of an equilibrium thermal transition. The nonequilibrium nature of the dynamical transition, however, leaves strong signatures on the statistics of the excitations. We observed three qualitatively different behaviors of the fluctuations in the number of excitations as a function of time, depending on the ramp being performed above, at, or below the dynamical critical point of the system, which are not affected by the duration of the switching process. As a result, a measure of the statistics of excitations, which should be accessible in ultracold atom experiments, could provide direct signatures of the dynamical transition as well as of aging and coarsening properties even in realistic systems such as the Bose-Hubbard model.

Bibliography

[1] A. Polkovnikov, K. Sengupta, A. Silva, and M. Vengalattore, Rev. Mod. Phys. **83**, 863 (2011).

[2] I. Bloch, J. Dalibard, and W. Zwerger, Rev. Mod. Phys. **80**, 885 (2008).

[3] T. Langen, R. Geiger, and J. Schmiedmayer, Annu. Rev. Condens. Matter Phys. **6**, 201 (2015).

[4] P. Calabrese and J. Cardy, Phys. Rev. Lett. **96**, 136801 (2006).

[5] M. Greiner, O. Mandel, T. W. Hänsch, and I. Bloch, Nature **419**, 51 (2002).

[6] G. Lamporesi, S. Donadello, S. Serafini, F. Dalfovo, and G. Ferrari, Nature Physics **9**, 656 (2013).

[7] T. W. B. Kibble, J. Phys. A: Math. Gen. **9**, 1387 (1976).

[8] W. H. Zurek, Nature **317**, 505 (1985).

[9] W. H. Zurek, Phys. Rep. **276**, 177 (1996).

[10] I. Bloch, J. Dalibard, and S. Nascimbène, Nature Physics **8**, 267 (2012).

[11] S. Trotzky, Y.-A. Chen, A. Flesch, I. P. McCulloch, U. Schollwöck, J. Eisert, and I. Bloch, Nature Physics **8**, 325 (2012).

[12] W. S. Bakr, A. Peng, M. E. Tai, R. Ma, J. Simon, J. I. Gillen, S. Fölling, L. Pollet, and M. Greiner, Science **329**, 547 (2010).

[13] J. F. Sherson, C. Weitenberg, M. Endres, M. Cheneau, I. Bloch, and S. Kuhr, Nature **467**, 68 (2010).

[14] C. Weitenberg, M. Endres, J. F. Sherson, M. Cheneau, P. Schauss, T. Fukuhara, I. Bloch, and S. Kuhr, Nature **471**, 319 (2011).

[15] M. Endres, M. Cheneau, T. Fukuhara, C. Weitenberg, P. Schauß, C. Gross, L. Mazza, M. C. Bañuls, L. Pollet, I. Bloch, and S. Kuhr, Science **334**, 200 (2011).

[16] M. Cheneau, P. Barmettler, D. Poletti, M. Endres, P. Schauß, T. Fukuhara, C. Gross, I. Bloch, C. Kollath, and S. Kuhr, Nature **481**, 484 (2012).

[17] T. Fukuhara, A. Kantian, M. Endres, M. Cheneau, P. Schauß, S. Hild, D. Bellem, U. Schollwöck, T. Giamarchi, C. Gross, I. Bloch, and S. Kuhr, Nature Phys. **9**, 235 (2013).

[18] T. Fukuhara, P. Schauß, M. Endres, S. Hild, M. Cheneau, I. Bloch, and C. Gross, Nature **502**, 76 (2013).

[19] M. Gring, M. Kuhnert, T. Langen, T. Kitagawa, B. Rauer, M. Schreitl, I. Mazets, D. Adu Smith, E. Demler, and J. Schmiedmayer, Science **337**, 1318 (2012).

[20] T. Langen, M. Gring, M. Kuhnert, B. Rauer, R. Geiger, D. Adu Smith, I. E. Mazets, and J. Schmiedmayer, Eur. Phys. J. ST **217**, 43 (2013).

[21] M. Kuhnert, R. Geiger, T. Langen, M. Gring, B. Rauer, T. Kitagawa, E. Demler, D. Adu Smith, and J. Schmiedmayer, Phys. Rev. Lett. **110**, 090405 (2013).

[22] D. Adu Smith, M. Gring, T. Langen, M. Kuhnert, B. Rauer, R. Geiger, T. Kitagawa, I. Mazets, E. Demler, and J. Schmiedmayer, New J. Phys. **15**, 075011 (2013).

[23] C.-L. Hung, V. Gurarie, and C. Chin, Science **341**, 1213 (2013).

[24] L. E. Sadler, J. M. Higbie, S. R. Leslie, M. Vengalattore, and D. M. Stamper-Kurn, Nature **443**, 312 (2006).

[25] S. Inouye, M. R. Andrews, J. Stenger, H.-J. Miesner, D. M. Stamper-Kurn, and W. Ketterle, Nature **392**, 151 (1998).

[26] C. Chin, R. Grimm, P. Julienne, and E. Tiesinga, Rev. Mod. Phys. **82**, 1225 (2010).

[27] F. Meinert, M. J. Mark, E. Kirilov, K. Lauber, P. Weinmann, A. J. Daley, and H.-C. Nägerl, Phys. Rev. Lett. **111**, 053003 (2013).

[28] J. Simon, W. S. Bakr, R. Ma, M. E. Tai, P. M. Preiss, and M. Greiner, Nature **472**, 307 (2011).

[29] S. Sachdev, K. Sengupta, and S. M. Girvin, Phys. Rev. B **66**, 075128 (2002).

[30] T. Kinoshita, T. Wenger, and D. S. Weiss, Nature **440**, 900 (2006).

[31] E. H. Lieb and W. Liniger, Phys. Rev. **130**, 1605 (1963).

[32] E. H. Lieb, Phys. Rev. **130**, 1616 (1963).

[33] J. von Neumann, Z. Phys. **57**, 30 (1929).

[34] S. Goldstein, J. L. Lebowitz, R. Tumulka, and N. Zanghì, Eur. Phys. J. H **35**, 173 (2010).

[35] J. M. Deutsch, Phys. Rev. A **43**, 2046 (1991).

[36] M. Srednicki, Phys. Rev. E **50**, 888 (1994).

[37] A. Peres, Phys. Rev. A **30**, 504 (1984).

[38] M. Rigol, V. Dunjko, and M. Olshanii, Nature **452**, 854 (2008).

[39] M. Rigol, Phys. Rev. Lett. **103**, 100403 (2009).

[40] M. Rigol and L. F. Santos, Phys. Rev. A **82**, 011604 (2010).

[41] L. F. Santos and M. Rigol, Phys. Rev. E **82**, 031130 (2010).

[42] T. N. Ikeda, Y. Watanabe, and M. Ueda, Phys. Rev. E **84**, 021130 (2011).

[43] M. Rigol and M. Srednicki, Phys. Rev. Lett. **108**, 110601 (2012).

[44] C. Neuenhahn and F. Marquardt, Phys. Rev. E **85**, 060101 (2012).

[45] S. Dubey, L. Silvestri, J. Finn, S. Vinjanampathy, and K. Jacobs, Phys. Rev. E **85**, 011141 (2012).

[46] R. Steinigeweg, J. Herbrych, and P. Prelovšek, Phys. Rev. E **87**, 012118 (2013).

[47] W. Beugeling, R. Moessner, and M. Haque, Phys. Rev. E **89**, 042112 (2014).

[48] G. Biroli, C. Kollath, and A. M. Läuchli, Phys. Rev. Lett. **105**, 250401 (2010).

[49] C. Kollath, A. M. Läuchli, and E. Altman, Phys. Rev. Lett. **98**, 180601 (2007).

[50] C. Gogolin, M. P. Müller, and J. Eisert, Phys. Rev. Lett. **106**, 040401 (2011).

[51] M. C. Bañuls, J. I. Cirac, and M. B. Hastings, Phys. Rev. Lett. **106**, 050405 (2011).

[52] B. Sutherland, *Beautiful Models: 70 Years of Exactly Solved Quantum Many-body Problems*, World Scientific, Singapore, 2004.

[53] J.-S. Caux and J. Mossel, J. Stat. Mech. Theor. Exp. **2011**, P02023 (2011).

[54] E. T. Jaynes, Phys. Rev. **106**, 620 (1957).

[55] E. T. Jaynes, Phys. Rev. **108**, 171 (1957).

[56] M. Rigol, V. Dunjko, V. Yurovsky, and M. Olshanii, Phys. Rev. Lett. **98**, 050405 (2007).

[57] M. Girardeau, J. Math. Phys. **1**, 516 (1960).

[58] M. Rigol, A. Muramatsu, and M. Olshanii, Phys. Rev. A **74**, 053616 (2006).

[59] M. Kollar and M. Eckstein, Phys. Rev. A **78**, 013626 (2008).

[60] P. Calabrese, F. H. L. Essler, and M. Fagotti, Phys. Rev. Lett. **106**, 227203 (2011).

[61] P. Calabrese, F. H. L. Essler, and M. Fagotti, J. Stat. Mech. Theor. Exp. **2012**, P07022 (2012).

[62] M. Fagotti and F. H. L. Essler, Phys. Rev. B **87**, 245107 (2013).

[63] M. A. Cazalilla, Phys. Rev. Lett. **97**, 156403 (2006).

[64] A. Iucci and M. A. Cazalilla, Phys. Rev. A **80**, 063619 (2009).

[65] M. A. Cazalilla, A. Iucci, and M.-C. Chung, Phys. Rev. E **85**, 011133 (2012).

[66] J. M. Luttinger, J. Math. Phys. **4**, 1154 (1963).

[67] D. C. Mattis and E. H. Lieb, Journal of Mathematical Physics **6**, 304 (1965).

[68] J.-S. Caux and R. M. Konik, Phys. Rev. Lett. **109**, 175301 (2012).

[69] M. Kormos, A. Shashi, Y.-Z. Chou, J.-S. Caux, and A. Imambekov, Phys. Rev. B **88**, 205131 (2013).

[70] M. Kormos, M. Collura, and P. Calabrese, Phys. Rev. A **89**, 013609 (2014).

[71] B. Pozsgay, J. Stat. Mech. Theor. Exp. **2013**, P07003 (2013).

[72] M. Fagotti and F. H. L. Essler, J. Stat. Mech. Theor. Exp. **2013**, P07012 (2013).

[73] M. Fagotti, M. Collura, F. H. L. Essler, and P. Calabrese, Phys. Rev. B **89**, 125101 (2014).

[74] D. Fioretto and G. Mussardo, New J. Phys. **12**, 055015 (2010).

[75] G. Mussardo, Phys. Rev. Lett. **111**, 100401 (2013).

[76] S. Sotiriadis, G. Takacs, and G. Mussardo, Phys. Lett. B **734**, 52 (2014).

[77] A. C. Cassidy, C. W. Clark, and M. Rigol, Phys. Rev. Lett. **106**, 140405 (2011).

[78] D. M. Gangardt and M. Pustilnik, Phys. Rev. A **77**, 041604 (2008).

[79] S. Ziraldo and G. E. Santoro, Phys. Rev. B **87**, 064201 (2013).

[80] G. Goldstein and N. Andrei, Failure of the GGE hypothesis for integrable models with bound states, arXiv:1405.4224 (2014).

[81] M. Mierzejewski, P. Prelovšek, and T. Prosen, Phys. Rev. Lett. **113**, 020602 (2014).

[82] B. Wouters, J. De Nardis, M. Brockmann, D. Fioretto, M. Rigol, and J.-S. Caux, Phys. Rev. Lett. **113**, 117202 (2014).

[83] B. Pozsgay, M. Mestyán, M. A. Werner, M. Kormos, G. Zaránd, and G. Takács, Phys. Rev. Lett. **113**, 117203 (2014).

[84] B. Pozsgay, J. Stat. Mech. Theor. Exp. **2014**, P09026 (2014).

[85] J. Berges, S. Borsányi, and C. Wetterich, Phys. Rev. Lett. **93**, 142002 (2004).

[86] A. Arrizabalaga, J. Smit, and A. Tranberg, Phys. Rev. D **72**, 025014 (2005).

[87] D. Podolsky, G. N. Felder, L. Kofman, and M. Peloso, Phys. Rev. D **73**, 023501 (2006).

[88] M. Moeckel and S. Kehrein, Phys. Rev. Lett. **100**, 175702 (2008).

[89] M. Moeckel and S. Kehrein, Ann. Phys. **324**, 2146 (2009).

[90] M. Moeckel and S. Kehrein, New J. Phys. **12**, 055016 (2010).

[91] M. Eckstein, M. Kollar, and P. Werner, Phys. Rev. Lett. **103**, 056403 (2009).

[92] M. Eckstein, M. Kollar, and P. Werner, Phys. Rev. B **81**, 115131 (2010).

[93] M. Kollar, F. A. Wolf, and M. Eckstein, Phys. Rev. B **84**, 054304 (2011).

[94] R. Barnett, A. Polkovnikov, and M. Vengalattore, Phys. Rev. A **84**, 023606 (2011).

[95] J. Marino and A. Silva, Phys. Rev. B **86**, 060408 (2012).

[96] A. Mitra, Phys. Rev. B **87**, 205109 (2013).

[97] M. Stark and M. Kollar, Kinetic description of thermalization dynamics in weakly interacting quantum systems, arXiv:1308.1610 (2013).

[98] M. Marcuzzi, J. Marino, A. Gambassi, and A. Silva, Phys. Rev. Lett. **111**, 197203 (2013).

[99] F. H. L. Essler, S. Kehrein, S. R. Manmana, and N. J. Robinson, Phys. Rev. B **89**, 165104 (2014).

[100] N. Nessi, A. Iucci, and M. A. Cazalilla, Phys. Rev. Lett. **113**, 210402 (2014).

[101] B. Bertini, F. H. L. Essler, S. Groha, and N. J. Robinson, Prethermalization and thermalization in models with weak integrability breaking, arXiv:1506.02994 (2015).

[102] T. Kitagawa, A. Imambekov, J. Schmiedmayer, and E. Demler, New J. Phys. **13**, 073018 (2011).

[103] F. Wegner, Ann. Phys. **506**, 77 (1994).

[104] S. Kehrein, *The Flow Equation Approach to Many-Particle Systems*, Springer Tracts in Modern Physics, Springer, Berlin Heidelberg, 2007.

[105] I. E. Mazets, T. Schumm, and J. Schmiedmayer, Phys. Rev. Lett. **100**, 210403 (2008).

[106] T. Kitagawa, S. Pielawa, A. Imambekov, J. Schmiedmayer, V. Gritsev, and E. Demler, Phys. Rev. Lett. **104**, 255302 (2010).

[107] T. Langen, S. Erne, R. Geiger, B. Rauer, T. Schweigler, M. Kuhnert, W. Rohringer, I. E. Mazets, T. Gasenzer, and J. Schmiedmayer, Science **348**, 207 (2015).

[108] M. Schirò and M. Fabrizio, Phys. Rev. Lett. **105**, 076401 (2010).

[109] M. Sandri, M. Schiró, and M. Fabrizio, Phys. Rev. B **86**, 075122 (2012).

[110] N. Tsuji, M. Eckstein, and P. Werner, Phys. Rev. Lett. **110**, 136404 (2013).

[111] N. Tsuji and P. Werner, Phys. Rev. B **88**, 165115 (2013).

[112] B. Sciolla and G. Biroli, Phys. Rev. Lett. **105**, 220401 (2010).

[113] A. Gambassi and P. Calabrese, Europhys. Lett. **95**, 66007 (2011).

[114] B. Sciolla and G. Biroli, J. Stat. Mech. Theor. Exp. **2011**, P11003 (2011).

[115] M. Sandri and M. Fabrizio, Phys. Rev. B **88**, 165113 (2013).

[116] A. Chandran, A. Nanduri, S. S. Gubser, and S. L. Sondhi, Phys. Rev. B **88**, 024306 (2013).

[117] B. Sciolla and G. Biroli, Phys. Rev. B **88**, 201110 (2013).

[118] P. Smacchia, M. Knap, E. Demler, and A. Silva, Phys. Rev. B **91**, 205136 (2015).

[119] A. Chiocchetta, M. Tavora, A. Gambassi, and A. Mitra, Phys. Rev. B **91**, 220302 (2015).

[120] P. Barmettler, M. Punk, V. Gritsev, E. Demler, and E. Altman, Phys. Rev. Lett. **102**, 130603 (2009).

[121] G. Mazza and M. Fabrizio, Phys. Rev. B **86**, 184303 (2012).

[122] L. D. Landau, Zh. Eksp. Teor. Fiz. **30**, 1058 (1956), [Sov. Phys. JETP 3, 920–925 (1957)].

[123] L. D. Landau, Zh. Eksp. Teor. Fiz. **32**, 59 (1957), [Sov. Phys. JETP 5, 101–108 (1957)].

[124] O. Costin, *Asymptotics and Borel Summability*, Monographs and Surveys in Pure and Applied Mathematics, CRC Press, Boca Raton, 2008.

[125] E. Coira, F. Becca, and A. Parola, Eur. Phys. J. B **86**, 55 (2013).

[126] V. M. Galitskii, Zh. Eksp. Teor. Fiz. **34**, 151 (1958), [Sov. Phys. JETP 7, 104–112 (1958)].

[127] M. Fabrizio, A. Parola, and E. Tosatti, Phys. Rev. B **44**, 1033 (1991).

[128] P. W. Anderson, Phys. Rev. **112**, 1900 (1958).

[129] R. Mélin, J. Phys. I France **5**, 159 (1995).

[130] R. Mélin, J. Phys. I France **5**, 787 (1995).

[131] M. Di Stasio and X. Zotos, Phys. Rev. Lett. **74**, 2050 (1995).

[132] E. G. Dalla Torre, E. Demler, T. Giamarchi, and E. Altman, Nature Phys. **6**, 806 (2010).

[133] A. Mitra and T. Giamarchi, Phys. Rev. Lett. **107**, 150602 (2011).

[134] A. Polkovnikov, Phys. Rev. B **72**, 161201 (2005).

[135] W. H. Zurek, U. Dorner, and P. Zoller, Phys. Rev. Lett. **95**, 105701 (2005).

[136] C. De Grandi and A. Polkovnikov, in *Quantum Quenching, Annealing and Computation*, edited by A. K. Chandra, A. Das, and B. K. Chakrabarti, Springer, Berlin Heidelberg, 2010, volume 802 of *Lecture Notes in Physics*, chapter 4.

[137] M. Eckstein and M. Kollar, New J. Phys. **12**, 055012 (2010).

[138] A. Polkovnikov and V. Gritsev, Nature Phys. **4**, 477 (2008).

[139] S.-J. Gu and H.-Q. Lin, Europhys. Lett. **87**, 10003 (2009).

[140] A. Messiah, *Quantum Mechanics*, Dover books on physics, Dover Publications, New York, 1961.

[141] S. Sachdev and A. P. Young, Phys. Rev. Lett. **78**, 2220 (1997).

[142] S. Sachdev, *Quantum Phase Transitions*, Cambridge University Press, Cambridge, 2011.

[143] P. Jordan and E. Wigner, Z. Phys. **47**, 631 (1928).

[144] J. Dziarmaga, Phys. Rev. Lett. **95**, 245701 (2005).

[145] E. Lieb, T. Schultz, and D. Mattis, Ann. Phys. **16**, 407 (1961).

[146] G. Szegő, Comm. Sém. Math. Univ. Lund [Medd. Lunds Univ. Mat. Sem.] **1952**, 228 (1952).

[147] G. Rigolin, G. Ortiz, and V. H. Ponce, Phys. Rev. A **78**, 052508 (2008).

[148] E. Barouch and B. M. McCoy, Phys. Rev. A **3**, 786 (1971).

[149] J.-P. Bouchaud, L. F. Cugliandolo, J. Kurchan, and M. Mézard, in *Spin Glasses And Random Fields*, edited by A. P. Young, World Scientific, Singapore, 1997, volume 12 of *Series on Directions in Condensed Matter Physics*.

[150] H. Janssen, B. Schaub, and B. Schmittmann, Z. Phys. B Condens. Matter **73**, 539 (1989).

[151] P. Calabrese and A. Gambassi, J. Phys. A: Math. Gen. **38**, R133 (2005).

[152] M. Buchhold and S. Diehl, Phys. Rev. A **92**, 013603 (2015).

[153] P. Gagel, P. P. Orth, and J. Schmalian, Phys. Rev. Lett. **113**, 220401 (2014).

[154] P. Gagel, P. P. Orth, and J. Schmalian, Phys. Rev. B **92**, 115121 (2015).

[155] M. Moshe and J. Zinn-Justin, Phys. Rep. **385**, 69 (2003).

[156] S. Sotiriadis and J. Cardy, Phys. Rev. B **81**, 134305 (2010).

[157] J. Berges and T. Gasenzer, Phys. Rev. A **76**, 033604 (2007).

[158] P. Calabrese and J. Cardy, J. Stat. Mech. Theor. Exp. **2007**, P06008 (2007).

[159] A. Kamenev, *Field Theory of Non-Equilibrium Systems*, Cambridge University Press, Cambridge, 2011.

[160] M. Abramowitz and I. A. Stegun, *Handbook of mathematical functions*, Dover Publications, New York, 1965.

[161] S. Sotiriadis, P. Calabrese, and J. Cardy, Europhys. Lett. **87**, 20002 (2009).

[162] A. J. Bray and M. A. Moore, Phys. Rev. Lett. **38**, 735 (1977).

[163] J. Zinn-Justin, *Quantum Field Theory and Critical Phenomena*, International series of monographs on physics, Clarendon Press, Oxford, 2002.

[164] A. J. Bray, Adv. Phys. **43**, 357 (1994).

[165] C. Godrèche and J. M. Luck, J. Phys. Condens. Matter **14**, 1589 (2002).

[166] L. F. Cugliandolo, C. R. Phys. **16**, 257 (2015), Coarsening dynamics / Dynamique de coarsening.

[167] S. L. Sondhi, S. M. Girvin, J. P. Carini, and D. Shahar, Rev. Mod. Phys. **69**, 315 (1997).

[168] M. van den Worm, B. C. Sawyer, J. J. Bollinger, and M. Kastner, New J. Phys. **15**, 083007 (2013).

[169] T. Langen, R. Geiger, M. Kuhnert, B. Rauer, and J. Schmiedmayer, Nature Phys. **9**, 640 (2013).

[170] M. Greiner, O. Mandel, T. Esslinger, T. W. Hänsch, and I. Bloch, Nature **415**, 39 (2002).

[171] S. Trotzky, P. Cheinet, S. Fölling, M. Feld, U. Schnorrberger, A. M. Rey, A. Polkovnikov, E. A. Demler, M. D. Lukin, and I. Bloch, Science **319**, 295 (2008).

[172] W. S. Bakr, J. I. Gillen, A. Peng, S. Fölling, and M. Greiner, Nature **462**, 74 (2009).

[173] T. Betz, S. Manz, R. Bücker, T. Berrada, C. Koller, G. Kazakov, I. E. Mazets, H.-P. Stimming, A. Perrin, T. Schumm, and J. Schmiedmayer, Phys. Rev. Lett. **106**, 020407 (2011).

[174] P.-E. Larré and I. Carusotto, Phys. Rev. A **92**, 043802 (2015).

[175] J. Berges, A. Rothkopf, and J. Schmidt, Phys. Rev. Lett. **101**, 041603 (2008).

[176] J. Berges and G. Hoffmeister, Nucl. Phys. B **813**, 383 (2009).

[177] C. Scheppach, J. Berges, and T. Gasenzer, Phys. Rev. A **81**, 033611 (2010).

[178] J. Berges and D. Sexty, Phys. Rev. D **83**, 085004 (2011).

[179] J. Berges and D. Sexty, Phys. Rev. Lett. **108**, 161601 (2012).

[180] A. Piñeiro Orioli, K. Boguslavski, and J. Berges, Phys. Rev. D **92**, 025041 (2015).

[181] J. Schole, B. Nowak, and T. Gasenzer, Phys. Rev. A **86**, 013624 (2012).

[182] M. Karl, B. Nowak, and T. Gasenzer, Phys. Rev. A **88**, 063615 (2013).

[183] P. C. Hohenberg and B. I. Halperin, Rev. Mod. Phys. **49**, 435 (1977).

[184] C. Godrèche and J. M. Luck, J. Phys. A: Math. Gen. **33**, 9141 (2000).